TAILORING ONE DIMENSIONAL NOVEL NANO STRUCTURES FOR SPECIFIC
APPLICATIONS USING TOOLS OF MOLECULAR MODELING

A THESIS SUBMITTED TO
THE GRADUATE SCHOOL OF NATURAL AND APPLIED SCIENCES
OF
MIDDLE EAST TECHNICAL UNIVERSITY

BY

OSMAN BARIŞ MALCIOĞLU

IN PARTIAL FULFILLMENT OF THE REQUIREMENTS

FOR

THE DEGREE OF DOCTOR OF PHILOSOPHY

IN

PHYSICS

MARCH 2008

Approval of the thesis:

TAILORING ONE DIMENSIONAL NOVEL NANO STRUCTURES FOR SPECIFIC APPLICATIONS USING TOOLS OF MOLECULAR MODELING

submitted by **OSMAN BARIŞ MALCIOĞLU** in partial fulfillment of the requirements for the degree of **Doctor of Philosophy in Physics department, Middle East Technical University** by,

Prof. Dr. Canan Özgen
Dean, Graduate School of **Natural and Applied Sciences**   _____

Prof. Dr. Sinan Bilikmen
Head of Department, **Physics**   _____

Prof. Dr. Şakir Erkoç
Supervisor, **Physics, METU**   _____

Examining Committee Members:

Prof. Dr.Salim Çıracı
Physics, Bilkent University   _____

Prof. Dr. Şakir Erkoç
Physics, METU   _____

Prof. Dr. Demet Gülen
Physics, METU   _____

Prof. Dr. Güngör Gündüz
Chemical Engineering, METU   _____

Prof. Dr. Hamit Yurtseven
Physics, METU   _____

Date: _____

"I hereby declare that all information in this document has been obtained and presented in accordance with academic rules and ethical conduct. I also declare that, as required by these rules and conduct, I have fully cited and referenced all material and results that are not original to this work."

Name Surname: Osman Barış Malcıoğlu
Signature:

ABSTRACT

TAILORING ONE DIMENSIONAL NOVEL NANO STRUCTURES FOR SPECIFIC
APPLICATIONS USING TOOLS OF MOLECULAR MODELING

Malcıoğlu, Osman Barış
Ph.D., Department of Physics
Supervisor: Prof. Dr. Şakir Erkoç

March 2008, 151 pages.

In this work, the use of theoretical tools of molecular modeling for tailoring 1D novel
nanomaterials is demonstrated. There are four selected nano-structures as examples,
each tailored for a specific demand of nano-technology that is yet to be fulfilled. For
the purpose of modeling/calculating the electronic and structural properties, various
methods of defining the interatomic interaction, such as empirical potential energy
functions, semi-empirical methods and density functional theory, are used. Each of
these methods have a different level of approximations leading to limitations in their
use. Furthermore, each method needs to be calibrated carefully in order to obtain
physically meaningful results. Examples being novel nano-structures, there does not
exist any experimental observations directly studying the material at hand. Thus, in
order to obtain a parameter set that best describes the system, a series of pre-existing
structures that are physically and/or chemically related are used. Among the methods
employed, the density functional theory (DFT) is certainly the most popular one, due to
its accuracy and more importantly the framework it provides for perturbative extensions
otherwise nearly impossible to calculate in Hartree-Fock level.

Keywords: Novel carbon nanomaterials, density functional theory, molecular-dynamics

ÖZ

UYGULAMAYA YÖNELIK TEK BOYUTLU NANO YAPILARIN MOLEKÜLER MODELLEME TEKNIKLERI KULLANARAK HAZIRLANMASI

Malcıoğlu, Osman Barış

Doktora , Fizik Bölümü

Tez Yöneticisi: Prof. Dr. Şakir Erkoç

Mart 2008, 151 sayfa.

Bu çalışmada, uygulamaya yönelik tek uzamlı karbon nanoyapıların molekül modelleme teknikleri kullanarak incelenmesi önerilmiş ve örneklendirilmiştir. Nanoteknoloji uygulamaları olabilecek dört farklı model incelenmiştir. Modellerin yapıları ve elektronik özelliklerinin hesaplanması için ampirik ve yarı ampirik potansiyeller, Yoğunluk Fonksiyoneli Kuramı gibi farklı yöntemler uygulanmıştır. Uygulanan her yöntemin barındırdığı farklı yakınsamalar uygulama alanlarında farklı kısıtlamalara yol açmakta, ve model hakkında farklı örneklemeler gerektirmektedir. Örnek olarak incelenen yapılar ve özellikler için uygun olan fonksiyoneller ve dalga fonksiyonu setini seçmek amacıyla kimyasal veya yapısal açıdan benzer yapılar göz önüne alınmıştır.

Elektronik özellikler için günümüzde yaygın olarak kullanılan Yoğunluk Fonksiyoneli Kuramı yöntemi kullanılmıştır. Bu kuramın sağladığı yapısal çerçeve ile farklı fiziksel özelliklerin hesaplanması için Hartree-Fock seviyesinde mümkün olmayan yakınsamalar yapılabilmektedir.

Anahtar Kelimeler: karbon nanomalzeme, Yoğunluk fonksiyonel kuramı, molekül-dinamiği

To my mother, family, and in memory of my father.

ACKNOWLEDGMENTS

Before anything else, I would like to express my deepest gratitude to my advisor Prof. Dr. Şakir Erkoç, with whom I have been studying more than eight years now. It was through his teachings, not only in the scientific sense, but also in terms of discipline and advisorship that this work you are about to read was possible.

I can still remember my first day in METU, the long queue at the registration desk, and the strangeness of the surroundings. It feels funny that this memory is older than eleven years now. I have seen my share of "circulation of people" within these years. Most of my friends I have met in my undergraduate years are long gone for other adventures, and now, the time of my departure comes near. I hope farewell in their journeys, maybe we will meet again someday.

There are a number of people I would like to acknowledge for their direct help and support in my Ph.D. years, although I am doubtful I will be able to express my gratitude in the extent they deserve within the constraints of this text.

First of all, I would like to thank everyone in our group in METU for their friendship and help, especially my partners in the micro anthropological entity formed by Emre Taşcı, Efe Yazgan and me. Every single day of coming to work was more interesting and fun than the previous one thanks to them. It should also be mentioned that although their line of work does not coincide directly with ours, Sezen Sekmen and Yasemin Yazgan are the honorary members of this socio-(a)pedagogical entity due to its very definition, and their contribution can not be overlooked. The cheerfulness and friendship

tradesperson working in a dull job, always in self denial for what I have missed. I have met with the other part of my family rather late, and in a time of great stress, and it is sad to see I have met them this late. Ferda Malcıoğlu, I hope you find yourself in the new field you have chosen, and achieve great success, Rana Güzeldağ, I hope you make your life meet your expectations to the fullest extent, once little ducklings, now little ladies, Berna, Birgül, and Birnur, I wish you a good life, support each other no matter what may life toss at you.

Before I conclude, I would like to thank everyone working in the sports facilities of METU, the trainers and workers, for the support and encouragement in time of need, and the ODTU-DOJO, which I am honored to be a part of and sad to meet all the beatiful people within so late.

TABLE OF CONTENTS

LIST OF TABLES

LIST OF FIGURES

xv

CHAPTER 1

THEORETICAL BACKGROUND

It should be noted beforehand that, this introductory text can be considered as a summary of information contained within the Refs. [1]-[9] (and more), for more detailed discussion, the reader should refer to them accordingly.

1.1 Introduction

Nano refers to a length scale, 10^{-9} m, and it is just that. The interesting part, or let me say "the problem" is the behavior of materials at that scale. Call it nanotechnology or nanoscience, depending whether you are in for engineering or scientific purposes, it does not matter, almost any field interested in physical entities and their applications are involved in some part or another. Exploring this scale, and tackling with the new problems attached, lead to a better understanding of the nature of materials and consequently their better use, which is what science and technology stands for. The subject lies shared within the intellectual domains of most of the basic sciences, primarily Physics and Chemistry. Biology, especially molecular biology, is special in its interest and contribution, due to majority of its subjects already being in the nanoscale.

In fact, this involvement is to the extent that biology can be considered as the working example nanotechnology. It is a source of inspiration for possible applications, and proof that concepts like "self-assembly", "molecular machines" are not eccentric novelties, but something nature has already excelled. As the understanding of this scale increases, almost all branches of engineering are also slowly transformed in order to accommodate the new set of rules. With the (gate) size of a transistor being as small as few nanometers nowadays, and consequent quantum effects coming more and more in the play, electronic engineering is one of the first to incorporate nanoscale effects (although rather covertly, due to commercial nature). Mechanical engineering is interested in the new rules this dimension introduce, and how to use them for more efficient mechanical work, reducing friction inside the existing engines, or exploring the possibility of creating useful mechanical work at nanometer scale. Even civil engineering and thus architecture are slowly transformed, with the advent of new, stronger and lighter materials. These examples may be expanded, but the essence of the story is the same, nanotechnology is slowly changing the world, where the subtle but strong quantum effects are recognized in everyday life. This transformation is considered to be crucial in most of the nations, and the exponential increase of the diverted effort in the literature these last years is a perfect indication of the importance the topic carries.

The peculiarity of the scale arises from being in the border of atomic and macroscopic worlds. As of all such "in the border" scales, this scale is challenging theoretically as much as it is experimentally. In the scale of (one or very few) atoms, there is quantum theory, which gives a huge amount of information on the structure, with its consequences not accustomed to in everyday life. In the scale of macroscopic materials (with the number of atoms contained is in the order of 10^{23}, practically uncountable) there is statistical physics, and empirical equations originating from experiments, which can predict the outcome of a specific stimulus, although it gives limited information on

intrinsic mechanisms. In principle these two scales are consistent, which is to say, quantum equations should reduce to their macroscopic equivalents in the limit where the elementary quantum of action (and the Dirac's constant $\hbar$) is negligible, accompanied with the expected loss of detail. But what happens just in between, when the structure of interest fits neither of the size criteria well? Nanoscale is just that. The number of atoms is too much for a basic quantum approach, the equations become so tangled that it is practically impossible to solve[1], and since the $\hbar$ and atomic/quantum effects attached to it can not be dismissed readily, macroscopic equations tend to be inadequate. What we need is the proper scaling of quantum equations. The application of wave mechanics to larger systems is not a new problem, on the contrary, since the quantum theory itself has its roots on the unexplained atomic phenomena, it was a very popular area of research in the pre-war era of 1923-1933. With the turn of events in 1933, nuclear and high energy physics gain more popularity, and it is not much later that significant achievements in this problem is made. The correlation with the advancements in computers also can not be neglected. The form of the equations are most suitable for iterative approaches, and the sheer quantity of iterations make the computers not a luxury but mandatory. This makes the capacity of the particular computer a physical limit on the problem that can be studied. Approximations lighten the load on the computer, thus via a sacrifice in generality and/or accuracy, the limitations are eased. Both computer science and methods available exponentially grew since then, and continue on growing. At some point, the necessity for approximations may cease to exists, but, as of now, the knowledge of physical and mathematical nature of approximations and their applicability is very important if not essential for someone involved in this field. Nowadays, the pure theoretical interest of the last century is replaced by the urge to explain empirical observations at the nanoscale. Theoretical methods benefit from the

---

[1]In fact, even for atoms larger than hydrogen one does need simplifications to separate the Hamiltonian and solve the electron related equations. But the modifications mentioned here is of higher level, the separated Hamiltonian also becomes intangible after a certain limit, and further simplifications come into play

increased number of experimentation, as the empirical data greatly reduce the strain of calculation, and in return, theoretical models provide the experiments a guide light on where to proceed, ultimately leading to better understanding of the phenomenon.

In this last decade, the popularity of the field increased exponentially. The quantity and quality of the available experimental information regarding the materials at this scale is getting better and better. Stronger theoretical models are formed and proposed in the literature frequently, along with new computational techniques that exploit the advent of computer capabilities to a better extent, reducing the number of approximations required. At this point, it is may be theorized that, using this already available information, one can extrapolate at least some of the physical properties for a novel nanomaterial that does not exist in the literature, within an acceptable margin of error. Due to nature of the theoretical models used, even for "ab-initio" density functional methods, this nano material modeling/engineering approach is strictly not a black box where you just turn the crank and wait for the results. One needs to choose the parametrization samples carefully, keeping in mind the expected physics and chemistry of the system, intervening with intuition when necessary. This work incorporates five self-contained examples of this approach to carbon nanomaterials, outlining the methods used in the calculation and modeling in detail. Carbon materials are well studied thanks to its popularity due to carbon nanotubes and Buckminsterfullerene, and thus they have a better understood nature. Before proceeding any further, a short introduction to the material is next.

1.2 The special importance of Carbon atom

There are numerous elements in the periodic table, each with its own set of unique properties. Among them, the carbon atom carries a special significance. The main reason of this lies within the realms of biology and organic chemistry. Carbon is seen to be functionalized in a huge number of ways in the subjects of these fields. The presence

is so strong that, in short, the life on earth is carbon based. But why not Silicon, or another element? The reason is in the unique ability in hybridization. Hybridization can be explained roughly as the intermixing of atomic orbitals of a particular atom in order to form stronger molecular bonds and permit different geometrical orientations[2]. Any two atomic orbitals with different shell designations that are close enough energetically can intermix to form a hybrid orbital. For example if one refers a sp hybridization, it translates as one s orbital and one p orbital intermixing to form two sp orbitals (See Figure 1.1).
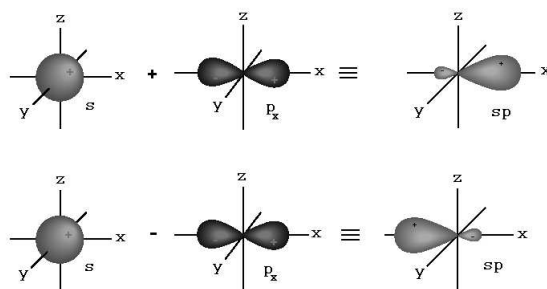
Figure 1.1: A graphical representation of sp hybridization.

The result is a better overlap and altered geometry. The process is common for most atoms, even the particular geometry of water can be explained by the hybridization of oxygen atom. In the case of carbon atom however, particular arrangement of valance electrons make one electron leaving s orbital to occupy one of the vacant p orbitals energetically viable, thus all sp hybridization variants (sp^1, sp^2 and sp^3) are available (Figure 1.2).

Furthermore, these hybrids are quite stable and favorable. Adding this the fact

---

[2]It is often pointed out that hybridization theory was indeed proposed in order to explain peculiar geometric orientations of some molecules.

(1 Triple + 1 Single bond) $4\mathrm{x}\ \frac{\uparrow}{\mathrm{sp}}$ = 4 Bonds (sp^3)

$\frac{\uparrow\downarrow}{s}\ \frac{\uparrow\ \ \uparrow}{p}$ → $\frac{\uparrow}{s}\ \frac{\uparrow\ \ \uparrow\ \ \uparrow}{p}$ → $3\mathrm{x}\ \frac{\uparrow}{\mathrm{sp}} + 1\mathrm{x}\ \frac{\uparrow}{p}$ = 3 Aromatic Bonds (sp^2)

$2\mathrm{x}\ \frac{\uparrow}{\mathrm{sp}} + 2\mathrm{x}\ \frac{\uparrow}{p}$ = 2 Double Bonds (sp)
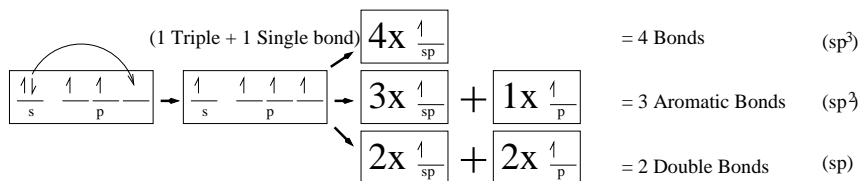
Figure 1.2: Schematic representations of possible bonding schemes of carbon. In non-hybridized form, 2 bonds are possible (1 triple and one single). sp^1 ,sp^2 and sp^3 hybridization leads to different bonding schemes and orders.

that the resulting geometries are in fact the geometrical basics that can be used to construct an infinite number of structures, carbon atom serves as the ultimate building block for complex functional molecules. One of the closest substitutes, silicone, lack the bond strength, and thus silane (analogous to hydrocarbon chains) are not as stable. In addition to this, silicon does not readily form double or triple bonds, and tend to react strongly to the presence of oxygen if not in its sp^3 hybridized state. The reason why the life is not silicon based here on earth is most probably this lack of hybridization capabilities.

Different hybridization schemes lead to various forms of carbon that are distinctively separate in behavior. Think of graphite and diamond, diamond has an incredible hardness, optical properties and it is much prized as an item of fashion, whereas graphite is flexible, black, conductive, and so common that it is often used as fuel!

1.3 Approximate and Conquer: A Solution to the Infamous Many Body Schrödinger Equation

When one approaches the problem with the usual analytical quantum formalism, the Hamiltonian encountered in its most general form looks like this:

$$\hat{H} = \hat{H}_{k,n} + \hat{H}_{k,e} + \hat{H}_{p,n-n} + \hat{H}_{p,e-e} + \hat{H}_{p,n-e} \tag{1.1}$$

in this equation, $\hat{H}_{k,n}$ and $\hat{H}_{k,e}$ are the kinetic energy contributions of the nuclei and the electrons respectively. $\hat{H}_{p,n-n}$, $\hat{H}_{p,e-e}$ and $\hat{H}_{p,n-e}$ are the interaction potential terms for nucleus–nucleus, electron–electron and nucleus–electron terms. The exact compositions of the Hamiltonians are unimportant at this point. The equation we are trying to solve is simply,

$$\left[\left(\hat{H}_{k,n} + \hat{H}_{p,n-n}\right) + \left(\hat{H}_{k,e} + \hat{H}_{p,e-e} + \hat{H}_{p,n-e}\right)\right] \Psi(\vec{X}, \vec{x}) = E.\Psi(\vec{X}, \vec{x}) \qquad (1.2)$$

(where $\vec{X}$ and $\vec{x}$ are the nuclear and electronic coordinates respectively). Alas, there is nothing simple about this equation, it is inseparable! One may try to solve this extremely complicated problem using some mathematical method being also (if not more) complex in its nature, but, the question is, do we require that much information? Not in this case, and in a majority of others. Instead, at this point, which may be called a crossroad of sorts, it is better to choose in which application the results will be used, and proceed accordingly. In the context of this discussion, the point of interest is somewhat limited, and thus considerable simplifications can be made. The price is the compromise of generality, but armed with the knowledge of what is lost, and what can still be done, the problem becomes solvable straightforwardly if not trivial.

A first level approach is to apply Born-Oppenheimer approximation. In this approximation, it is pointed out that the electrons move so much faster than the nuclei such that the corresponding part of the wave function adjusts itself to a new configuration almost instantly. Thus the equation can be investigated in two parts, an electronic and a nuclear part which are assumed to be independent. The rest follows easily,

$$\Psi(\vec{X}, \vec{x}) = \Psi_n(\vec{X})\Psi_e(\vec{X}, \vec{x}) \qquad (1.3)$$

$$\left(\hat{H}_{k,n} + \hat{H}_{p,n-n}\right) \Psi_n(\vec{X})\Psi_e(\vec{X}, \vec{x}) \qquad (1.4)$$

$$+ \left(\hat{H}_{k,e} + \hat{H}_{p,e-e} + \hat{H}_{p,n-e}\right) \Psi_n(\vec{X})\Psi_e(\vec{X}, \vec{x})$$

$$\simeq \Psi_e(\vec{X}, \vec{x}) \left(\hat{H}_{k,n} + \hat{H}_{p,n-n}\right) \Psi_n(\vec{X}) \qquad (1.5)$$

$$+\Psi_n(\vec{X})\left(\hat{H}_{k,e} + \hat{H}_{p,e-e} + \hat{H}_{p,n-e}\right)\Psi_e(\vec{X},\vec{x})$$

$$= E.\Psi_n(\vec{X})\Psi_e(\vec{X},\vec{x})$$

$$\frac{\left(\hat{H}_{k,n} + \hat{H}_{p,n-n}\right)\Psi_n(\vec{X})}{\Psi_n(\vec{X})} + \frac{\left(\hat{H}_{k,e} + \hat{H}_{p,e-e} + \hat{H}_{p,n-e}\right)\Psi_e(\vec{X},\vec{x})}{\Psi_e(\vec{X},\vec{x})} \qquad (1.6)$$

$$= (E_n + E_e)$$

and since both parts must be independent (first fractional depends only on nuclear coordinates, whereas second fractional depends also on electronic coordinates), we are left with two slightly coupled equations

$$\hat{H}_e\Psi_e(\vec{X},\vec{x}) = E_e\Psi_e(\vec{X},\vec{x}) \qquad (1.7)$$

$$\hat{H}_n\Psi_n(\vec{X}) = E_n\Psi_n(\vec{X}) \qquad (1.8)$$

Notice that in Eq. 1.5 contributions like

$$-\frac{\hbar^2}{2M_k}\nabla^2_{\vec{X}}\Psi_e(\vec{X},\vec{x}) \qquad (1.9)$$

(kinetic energy of the nuclei originating from the electronic part of the wave function) are ignored, and although this is feasible in our problem, it is not always justified. Some very important effects are now "out of reach". Among the lost are the superconductivity effect and electron charge- or spin-density waves. But via this loss of generality, the equations become more solvable, and in the context of this text, the trade off is more than acceptable. The remaining electron integrals can be solved using various methods, generally in a self-consistent manner, each with its own advantage and disadvantage, leading to electron configuration information with varying detail. Looking at Equation 1.8, one immediately recognize it as the quantum analog for the equations of motion of a particle under a potential, thus, in the separated equation, the nuclei can now be treated semi-classically (depending on the boundary conditions).

The dependence on electronic coordinates is not obvious in Equation 1.8 at first sight. After all, $\vec{x}$ does not appear anywhere within. However, as the common sense

dictates, this can not be the case, so lets investigate where does the effects of electron configuration come into play:

The equation of motion for nuclei can be written as simplistic as:

$$\vec{F}_i = M_i \vec{a}_i \tag{1.10}$$

where $\vec{F}_i$ is the force acting on the ith nucleus, and $M_i, \vec{a}_i$ are the mass and acceleration accordingly. Basic Newtonian equation of motion that reduce the nuclei to point particles. The sole requirements for the reduction in mathematical terms are a smooth potential energy function and large enough boundary. For now, lets assume these requirements are fulfilled, and proceed. The problem is now reduced to finding the force on the ith nucleus, or the force field using a more general name. This can be done using numerous ways, but you guessed it correctly, it does depend on the configuration of electrons. The key point is to remember that the equation of motion for the nuclei should be defined through the full Hamiltonian, not only through the nuclear part, as the two parts are not completely uncoupled.

1.4   Handling the electronic equation of motion

Due to coupling in the electronic and nuclear parts of the Hamiltonian, any arrangement in nuclear coordinates lead to a different energy in the electronic part. If you are trying to determine the nuclear positions in the structure, this poses a big problem, as these kind of equations almost always prove to be impossible to solve by traditional analytical methods. However, they can easily be solved iteratively. You start with an initial set of nuclear coordinates, calculate the total Hamiltonian and its spatial gradient, and move the nuclei (with your favorite method) arriving at a new set of coordinates. In these new coordinates the electronic part needs to be recalculated, and you need to start over the whole procedure again. This continues until a preset convergence criteria, usually when the variation in total energy is negligible. In this sense, the electronic part of the Hamiltonian is the key to the solution.

Various levels of approximation and different approaches can be used in order to solve the problem, but except from a few simplistic methods, these all require computers. The methods can be classified in ab-initio, semi-empirical, and density functional branches. Ab-initio methods try to solve wave-function for electrons employing mathematical shortcuts and approximations, without any empirical data. Although the precision and diversity of information obtained is excellent, the complexity of the wave-function significantly limits the applicability in this approach. Density functional method replaces the differential equation for wave-function with an integral equation for the density, eliminating some (excess in our case) information thus simplifying the problem with minimum sacrifice, at least in a number of cases. This method will be detailed in the following section. Semi-empirical methods tries to incorporate empirical data to simplify the equation for electronic wave-function, but as all empirical methods, parametrization is required. The problematic part is always the electron-electron interaction terms, and usually all the parametrization comes into play when trying to approximate these integrals with (a series of) one electron equations. Two such examples, AM1 [10] and PM3 [11, 12, 13] which are both descendants of modified neglect of differential orbitals approximation, are of most importance in this context, due to their significantly reduced form (translates as being cheaper computationally) and wide applicability (a lot of parameter sets exist in the literature).

1.4.1 An alternative for wave-functions in the quest for observables

Seemingly, the most straightforward method we can choose is to find the electron wave-function through the electronic part of the Hamiltonian

$$\hat{H}_e \Psi_e(\vec{X}, \vec{x}) = E_e \Psi_e(\vec{X}, \vec{x}) \tag{1.11}$$

However, even for a simple molecule, say Benzene, the wave-function depends on 126 spatial coordinates and 42 spin coordinates. Of course we can try to approximate this equation, as briefly mentioned in the previous chapter, various methods exist, but before

trying to tackle this problem, there is an important question: Do we really need so much detail in describing our system? Commonly experimental observables depend only on spatial coordinates of the species considered. Consider such an operator:

$$\hat{A} = \sum_n a_1(\vec{r}_n) \tag{1.12}$$

the expectation is

$$\int d\vec{r}_1 \ldots d\vec{r}_N \left\langle \Psi\left(\vec{r}_1 \ldots \vec{r}_N\right)\right| \hat{A} \left|\Psi\left(\vec{r}_1 \ldots \vec{r}_N\right)\right\rangle \tag{1.13}$$

the above integral can be re-written using the density operator

$$a_1(\vec{r}_n) = \int a_1(\vec{s})\delta(\vec{r}_n - \vec{s})\, d\vec{s} \tag{1.14}$$

$$\rightarrow \int d\vec{r}_1 \ldots d\vec{r}_N \left\langle \Psi\left(\vec{r}_1 \ldots \vec{r}_N\right)\right| \sum_n a_1(\vec{r}_n) \left|\Psi\left(\vec{r}_1 \ldots \vec{r}_N\right)\right\rangle \tag{1.15}$$

$$= \int \left[\int d\vec{r}_1 \ldots d\vec{r}_N \left\langle \Psi\left(\vec{r}_1 \ldots \vec{r}_N\right)\right| \sum_n \delta(\vec{r}_n - \vec{s}) \left|\Psi\left(\vec{r}_1 \ldots \vec{r}_N\right)\right\rangle \right] a_1(\vec{s})\, d\vec{s} \tag{1.16}$$

$$= \int \rho(\vec{s})a_1(\vec{s})\, d\vec{s} \tag{1.17}$$

to depend only on the electron density. Similar reductions exist for operators of more complicated nature such as:

$$\hat{A} = \sum_{n \neq m} a_2(\vec{r}_n, \vec{r}_m) \tag{1.18}$$

consequently, most of the coordinates residing in the wave-function turn out to be nothing more than redundancies for such cases, and, if a reformulation that bypasses the wave-functions exists, even for the more complicated operator presented above, only 6 spatial and 2 spin coordinates defining the density will be sufficient, independent of the number of electrons system contains. Gladly, such a formulation does exist, the Density Functional Theory (DFT) [3].

---

[3]Possibly the first such formulation is the Thomas and Fermi $X\alpha$ method, which is an approximation to solving the Schrödinger equation. Due to its nature, it will not be further mentioned here.

In 1964, Hohenberg and Kohn [14] have shown that it is *possible* to calculate all the *ground state* properties only through the knowledge of electron density. The proof is exceptionally simple. Split the potential energy term in the electron equation into two parts, the electron–electron interaction term, and another term consisting of a series of one-body interaction terms

$$\hat{H}_e = \left[\sum_{i=1}^N -\frac{1}{2}\nabla_{\vec{r_i}}^2 + \sum_{i \neq j}^N \frac{1}{|\vec{r_i} - \vec{r_j}|} \right] + \sum_{i=1}^N V_{ext}(\vec{r_i}) = \hat{H}_{fe} + \hat{V}_{ext} \qquad (1.19)$$

this series of one-body interaction terms, called the "external potential", is assumed to be a near complete description of all the relevant stimuli to an otherwise free gas of electrons (the square bracketed term). This term may correspond only to nuclei, or a combination that also include external fields applied to the matter depending on the system under study. The square bracketed part is common for all the possible problems, thus, what determines the exact behavior of electron distribution, and consequently the uniqueness of the particular system under consideration, is solely the external potential.

Now consider two *different* external potentials and the corresponding Hamiltonians

$$\hat{H}_1 = \hat{H}_{fe} + \hat{V}_{ext} \; ; \; \hat{H}_2 = \hat{H}_{fe} + \hat{V}'_{ext} \; ; \; \hat{V}_{ext} \neq \hat{V}'_{ext} \qquad (1.20)$$

define the *ground states* of these two distinct Hamiltonians as

$$\hat{H}_1\Psi_1 = E_1\Psi_1 \; ; \; \hat{H}_2\Psi_2 = E_2\Psi_2 \; ; \; \Psi_1 \neq \Psi_2 \qquad (1.21)$$

assume both wave-functions lead to same density

$$\rho(\vec{r}) = \int d\vec{r}_1 \ldots d\vec{r}_N \, \langle \Psi_1 \left(\vec{r}_1 \ldots \vec{r}_N \right)| \sum_n \delta(\vec{r}_n - \vec{r}) \, |\Psi_1 \left(\vec{r}_1 \ldots \vec{r}_N \right)\rangle \qquad (1.22)$$

$$= \int d\vec{r}_1 \ldots d\vec{r}_N \, \langle \Psi_2 \left(\vec{r}_1 \ldots \vec{r}_N \right)| \sum_n \delta(\vec{r}_n - \vec{r}) \, |\Psi_2 \left(\vec{r}_1 \ldots \vec{r}_N \right)\rangle \qquad (1.23)$$

since we are dealing with ground states, and Ψ_2 is not the ground state of $\hat{H}_1$,

$$\langle \Psi_2 | \, \hat{H}_1 \, | \Psi_2 \rangle > \langle \Psi_1 | \, \hat{H}_1 \, | \Psi_1 \rangle = E_1 \qquad (1.24)$$

12

$$E_1 \quad < \quad \langle \Psi_2 | \hat{H}_1 | \Psi_2 \rangle = \langle \Psi_2 | \hat{H}_1 - \hat{H}_2 + \hat{H}_2 | \Psi_2 \rangle \tag{1.25}$$

$$= \langle \Psi_2 | \hat{H}_1 - \hat{H}_2 | \Psi_2 \rangle + \langle \Psi_2 | \hat{H}_2 | \Psi_2 \rangle \tag{1.26}$$

$$= \langle \Psi_2 | \hat{V}_{ext} - \hat{V}'_{ext} | \Psi_2 \rangle + E_2 \tag{1.27}$$

$$= \int \rho(\vec{r}) \left[\hat{V}_{ext} - \hat{V}'_{ext} \right] d\vec{r} + E_2 \tag{1.28}$$

$$E_1 - E_2 \quad < \quad \int \rho(\vec{r}) \left[\hat{V}_{ext} - \hat{V}'_{ext} \right] d\vec{r} \tag{1.29}$$

but this is also valid other way around!

$$\langle \Psi_1 | \hat{H}_2 | \Psi_1 \rangle > \langle \Psi_2 | \hat{H}_2 | \Psi_2 \rangle = E_2 \tag{1.30}$$

leading to

$$E_2 - E_1 < \int \rho(\vec{r}) \left[\hat{V}'_{ext} - \hat{V}_{ext} \right] d\vec{r} \tag{1.31}$$

or

$$E_1 - E_2 > \int \rho(\vec{r}) \left[\hat{V}_{ext} - \hat{V}'_{ext} \right] d\vec{r} \tag{1.32}$$

which is just the opposite of Equation 1.29. They can not be both true, the only logical conclusion is that our initial assumption of two different external potentials leading to same ground state charge density should be wrong. Thus, electron charge density is an unique property of the system. Now assume we know this density, ρ, which can be calculated from the N–electron ground state wave-function Ψ_0.

$$E_e = \langle \Psi_0 | \hat{H}_e | \Psi_0 \rangle \tag{1.33}$$

since Ψ_0 is the ground state

$$E_e = \min_{\Psi} \langle \Psi | \hat{H}_e | \Psi \rangle \tag{1.34}$$

we now know that ρ is an unique property of the system, thus we can safely state

$$E_e = \min_{\Psi \to \rho} \langle \Psi | \hat{H}_e | \Psi \rangle \tag{1.35}$$

or

$$E_e = E_e [\rho] = \min_{\Psi \to \rho} \langle \Psi | \hat{H}_e | \Psi \rangle \tag{1.36}$$

where we have written E_e as a *functional* of ρ. Being an unique variable, variational principle is valid

$$E_e\left[\rho'\right] \geq E_e\left[\rho\right] \tag{1.37}$$

this, in fact, is a whole new perspective for our problem: If a practical way exists for calculating the energy through the density, calculating the N–electron wave-function is no longer obligatory. Hohenberg-Kohn theorems does not provide such a framework, only the proof of existence. Lets see what we can do. Variational principle being valid, the ground state density of the system can be found through

$$\frac{\delta E_e\left[\rho\right]}{\delta\rho} = \lim_{\delta\rho \to 0}\left(\frac{E_e\left[\rho + \delta\rho\right] - E_e\left[\rho\right]}{\delta\rho}\right) = 0 \tag{1.38}$$

where $\frac{\delta}{\delta\rho}$ is called a *functional derivative*. Furthermore, we require that the system has a predetermined constant number of electrons (otherwise nasty things like charged constituents separating due to Coulomb repulsion may occur)

$$\int \rho(\vec{r})\,d\vec{r} = N \tag{1.39}$$

combining these two criteria via Lagrange multipliers an action integral for the ground state is obtained

$$\frac{\delta}{\delta\rho(\vec{r})}\left\{E_e\left[\rho(\vec{r})\right] - \mu\left[\int \rho(\vec{r})\,d\vec{r} - N\right]\right\} = 0 \tag{1.40}$$

Lets proceed further by expanding the E_e term. This term corresponds to the electronic Hamiltonian:

$$\hat{H}_e = \left[\sum_{i=1}^{N} -\frac{1}{2}\nabla^2_{\vec{r}_i} + \sum_{i \neq j}^{N} \frac{1}{|\vec{r}_i - \vec{r}_j|}\right] + \sum_{i=1}^{N} V_{ext}(\vec{r}_i) = \hat{T} + \hat{V} + \hat{V}_{ext} \tag{1.41}$$

the kinetic energy part depends only on the single particle coordinates, thus it belongs to the family mentioned in Equation 1.12. $\hat{V}_{ext}$ also belongs to that family by definition, thus we can write

$$\hat{T} \to T\left[\rho\right] \quad \hat{V}_{ext} \to V_{ext}\left[\rho\right] \tag{1.42}$$

but there is a problematic part. The Coulombic interaction part is a many body term, and can not easily be cast into a form consisting only of one particle densities i.e.:

$$\int \frac{\rho(\vec{r}, \vec{r'})}{|\vec{r} - \vec{r'}|}\, d\vec{r}d\vec{r'} \neq \int \frac{\rho(\vec{r})\rho(\vec{r'})}{|\vec{r} - \vec{r'}|}\, d\vec{r}d\vec{r'} \qquad (1.43)$$

which is mandatory in our derivation. Using a rather complicated expansion this term can be *approximated*[4] as

$$\int \frac{\rho(\vec{r}, \vec{r'})}{|\vec{r} - \vec{r'}|}\, d\vec{r}d\vec{r'} \approx \int \frac{\rho(\vec{r})\rho(\vec{r'})}{|\vec{r} - \vec{r'}|}\, d\vec{r}d\vec{r'} + \hat{E}_{xc} \qquad (1.44)$$

where $\hat{E}_{xc}$ contains all the second order effects not present in the $\int \frac{\rho(\vec{r})\rho(\vec{r'})}{|\vec{r}-\vec{r'}|}\, d\vec{r}d\vec{r'}$, such as exchange and correlation. The total electronic energy is now

$$E_e = T[\rho] + V_{ext}[\rho] + V[\rho] + E_{xc} \qquad (1.45)$$

$$= T[\rho] + \int V_{ext}(\vec{r})\rho(\vec{r})\, d\vec{r} + \int \frac{\rho(\vec{r})\rho(\vec{r'})}{|\vec{r} - \vec{r'}|}\, d\vec{r}d\vec{r'} + E_{xc} \qquad (1.46)$$

$$= T[\rho] + \int V_{ext}(\vec{r})\rho(\vec{r})\, d\vec{r} + \int V_C(\vec{r})\rho(\vec{r})\, d\vec{r} + E_{xc} \qquad (1.47)$$

placing this into the action integral

$$\frac{\delta E_e[\rho]}{\delta \rho} = \frac{\delta T[\rho]}{\delta \rho} + V_{ext}(\vec{r}) + V_C(\vec{r}) + \frac{\delta E_{xc}}{\delta \rho} = \mu \qquad (1.48)$$

The only problem we have now is the many-body nature of the exchange-correlation term. In 1965, Kohn and Sham introduced an ingenious trick [15]. Consider a system of N *non-interacting* particles that have the same density and same energy as our electron system. These particles are strictly *not* electrons, thus the describing Hamiltonian is completely different,

$$\hat{H} = \left[\sum_{i=1}^{N} \left(-\frac{1}{2} \nabla^2_{\vec{r_i}} + V_{eff}(\vec{r_i}) \right) \right] \quad E_e = T_0[\rho] + \int V_{eff}(\vec{r})\rho(\vec{r})\, d\vec{r} \qquad (1.49)$$

---

[4]If an analytical method for calculating E_{xc} exactly for free electron system existed, this term would be exact

but being non-interacting, the form is considerably simpler. Following the same steps, and since the total energy of both the systems is the same it is seen that

$$\frac{\delta T\left[\rho\right]}{\delta \rho} + V_{ext}(\vec{r}) + V_C(\vec{r}) + \frac{\delta E_{xc}}{\delta \rho} \equiv \frac{\delta T_0\left[\rho\right]}{\delta \rho} + V_{eff}(\vec{r}) \quad (1.50)$$

thus the effective potential should be equivalent to

$$V_{eff}(\vec{r}) \equiv \frac{\delta T\left[\rho\right]}{\delta \rho} - \frac{\delta T_0\left[\rho\right]}{\delta \rho} + V_{ext}(\vec{r}) + V_C(\vec{r}) + \frac{\delta E_{xc}}{\delta \rho} \quad (1.51)$$

surely this is an approximation, since effectively we are modeling a many–body system with a single body potential, but if Hohenberg-Kohn theorems hold true, sharing exactly the same density, both Hamiltonians should return the same ground state observables, even they are of completely different nature! Solution to this model Hamiltonian is simple if not trivial, but one must keep in mind that the orbitals are not those of electrons in our system, luckily, for most of the cases, it has been empirically found that the two has correspondence.

1.4.2 Nature of the interaction potential

The trickiest part in any problem is thus to model/choose the "Effective potential". Apart from the $V_{ext}(\vec{r})$ and $V_C(\vec{r})$, which are easily calculable, one can group all the remaining terms into a parametric function, aptly named as V_{xc}. Remember $\hat{E}_{xc}$ is an operator belonging to the free electron part of the Hamiltonian. Notice that other grouped term is also of the same nature, belonging to the free-electron part of the electronic Hamiltonian. Thus, in principle, V_{xc} does not depend on the specific problem, but in reality, due to its complicated nature, V_{xc} is often parametrized, and although this parametrization is not carried out with a specific material in mind, one must know which approximation works best for the system at hand. Most of the debates density functional theory being an ab-initio method or not arise from this.

There are numerous ways one can approximate the V_{xc}. Possibly the simplest one is to use the local density approximation (LDA). In this approximation exchange and

correlation effects are calculated through a model called the homogeneous electron gas (see Chapter 5 in Ref. [16] for details) . In this model, electron density is assumed to be constant and thus V_{xc} depends only on the electron density at some point. Although crude, this approximation works very well for materials that have slowly varying electron density, including many crystal bulk structures, and it may be extended to include spin (LSDA) . The functional by Perdew & Zunger [17] can be shown as an example. A first order correction is the non-local-density approximations, more widely known as the generalized gradients approximation (GGA). In this approximation the dependence on gradients $\left|\vec{\nabla}\rho\right|, \nabla^2\rho\ldots$ are also included in the V_{xc}. GGA methods are almost always as accurate as LDA in the systems which LDA describe well. In addition GGA methods are able to handle structures in which LDA is known to be problematic, like the those containing more weakly interacting parts, such as hydrogen-bonded sections. However, in some cases, cancellation of errors lead to LDA performing better than GGA. A few examples of GGA functionals are due to Becke [18], Perdew [19], Perdew&Wang [20].

In the beginning of 1990s, a new method for approximating the V_{xc} leading to even more accurate energies and structure made its appearance [21]. This family of methods, called hybrid methods, rely on the adiabatic connection approach [22].

Remember our fictitious and approximated system that gives the same density and same energy as the electronic part of the Hamiltonian

$$\hat{H} = \left[\sum_{i=1}^{N}\left(-\frac{1}{2}\nabla_{\vec{r_i}}^2 + V_{ext}(i) + V_C(i) + V_{xc}(i)\right)\right] \tag{1.52}$$

the most profound approximation here is that we have replaced the many-particle operator E_{xc} with a single particle operator V_{xc}. Lets assume an adiabatic connection in this transition exists via a control parameter λ

$$\hat{H}_\lambda = \left[\sum_{i=1}^{N}\left(-\frac{1}{2}\nabla_{\vec{r_i}}^2 + V_{ext}(i) + V_C(i) + V_\lambda(i)\right) + \lambda\sum_{i\neq j}^{N}V_{ee}(i,j)\right] \tag{1.53}$$

V_{ee} contains E_{xc} directly, whereas V_λ has just the single body terms. Thus, when $\lambda = 0$ the system is fully non-interacting, and when $\lambda = 1$ the system is fully interacting.

V_λ is modeled such that the density and the energy of our model system is always the same as the original electronic Hamiltonian, independent of λ.

Using the Hellman-Feynman theorem [23, 24]

$$\frac{\partial}{\partial \lambda} \langle \Psi_\lambda | \hat{H}_\lambda | \Psi_\lambda \rangle = \langle \Psi_\lambda | \frac{\partial \hat{H}_\lambda}{\partial \lambda} | \Psi_\lambda \rangle \tag{1.54}$$

and

$$f(b) = f(a) + \int_a^b \frac{df}{dx} \, dx \tag{1.55}$$

one obtains

$$
\begin{aligned}
\langle \Psi_1 | \hat{H}_1 | \Psi_1 \rangle &= \langle \Psi_0 | \hat{H}_0 | \Psi_0 \rangle + \int_0^1 \frac{\partial}{\partial \lambda} \langle \Psi_\lambda | \hat{H}_\lambda | \Psi_\lambda \rangle \, d\lambda && (1.56) \\
&= \langle \Psi_0 | \hat{H}_0 | \Psi_0 \rangle + \int_0^1 \langle \Psi_\lambda | \frac{\partial}{\partial \lambda} \hat{H}_\lambda | \Psi_\lambda \rangle \, d\lambda && (1.57) \\
&= \langle \Psi_0 | \hat{H}_0 | \Psi_0 \rangle + \int_0^1 \langle \Psi_\lambda | \hat{V}_{ee} + \frac{\partial}{\partial \lambda} \hat{V}_\lambda | \Psi_\lambda \rangle \, d\lambda && (1.58) \\
&= \langle \Psi_0 | \hat{H}_0 | \Psi_0 \rangle + \int_0^1 \langle \Psi_\lambda | \hat{V}_{ee} | \Psi_\lambda \rangle \, d\lambda && (1.59) \\
&\quad + \int_0^1 \langle \Psi_\lambda | \frac{\partial \hat{V}_\lambda}{\partial \lambda} | \Psi_\lambda \rangle \, d\lambda && (1.60)
\end{aligned}
$$

the $\hat{V}_\lambda$ is tailored to be a one-body operator depending only on the coordinates, thus

$$\int_0^1 \langle \Psi_\lambda | \frac{\partial \hat{V}_\lambda}{\partial \lambda} | \Psi_\lambda \rangle \, d\lambda = \int_0^1 \int \rho(\vec{r}) \frac{\partial V_\lambda(\vec{r})}{\partial \lambda} \, d\vec{r} d\lambda \tag{1.61}$$

remembering our initial requirement that $\rho(\vec{r})$ is independent of λ

$$\int_0^1 \int \rho(\vec{r}) \frac{\partial V_\lambda(\vec{r})}{\partial \lambda} \, d\vec{r} d\lambda = \int \rho(\vec{r}) \int_0^1 \frac{\partial V_\lambda(\vec{r})}{\partial \lambda} \, d\lambda d\vec{r} \tag{1.62}$$

$$= \int \rho(\vec{r}) V_1(\vec{r}) \, d\vec{r} - \int \rho(\vec{r}) V_0(\vec{r}) \, d\vec{r} \tag{1.63}$$

we obtain

$$
\begin{aligned}
\langle \Psi_1 | \hat{H}_1 | \Psi_1 \rangle &= \langle \Psi_0 | \hat{H}_0 | \Psi_0 \rangle + \int_0^1 \langle \Psi_\lambda | \hat{V}_{ee} | \Psi_\lambda \rangle \, d\lambda && (1.64) \\
&\quad + \int \rho(\vec{r}) V_1(\vec{r}) \, d\vec{r} - \int \rho(\vec{r}) V_0(\vec{r}) \, d\vec{r} && (1.65)
\end{aligned}
$$

inserting $\hat{H}_1$ and $\hat{H}_0$ into place and canceling out the relevant terms, we are left with an interesting equality

$$\langle \Psi_1 | \hat{V}_{ee} | \Psi_1 \rangle = \int_0^1 \langle \Psi_\lambda | \hat{V}_{ee} | \Psi_\lambda \rangle \, d\lambda \tag{1.66}$$

this may seem as added complexity, but in reality, it permits fine tuning of the electron-electron interaction approximation. The many–body operator can be split into exchange and correlation parts to be investigated separately

$$\hat{V}_{ee} = \hat{V}_x + \hat{V}_c \tag{1.67}$$

The correlation part is best handled with the usual methods, such as GGA, but the exchange part can be handled in a different manner now. The integral can (crudely) be approximated as

$$\int_0^1 f(x) \, dx \approx a_1.f(1) - a_2.f(0) \tag{1.68}$$

where a_1, a_2 can be treated as fitting parameters. The exchange correlation energy is now

$$E_{xc} = a_1 E_{x;HF} + a_2 E_{x;LSD} + E_{c;LSD} + a_x \Delta E_{x;NLSD} + a_c \Delta E_{c;NLSD} \tag{1.69}$$

where $E_{x,HF}$ is an exchange term calculated through Hartree-Fock equations representing the $\lambda = 1$ case, and $E_{x;LSD}$ is the Local (spin) density approximated exchange energy representing the $\lambda = 0$ case. The correlation term $E_{c;LSD}$ is calculated directly (through LSD), and the Δ terms are the corrections due to non-local parts for the exchange and correlation. An additional constraint is due to normalization requirement in the approximation to the integral

$$a_1 + a_2 = 1 \tag{1.70}$$

thus by a simple transformation $a_1 = a_0 \; a_2 = 1 - a_0$ the number of parameters can be reduced

$$E_{xc} = E_{x;LSD} + a_0 \left[E_{x;HF} - E_{x;LSD} \right] + E_{c;LSD} + a_x \Delta E_{x;NLSD} + a_c \Delta E_{c;NLSD} \tag{1.71}$$

$[E_{x;HF} - E_{x;LSD}]$ is a functional that can be approximated using models. This three parameter expression is due to Becke [21]. In the original paper Becke found

$$a_0 = 0.2 \ \ a_x = 0.72 \ \ a_c = 0.81 \tag{1.72}$$

In the calculations utilizing this approximation, acronym "B3xxx" is used where "xxx" denote the nature of the non-local correction terms. Probably the most popular choice for this correction terms is the GGA of Lee Yang and Parr [25], resulting in the B3LYP hybrid exchange correlation functional.

Although these methods provide a functional describing the potential electrons move on, there exists a problem, the functional depends on the density of electrons, which we are trying to find from this equation itself! The solution to this problem is an iterative procedure called the self consistent field method. With an initial guess on electron density, a potential term is written, which in turn is used to calculate a new density. This goes on until the change in total energy between two consecutive densities is negligible. The method relies on the hermiticity of the Hamiltonian, and can be considered to be crudely resembling the LU decomposition orthoganilaztion scheme when written in matrix form. Thus, for this method to work, a good representation of the orbitals making the Hamiltonian matrix as close to being (n-)diagonal as possible is mandatory.

1.4.3 Representing the orbitals

Computational nature of the problem is inevitable at this point, and this introduces a number of complexities in handling the equations. The biggest problem is due to discretization. The exact computational techniques and problems encountered encountered along the course of transformation will not be detailed here, but it will suffice to say that discretization requires a number of modifications in our equations. Probably the most consequential one is transforming the eigenvalue equation into a matrix equation. In matrix notation, the wave-functions need to be represented in terms of a series

of orthogonal functions.

$$\Psi = \sum_i c_i \psi_i \tag{1.73}$$

as long as they form an complete set, any function can be used in the expansion. One may be tempted to use Slater type orbitals in the expansion, after all only a few of them will be required to form a complete set describing any atomic wave-function, but computationally they are rather hard to work with. Instead, a primitive Gaussian is very much alike in appearance, and it is much easier to handle. There are compromises, since no systematic way exists to prepare a complete orthogonal set from Gaussian functions. In literature, especially in chemistry related works, basis sets composed of primitive Gaussian are extensively used. They require a lot of inspiration and intuition both to prepare and use, and thus there are many branches, each designed with a specific family of materials in mind, but only two branches will be mentioned here, in relevance to this context.

"Minimal basis sets" are composed of linear combinations of Gaussian functions, and they are denoted by the notation STO-nG , where n is the number of primitive Gaussians. After a certain complexity, this kind of basis sets become very unwieldy, thus, calculations utilizing these wave-functions are often limited to be crude.

In a structure, not all the electrons contribute to the bonds, some of them are attached to the nuclei so strongly that, the bonding energy does not alter their configuration significantly. These electrons can be classified as the core electrons, and the corresponding wave-functions need not to be described with as much detail. The interesting part is due to the remaining electrons, or valance electrons. "Split-Valance" basis sets treat core electrons and valance electrons with different complexity. Using the Pople notation, these sets are denoted as $X - Y_1 \ldots Y_n g$ where X is the number of primitive Gaussians describing the core electrons and $Y_1 \ldots Y_n$ give the number of primitive Gaussians used in creating the multiple basis functions describing the valance orbitals

(and n is the number of basis functions). This kind of basis sets can be extended with polarization or diffusion functions, denoted by * or + in the end.

Gaussian is a localized function, thus an orbital defined through Gaussians is also localized. Although very welcome in molecular structures, this becomes rather unwieldy in periodic systems, such as crystals. An alternative to Gaussian function is the plane waves. Basically, the plane wave representation of any arbitrary wave-function is possible, but in practice, since a computer can not deal with an infinite number of plane waves, and high frequency plane waves are problematic to describe when discretized, localized orbitals tend to be a problem. Possibly the biggest advantage of using plane waves is that it provides a systematic way of increasing level of detail in describing the orbital, thus SCF convergence is achievable in a systematic manner for any given system. In Gaussian formalism, if you start with a "non-suitable" basis set, most probably you will end up without a solution for the electronic wave-function in the SCF iteration, and without a systematic method of increasing the level of detail, one is obliged to understand the chemical nature of the system under study before initiating. This is where intuition comes into play.

In describing orbitals through plane-waves, the section of wave-functions in close proximity with the nuclei pose a problem, since they tend to oscillate rapidly, and thus require high frequency plane-waves in their description. Some orbital wave-functions, namely those belonging to the core levels, entirely exist in this localized domain. Similar to split-valance Gaussian orbitals, core and valance electron orbitals can be split without much sacrifice. However this time, in order to avoid high frequency plane-waves, the localized sections of *all* the orbitals need to be truncated. This dictates a further modification to electronic Hamiltonian. A well behaving wave-function can be written as a linear combination of a localized and a non-localized part.

$$\Psi = \phi + \sum_c b_c \psi_c \tag{1.74}$$

where ψ_c denote the localized part. Since Ψ is *not* one of the core wave-functions of the

system

$$\langle \psi_c \,||\, \Psi \rangle = 0 \tag{1.75}$$

and thus

$$
\begin{aligned}
0 &= \langle \psi_c \,||\, \phi \rangle + \sum_{c'} b_{c'} \langle \psi_c \,||\, \psi_{c'} \rangle \tag{1.76} \\
&= \langle \psi_c \,||\, \phi \rangle + b_c \tag{1.77}
\end{aligned}
$$

$$b_c = -\langle \psi_c \,||\, \phi \rangle \tag{1.78}$$

The equation we are trying to solve is

$$\hat{H}_e \Psi = \epsilon \Psi \tag{1.79}$$

ϕ can be taken as a smooth function. In order to eliminate the problematic ψ_c, lets assume that the localized wave-functions are already eigenfunctions of the electronic Hamiltonian. The right hand side becomes

$$
\begin{aligned}
\hat{H}_e \Psi(\vec{r}) &= \hat{H}_e \left[\phi(\vec{r}) + \sum_c b_c \psi_c(\vec{r}) \right] \tag{1.80} \\
&= \hat{H}_e \phi(\vec{r}) + \sum_c b_c \hat{H}_e \psi_c(\vec{r}) \tag{1.81} \\
&= \hat{H}_e \phi(\vec{r}) + \sum_c b_c \epsilon_c \psi_c(\vec{r}) \tag{1.82} \\
&= \hat{H}_e \phi(\vec{r}) - \sum_c \int \psi_c^*(\vec{r}_1) \phi(\vec{r}_1) d\vec{r}_1 \epsilon_c \psi_c(\vec{r}) \tag{1.83}
\end{aligned}
$$

and the left hand side is

$$
\begin{aligned}
\epsilon \Psi(\vec{r}) &= \epsilon \left[\phi(\vec{r}) + \sum_c b_c \psi_c(\vec{r}) \right] \tag{1.84} \\
&= \epsilon \phi(\vec{r}) - \sum_c \int \psi_c^*(\vec{r}_1) \phi(\vec{r}_1) d\vec{r}_1 \epsilon \psi_c(\vec{r}) \tag{1.85}
\end{aligned}
$$

equating both sides we obtain

$$\hat{H}_e \phi(\vec{r}) + \sum_c (\epsilon - \epsilon_c) \int \psi_c^*(\vec{r}_1) \phi(\vec{r}_1) d\vec{r}_1 \psi_c(\vec{r}) = \epsilon \phi(\vec{r}) \tag{1.86}$$

which can be written as

$$\left(\hat{H}_e + \hat{V}_{ps} \right) \phi(\vec{r}) = \epsilon \phi(\vec{r}) \tag{1.87}$$

it is often a good approximation that

$$\hat{V}_{ps} \rightarrow V_{ps}(\vec{r}) \tag{1.88}$$

(i.e. the operator is approximated to be a function). $V_{ps}(\vec{r})$ is called the "pseudo potential" [26], and represents an additional correction to all the previous terms (exchange, correlation etc.) due to replacing the close proximity region with the smoother function $\phi(\vec{r})$. Non local extensions to approximation such as $V_{ps}(\vec{r}, \vec{r}')$ are also possible.

In writing equation 1.87, it is automatically assumed that

$$\int_0^\infty |\phi|^2 \, dr = 1 \tag{1.89}$$

naturally

$$\int_0^\infty |\Psi|^2 \, dr = 1 \tag{1.90}$$

thus

$$\int_0^\infty |\phi|^2 \, dr = \int_0^\infty |\Psi|^2 \, dr = 1 \tag{1.91}$$

the above equation makes sure that the valance density obtained for both the all-electron calculation and the pseudo-potential scheme are the same. This is called the "norm conservation" criteria, and the pseudo-potentials using this restriction are called "norm-conserving" pseudo potentials. It is possible to ease this criteria to obtain much smoother pseudo-potentials [27]. In this scheme the valance density is partitioned into "hard" and "soft" sections.

$$n(r) = \sum_n \left[|\phi_n|^2 + \sum_{ij} Q_{ij} \langle \phi_n \, || \, \beta_j \rangle \langle \beta_i \, || \, \phi_n \rangle \right] \tag{1.92}$$

where β_i are projector functions depending on the ionic positions. Q_{ij} is called the augmentation function

$$Q_{ij} = \psi_i^* \psi_j - \phi_i^* \phi_j \tag{1.93}$$

24

in which ψ_i are the all electron wave-functions and ϕ_j are pseudo wave-functions that do not conserve norm at all. By modeling β_i, minding the orthogonalization

$$\left\langle \phi_i \left| 1 + \sum_{ij} \int Q_{ij}(\vec{r})d\vec{r} |\beta_i\rangle \langle\beta_j| \right| \phi_j \right\rangle = 1 \qquad (1.94)$$

pseudo potentials that require significantly lower cutoff in describing the system without noticeable compromise can be obtained. However, due to additional parametrization through the β_i makes generalization of these pseudo-potentials difficult.

When using a pseudo-potential, one must be aware that the definition is not unique, and always more than one solution exists for the system at hand. There are many parameters, including the decision where core levels start, that determine the capability of a particular wave-function describing structure at hand. Combined with the other parameters buried in, for example, exchange and correlation functions, DFT is hardly a black box where only turning the crank is required. Careful pre-modeling and keeping track of the effects due to numerous parameters is mandatory.

1.5 The possibility of a classical treatment to the problem of structural mechanics.

Atoms and molecules are strictly quantum objects. Being of this nature, there are numerous phenomena related not explainable using the formalisms of classical physics. However, in the essence, we have seen that a semi-classical equation of motion can be derived. In this respect, is it possible to continue the approximations and derive a simple model for the equations of motion for the nuclei in a complicated quantum problem?

The answer is yes, as long as you are willing to sacrifice (a lot of) generality and information. If the desired information is structural properties, this action can be justified. Apart from means of just simplifying, the electron integrals may be avoided completely using empirical data. The idea follows from the old notion of "normal" arrangement of atoms. Using a more mathematical sense, the idea can be summarized as

the tendency to minimize configuration energy. An abstract mathematical entity called the potential surface is introduced, and using "normal" arrangements, it is parametrized. This potential energy function is directly related to the enthalpy of the molecule due to its nature, but it is not exactly enthalpy, since thermal motion and temperature dependent contributions are absent. For the definition of this potential surface, the old idea of stick bonds between atoms can be used. When the bonds are modeled as elastic, springy sticks, and mechanical properties such as stiffness, torsion resistance etc. are assigned, the parametrization completely replaces the electron integrals. Since the electron integrals are no longer involved, the point particles previously treated as nuclei can now be renamed as atoms. Adding atom type information to these point particles is a necessity due to the problem of assigning correct parameters for the bonds. This type of approach is called molecular mechanics method. The basic ideas behind the procedure can be traced back to a paper of D. H. Andrews in 1930, but the real utilization does not start until 1946 due to advancements in computer technology. In its most basic form, the potential surface in molecular mechanics method consists of these separate sums (see Figure 1.3 for graphical representation):

$$V = \sum V_{stretch} + \sum V_{bend} + \sum V_{torsion} + \sum V_{\text{non-bonded}} \qquad (1.95)$$
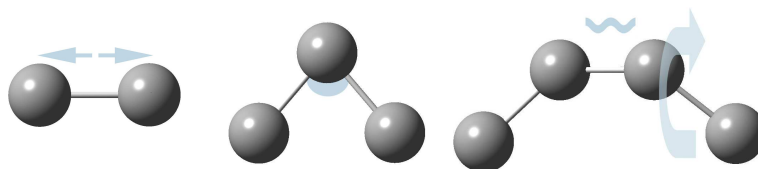
Figure 1.3: Stretch, bend and torsion using ball&stick representation of atoms. non-bonded interaction is not shown, as it is omnidirectional without bond requirement.

Each sum covers all the bonds in the structure, and depending on the nature, sometimes the spatial orientation of more than two atoms are used. The count of individual atoms contributing to the interaction term is referred as the order of the equation. Non-bonded atoms interaction term is a special case in this matter, due to its omnidirectional and seamless nature. Additional terms may be added, in order to account for special behavior. The most common examples for these additional terms are the hydrogen bond and electrostatic interaction.

There are numerous parameter sets for molecular mechanics, and each set has its own application domain. In order to name a few frequently used, there are MM+ [28, 29] , AMBER [30, 31, 32] , BIO+ [33, 34] and OPLS [35, 36] parameter sets . MM+ is a large parameter set, but it works best for thermodynamical and structural properties of small non-polar molecules. The unique feature of the MM+ force field separating it from the others listed is in the way it treats bonds and angles. In the corresponding bond and angle interaction terms, MM+ utilize a functional with different order along with the standard quadratic. MM+ also contains a stretch-bend cross term, called a Urey-Bradley term. A Urey-Bradley term includes 1-3 interactions, which are critical for accurately simulating molecules. For example, the bond angles for heavy atoms in cyclo butane are compressed, compared to the natural bond angle for C sp^3 orbitals, and the carbon-carbon bonds have higher p character. This results in a weaker bond and an increased carbon-carbon bond length. A Urey-Bradley term allows for these structural changes and recognizes the unique 1-3 interactions which occur in strained molecules. AMBER and OPLS are parameterized for certain proteins and some crystals. BIO+, which is based on CHARMM, on the other hand, focuses on certain macromolecules and ignores lone pairs. In this latter parameter sets, point charges are utilized in calculating electrostatic forces, whereas MM+ uses bond dipoles, resulting in the unreliability in charged and/or polar systems. MM+ is the most popular force field in our context.

The molecular mechanics method works best when the particular parameter set used

is not too deviant from the configuration it is parameterized for. One drawback (and sometimes the advantage) of the molecular mechanics method in general is that the bond configuration for each particle is to be input beforehand and this may not be always preferable. The correct parameterization requires more than atom type information. For example, as stated earlier, the behavior of carbon is very different in their various hybrid forms. In some cases, in order to make the force field utilise the correct parameter set, the nature of the bonds must also be input along with the always required connectivity information, and in the end, this pretty much dictates a particular geometry preventing another occurence. Additional methods for re-configuring bonds with each motion on the fly can be devised, but in this formalism, the re-configuration criteria introduces much unwelcome discontinuities, and it is not always reliable.

The best use for molecular mechanics is the calculation of vibrational spectra of known/given molecules and the geometry optimization procedure. In geometry optimization, pre-given bond configuration dictate the resultant geometry, making it quite useful for obtaining an initial structural geometry for molecules. A discussion on how to locate the minimum in a multidimensional energy surface (created by the molecular mechanics force field in our case) can be found in ref. [37].

Instead of modeling bonds as rigid entities of their own, a geometrical expansion for the abstract potential can be employed. The main advantage in doing so is that now the system is capable of seamless geometric reconfiguration. The necessity for pre-entering bond configuration is now lifted, as the potential energy function now only uses the spatial coordinates of atoms. An energy is assigned for each preferred geometrical configuration, along with some transition parameters, and the mathematical form of the potential energy function guarantees a smooth behavior for all geometries. Although there is a slight increase in computation time, system behavior is now somewhat more realistic for the problem at hand. This geometrical expansion procedure will be called as potential energy function method, or PEF method in short, hereafter in this chapter.

The PEF method has a better applicability for Molecular Dynamics calculations. Being an analytical function, the most distinctive property in an empirical potential energy function is its mathematical form. One has to formulate one such that it can incorporate a majority of experimental geometrical configurations, for the sake of wider applicability, while considering the mathematical complexity and the smooth behavior. In terms of mathematics, the continuity and smoothness for the PEF is guaranteed if one can expand it using a series of well behaved functions like:

$$E_p = \phi_2 + \phi_3 + \phi_4 + \dots \tag{1.96}$$

where ϕ_n is the n-body interaction term. These "interaction" terms are mathematical functions that translate a particular geometry to energy. Each interaction term spans all the atoms in the structure, the number of bodies involved for a particular interaction term dictate the geometrical configurations it can be used to explain. For example, two body interaction term ϕ_2 may only parameterize inter-atomic distances, whereas, three body interaction term ϕ_3 add "angles" to the mix. Each of these interaction terms must be smooth and well behaving within itself. Wider applicability demands an expansion with more interaction terms, while complexity problem demands less. It is assumed that the series is rapidly converging, and interaction terms higher than four are almost never used[5].

In order to calculate the force, the required quantity is the gradient of the PEF. Depending on the type of the problem, one must choose a functional describing the behavior of the system adequately. The PEFs are grouped according to this form; in this text, the following grouping is employed:

$$\Phi_I \quad = \quad \phi_2 \tag{1.97}$$

$$\Phi_{II} \quad = \quad \phi_2 + \phi_3 \tag{1.98}$$

$$\Phi_{III} \quad = \quad \phi_2 + \phi_3 + \phi_4 \tag{1.99}$$

---

[5]Nearly all the features of complex geometries are covered after order four.

for example, a group one potential Lennard-Jones PEF has a functional form:

$$\Phi = \phi_2 = \sum_{i<j} U_{ij} \tag{1.100}$$

$$U_{ij} = 4\epsilon \left[\left(\frac{\sigma}{r_{ij}} \right)^{12} - \left(\frac{\sigma}{r_{ij}} \right)^{6} \right] \tag{1.101}$$

The applicability of this group of potentials is severely limited to situations where spherical symmetry allows non directional interaction (such as Van der Waals interaction) or where only one geometry is permissible due to particular property of the element (Metallic crystals). In the presence of covalent bonds, necessity for higher order interaction terms is obvious. For a detailed discussion on many PEFs, please refer to Refs. [4, 5].

Interaction of carbon atoms is rather well studied in the last two decades, resulting in very well parameterized potential energy functions. There are two widely used PEFs in the matter. One of the most suitable in our case is the Tersoff PEF [38, 39]. Although formulated for Silicon at first, later revisions cover Carbon atom in various hybrid forms. In Tersoff PEF, the total interaction energy of a system of particles is taken to be the sum of total two–body and total three–body contributions

$$\Phi = \phi_2 + \phi_3 \tag{1.102}$$

This is a group II potential. Total two–body and three–body energies are expressed, respectively, as

$$\phi_2 \;=\; A \sum_{i<j}^{N} U_{ij}^{(1)} \tag{1.103}$$

$$\phi_3 \;=\; -B \sum_{i<j}^{N} U_{ij}^{(2)} \left[1 + \beta^n \left(\sum_{k \neq i,j}^{N} W_{ijk} \right)^{n} \right]^{-1/2n} \tag{1.104}$$

here U_{ij} and W_{ijk} represent the two–body and three–body interactions, respectively.

$$U_{ij}^{(1)} \;=\; f_c(r_{ij}) \exp(-\lambda_1 r_{ij}) \tag{1.105}$$

$$U_{ij}^{(2)} \;=\; f_c(r_{ij}) \exp(-\lambda_2 r_{ij}) \tag{1.106}$$

$$W_{ijk} \;=\; f_c(r_{ik}) g(\theta_{ijk}) \tag{1.107}$$

where

$$g(\theta_{ijk}) = 1 + \frac{c^2}{d^2} - \frac{c^2}{d^2 + (h - \cos\theta_{ijk})^2} \tag{1.108}$$

(this part handles angle to energy parameterization)

$$f_c(r) = \begin{cases} 1 & \text{for} \quad r < R - D \\ \frac{1}{2} - \frac{1}{2}\sin[\frac{\pi}{2}(r - R)/D] & \text{for} \quad R - D < r < R + D \\ 0 & \text{for} \quad r > R + D \end{cases} \tag{1.109}$$

(and this part is a cutoff function which satisfies smoothness and continuity criteria). In effect, U_{ij} and W_{ijk} convert the geometrical information to energy via a set of parameters.

The Brenner potential has a similar functional form

$$\Phi = \phi_2 + \phi_3 \tag{1.110}$$

This is also a group II potential. Total two–body and three–body energies are expressed, respectively, as [40]

$$\phi_2 = \sum_{i<j}^{N} U_{ij} \tag{1.111}$$

$$\phi_3 = \sum_{i<j,k}^{N} W_{ij,k} \tag{1.112}$$

here again U_{ij} and $W_{ij,k}$ represent the two–body and three–body interactions, respectively.

$$U_{ij} = f_c(r_{ij})V_R(r_{ij}) \tag{1.113}$$

$$W_{ij,k} = f_c(r_{ij})V_A(r_{ij})b_{ij,k} \tag{1.114}$$

the cutoff function $f_c(r_{ij})$ is exactly the same of Tersoff PEF

$$V_R(r_{ij}) = \frac{D_e}{S - 1}e^{-\beta\sqrt{2S}(r_{ij}-r_e)} \tag{1.115}$$

$$V_A(r_{ij}) = -\frac{SD_e}{S - 1}e^{-\beta\sqrt{2/S}(r_{ij}-r_e)} \tag{1.116}$$

$$b_{ij,k} = (1 + z_{ij,k})^{-n} \tag{1.117}$$

$$z_{ij,k} = \sum_{k \neq i,j} f_c(r_{ik}) g(\theta_{ijk}) e^{m(r_{ij} - r_{ik})} \tag{1.118}$$

three body contribution comes from[6]

$$g(\theta) = \alpha \left\{ 1 + \frac{c^2}{d^2} - \frac{c^2}{d^2 + (h + \cos \theta_{ijk})^2} \right\} \tag{1.119}$$

In its later modified form, Tersoff and Brenerr PEFs are almost equivalent in behavior, with Brenner potential having an increased interaction range whereas Tersoff PEF having a simpler mathematical form. Tersoff utilizes bulk data extensively in parameterizing the PEF, whereas Brenner uses molecular data. Consequently, in their original forms, they do have some significant intrinsic differences. The major difference is the bond-order terms in Brenner PEF, solving some problems in Tersoff PEF, but, due to some torsion related misbehavior, it is often neglected in nanostructure related calculations. Further improved PEFs are available in the literature, but their necessity for the problem at hand can be debated, especially for larger structures.

The major drawback in PEF method is in its inaccuracy in vibrational spectra. The parameterization and functional form is focused on the geometric reconfiguration, but the vibrational spectra is better modeled with the expansion used in molecular mechanics.

If one is not satisfied by a pure empirical treatment, and require more information, then electron integrals must also be put into action. Due to expensive nature of these integrals, the size of structures that can be investigated will be severely limited making this procedure a good practice only if one can not find/formulate a good enough empirical many body potential. Otherwise it is always possible to perform electronic calculations on the obtained final structure.

As it can be seen, although the equations involved are greatly simplified in the previous section, we still need a second level of assumptions and approximations, choosing

---

[6]Notice that this is also the same as Tersoff one, the sign change is due to parameterization.

Table 1.1: The empirical parameters of the Tersoff PEF for carbon [39]:

Parameter	Value
A	1393.6 eV
B	346.74 eV
λ_1	3.4879 Å^{-1}
λ_2	2.2119 Å^{-1}
β	1.5724×10^{-7}
n	0.72751
c	38049
d	4.3484
h	-0.57058
R	1.95 Å
D	0.15 Å

Table 1.2: The empirical parameters of the Brenner PEF [40]:

Parameter	Value
D_e	6.325 eV
r_e	1.28 Å
β	1.5 Å^{-1}
S	1.29 Å^{-1}
n	0.8047
α	0.0113
c	19.0
d	2.5
h	1.0
m	2.25 Å^{-1}
R	2.1 Å
D	0.2 Å

one according to the problem. In summary, Electron integrals are expensive. They can be simplified by inclusion of empirical data accompanied by the loss of generality, or basis set formalism can be used, compromising the accuracy. The results are accurate up to a predetermined level, however, the procedure still is not trivial. If a suitable set of parameters exist, one can use Molecular mechanics or PEF methods, but the accuracy of the outcome solely depends on the correct parameterization, which is problem specific at least. Molecular mechanics permit a wider range of application by its nature, and it is more accurate in vibrational spectra but generally PEF methods are more realistic in geometric reconfiguration.

1.6 Statistical Mechanics at the scale of few atoms

Having established the equations of motion for the system in last two sections, we now have a physical model describing the motion of atoms within a structure. But this model by itself is not capable of providing information we are looking for. What we are looking for is the measurable structural properties of the system and this requires statistical mechanics intervention.

Thermodynamics does not concern itself with the intrinsics of the system such as atoms and molecules, they are certain to be intangibly complex for a macroscopic body, and the topic itself precedes atomic and molecular theories. Instead, the observables of the system are interlinked via the use of a set of postulates such that one can estimate one by measuring others in a given environment. Statistical mechanics, on the other hand, focuses on the derivation of these observables from the first principles. The combination of statistics and mechanics (classical and quantum) at the microscopic level leads to thermodynamics itself, meaning the spectroscopic data of individual molecules can lead to observables at the bulk scale. But, similar to everything involving statistics, the system needs to be defined carefully, and restrictions must be put in place. A most obvious first necessity is that the number of available states for this systems must be vast, so what is the state of our system?

The force field obtained in the previous chapter permit us to formulate the energetics of a system for a given spatial configuration $\mathbf{x}$. Lets call this energy function $H(\mathbf{x})$, where, in our case, H no longer stands for the true Hamiltonian of the structure, but instead the classical one obtained from equations of motion. The $\mathbf{x}$ designate the particular geometrical configuration system is in. For a given structure, even with limited number of atoms contained within, the number of geometrical configurations with essentially the same energy is enormous, and due to all of them being in the same energy, they are all available. So, if we label these individual configurations as the state, and the ensemble of geometric configurations as the system, due to vastness of available

states, we are in the realm of statistical mechanics.

In our case, an ensemble of such configurations is not completely independent, since, the necessity dictate that it should prepared in a manner that it contains configurations "resembling[7]" the system of question. This way, we can be sure that the calculated observable is for the structure at hand, but not for a random geometry with same number of atoms.

As previously mentioned, statistical predictions require restrictions on the configuration space. These restrictions are named in terms of postulates utilized in obtaining observables:

- The micro–canonical ensemble: The constants of the configurations are the number of particles (N), the volume (V) and the internal energy(E). An alternative nomenclature is (NVE) ensemble.

- The canonical ensemble: (N), (V) and temperature (T) of the ensemble is constant. Alternative nomenclature is (NVT) ensemble.

- The isothermal–isobaric ensemble: Pressure (P), (T), and (N) are constants. Hence it may be called (NPT) ensemble.

- The grand canonical ensemble: (N) may vary to achieve constant chemical potential μ but the (V) and (T) are constants. So the other name is (μVT) ensemble.

In order to carry on, we need to define the ensemble we are working in. There is not much freedom of choice within our context, the goal is clear, we are trying to obtain observables for an isolated interacting set of atoms in a heat bath. Being isolated, there is no atom leaving or entering the system, thus the number of particles (N) is constant, and we have to be controlling the ambient temperature to observe its effects (constant T). The foundation principle of molecular thermodynamics clearly state that micro-canonical ensemble should be used for isolated molecules, but it is already eliminated.

---

[7]i.e. they have similar geometrical configurations, same kind of atoms etc.

The point of debate lies within the definition of heat bath. In macroscopic dimensions, the nature of the heat bath is almost always not a point of concern, but in molecular size, nearly all the heat transfer mechanisms has a huge and discontinuous impact on the system. At this point, one may choose to include the elements of heat bath into structure for more realistic representation, or take the heath bath concept to a more abstract level for focusing on the properties of system only. We will proceed with the second, due to special properties of the carbon nanostructures. This way, the contact with heat bath becomes a conceptual one, avoiding alteration of structure and the complications related.

At this point, a choice has to be made: Either the pressure or the volume of the container should remain constant. Although many constant pressure scenarios can be devised that can be used for similar purposes (i.e. [41]), a constant volume environment is somewhat more suited in our case, especially due to the nature of the heath bath. Thus, canonical ensemble will be assumed for the rest of this text, if not otherwise mentioned.

In systems having statistical nature, measurable physical quantities, namely the observables, appear as averages over some space of configurations.

$$\langle A \rangle = Z^{-1} \int A(\mathbf{x}).f(H(\mathbf{x})) \mathrm{d}\mathbf{x} \qquad (1.120)$$

$$Z = \int f(H(\mathbf{x})) \, \mathrm{d}\mathbf{x} \qquad (1.121)$$

$\langle A \rangle$ is called the ensemble average of the system. First problem in a calculation arises from the definition of this integral. In a computation for an observable, say the temperature, one can consider a large number of "resembling" configurations, or propagate system through a trajectory in phase space and evaluate kinetic energy along the path instead. First choice leads to famous Monte Carlo algorithms, whereas the latter leads to molecular dynamics, which will be emphasized within this context due to its ability of describing dynamics of the system. Using a trajectory along the phase

space instead of ensemble averaging is called the time average and in integral form it can be represented as:

$$\bar{A}_t = (t - t_0)^{-1} \int_{t_0}^{t} A(\mathbf{x}(\tau)\mathrm{d}\tau \tag{1.122}$$

and via the ergodicity theorem

$$\langle A \rangle = \bar{A}_\infty \tag{1.123}$$

but yet again, observation time can not possibly be infinite as it requires an infinite calculation time, so we must be content with something like

$$\langle A \rangle \approx \bar{A}_t \tag{1.124}$$

after all, the system should reach an equilibrium after a sufficient amount of time, and apart from fluctuations, major deviations in energy become highly improbable in equilibrium. A system in such a condition is called a relaxed system.

At this point one may argue that assumed weak interaction when calculating the energy of the system is not valid for our case, and instead of above, one has to use something like

$$f \rightarrow f(H_1(\mathbf{x}), H_2(\mathbf{x}), \ldots) \tag{1.125}$$

$$Z \rightarrow \int_1 \int_2 \ldots f(H_1(\mathbf{x}), H_2(\mathbf{x}), \ldots)\mathrm{d}\mathbf{x} \tag{1.126}$$

where each "atom" is treated separately according to its surroundings. But the sheer complexity of this integral is on the level of electron integrals if not more, and it is clear that it must be avoided. The trick is to use the continuity and well behavior of potential function. These two properties guarantee that for a small enough time interval, interaction potential can be considered constant, thus the above partition function is valid. Since in this context we will be employing discrete integration methods that utilize geometrical interpretation of integration, small time intervals is already a necessity. The overall error is negligible in the relaxed structure. The choice of "small enough" time interval depends on the nature of the system and the method of integration employed, thus it may be considered as a parameter itself.

Apart from finite observation time, there are also some finite size effects on the system. Although number of states for a given energy is vast, it is not infinite as it should be, and this introduces some major fluctuations. In order to cope with the problem, special boundary conditions are imposed, which will be discussed in the next chapter. This seemingly disadvantage can be utilized in a number of ways, though. For example specific heat of the system

$$C_V = -\frac{\partial}{\partial T}\left(T^2 \frac{\partial (F/T)}{\partial T}\right)_V \tag{1.127}$$

can be approximated from the fluctuations in temperature.

$$\delta(T) = \frac{\langle T \rangle^2 - \langle T^2 \rangle}{\langle T \rangle^2} = 1 - \frac{\langle T^2 \rangle}{\langle T \rangle^2} \tag{1.128}$$

$$\frac{\langle T^2 \rangle}{\langle T \rangle^2} = \frac{\left\langle T \frac{\partial E}{\partial T}\frac{\partial T}{\partial S}\right\rangle}{\langle T \rangle^2} = \frac{3}{2}NK_B \frac{\langle T \rangle}{\langle T \rangle}\frac{1}{\left\langle T\frac{\partial S}{\partial T}\right\rangle} = \frac{3}{2}NK_B \frac{1}{\langle C_v \rangle} \tag{1.129}$$

$$\frac{\langle T \rangle^2 - \langle T^2 \rangle}{\langle T \rangle^2} = \left(1 - \frac{3K_B N}{2C_v}\right) \tag{1.130}$$

(where an ideal gas of non-interacting point particles are considered) and thus difficult free energy calculation may be avoided. Notice that for an ideal canonical ensemble where temperature fluctuation is zero, above equation reduces to

$$C_v = \frac{3}{2}NK_B \tag{1.131}$$

which is the heat capacity due to translational motion in an ideal gas. The level of detail can be increased according to needs, for example using Debye approximation, and a more realistic definiton of equation of states.

The temperature argument is enforced as a velocity distribution to the system. Thus, what we need now is a suitable one. Using the fundamental law of thermodynamics

$$dE = -PdV + \mu dN + TdS \tag{1.132}$$

the principle of equal weight, and the definition of canonical ensemble where N, V and T are constants, the partition function and thermodynamic function for this ensemble

can be obtained as

$$Z(N, V, T) = \int_0^\infty e^{-E/K_B T} \Omega(E, V, N) dE \qquad (1.133)$$

$$F(N, V, T) = -K_B T \log Z(N, V, T) \qquad (1.134)$$

where Ω is the density of states of the system.

These two equations may be utilized for obtaining various bits of information on observables of the system. But, as of now, what we are interested in is the inclusion of temperature parameter to the equations of motion obtained in the previous section.

The heat of a system is interrelated with the internal kinetic energy. Thus, if we can find a distribution function suitable for our case, we can assign corresponding velocities to achieve a specific temperature. In order to do this, we need to know the particular distribution of momentum for a system in a given temperature. Without going in to further details, the three dimensional density of states in momentum space for a given translational momentum interval in the non-relativistic limit is simply [8]

$$f(p)dp = \frac{V 4\pi p^2 dp}{h^3} \qquad (1.135)$$

using this, the partition function for translational momentum becomes

$$Z_1^{tr} = \int_0^\infty \frac{V 4\pi p^2 dp}{h^3} \exp(-\beta p^2/2m) \qquad (1.136)$$

the integral is a common one with result

$$Z_1^{tr} = V \left(\frac{2\pi m K_B T}{h^2} \right)^{3/2} \qquad (1.137)$$

since the energy corresponding to a particular translational momentum state is

$$\epsilon = \frac{1}{2m} p^2 \qquad (1.138)$$

and the number of molecules with this state is

$$\bar{n} = N \frac{1}{Z_1^{tr}} \exp(-\beta \epsilon) \qquad (1.139)$$

we obtain a distribution of the form

$$\bar{n}(p) = \frac{N}{V}\left(\frac{2\pi m K_B T}{h^2}\right)^{-3/2}\exp(-p^2/2mK_BT) \qquad (1.140)$$

if the p is replaced by mv, we obtain the desired probability distribution for the speed

$$\mathbf{P}(v)dv = 4\pi v^2 dv \left(\frac{2\pi m K_B T}{h^2}\right)^{-3/2}\exp(-mv^2/2K_BT) \qquad (1.141)$$

This is called the Maxwell speed distribution. Using this speed distribution for the each Cartesian component, one obtains a spherically symmetric velocity distribution called the Maxwell velocity distribution. Before carrying on, some details on this distribution are worth mentioning. The most probable speed for this distribution, v_m, can be calculated from $\frac{d\mathbf{P}}{dv} = 0$, which gives:

$$\left(-\left(\mathrm{k}_B T\right)^{-1}mve^{-\left(\mathrm{k}_B T\right)^{-1}(mv^2/2)}\right)v^2 + e^{-\left(\mathrm{k}_B T\right)^{-1}(mv^2/2)}(2v) = 0 \qquad (1.142)$$

from this equality one obtains:

$$v_m = \sqrt{\frac{2\mathrm{k}_B T}{m}} \qquad (1.143)$$

average or arithmetic mean of the distribution is

$$\bar{v} = \frac{1}{N}\sum v\mathbf{P}(v) \qquad (1.144)$$

$$= \frac{4}{\sqrt{\pi}v_m^3}\int_0^\infty v^3 e^{-v^2/v_m^2}dv = \frac{2}{\sqrt{pi}}v_m \qquad (1.145)$$

the root–mean–square of the distribution is

$$v_{\mathrm{rms}} = \sqrt{\bar{v^2}} = \left(\frac{4}{\sqrt{\pi}v_m^3}\int_0^\infty v^4 e^{-v^2/v_m^2}dv\right) \qquad (1.146)$$

$$= \frac{3}{2}v_m \qquad (1.147)$$

summary of this distribution is given in Table 1.3.

The distribution serves as an initial step for assigning velocities to the molecules, if enforced exclusively it will break the equations of motion. However, in order to enforce canonical ensemble, a control over the temperature is required. This is done by introducing a constraint function.

Table 1.3: Maxwell distribution of speeds.

name	value
Distribution function	$4\pi n \left(\dfrac{(\mathrm{k}_B T)^{-1} m}{2\pi} \right)^{3/2} e^{-(\mathrm{k}_B T)^{-1}(mv^2/2)} v^2 dv$
Most Probable speed	$v_m = \sqrt{\dfrac{2\mathrm{k}_B T}{m}}$
Arithmetic mean of the speed	$\bar{v} = \sqrt{\dfrac{2.55\mathrm{k}_B T}{m}}$
Root–mean–square of the speed	$v_{rms} = \sqrt{\dfrac{3\mathrm{k}_B T}{m}}$

The constraint may be a nonholonomic constraint on the velocity like (iso kinetic MD)

$$A = \frac{1}{2} \sum_i m v_i^2 = \text{const.} \tag{1.148}$$

or one may introduce a vanishing proportionality constant depending on the temperature of the system at specific time (Gaussian iso kinetic MD)

$$\frac{1}{2} \sum_i m v_i^2 = \alpha t \tag{1.149}$$

Velocity restraint is a more straightforward method. At predetermined time intervals, a velocity rescaling factor is used to keep temperature at a constant level. The timing is somewhat critical, if it is too tight, correct energetics of the system is disturbed, if it is too relaxed, the ensemble can no longer be considered as canonical. This is yet another control parameter depending on the system. Lets see how we can obtain such a restraint. In a thermodynamical system the velocities and the temperatures should be interrelated as:

$$\text{Total Kinetic Energy} = \frac{\text{Degrees of Freedom}}{2} \times \mathrm{K}_B \times T \tag{1.150}$$

using this definition, one can easily come up with a rescaling factor for velocities as:

$$\alpha = \left[(3N) \,\mathrm{k}_B T_{\text{ref}} / \sum_i m v_i^2 \right]^{1/2} \tag{1.151}$$

In this formula N is the number of moving particles. Notice that there are $(3N - 4)$ degrees of freedom due to constraints imposed on total linear momentum and total

kinetic energy but keeping in mind that N is often very large, and constraints imposed are flexible, it is a common practice to just use (3N) instead. T_{ref} or T_r in short stands for the reference temperature of the system. The actual temperature of the system may be different than T_r due to previously mentioned reasons.

1.6.1 Boundary conditions

As mentioned a few times before, our ability to use statistical mechanics lies in the identification of the system, so that the appropriate postulate may be chosen. The knowledge on structure supply some of the information, and we now have a control on temperature, but there is something missing: the vicinity of the molecule. In terms of mathematics, one needs to define an enclosed space, even if it is of infinite volume, in order to proceed. The boundary of this volume provides the missing piece of information, ultimately defining the postulate.

There is no restriction on the shape or size of this volume, as long as it is bigger than the system at hand. But there are some special considerations. One such special consideration is the periodic boundary condition. This condition defines an enclosed space such that when an atom leaves a boundary it re–enters through the opposite one. Thus it is a necessity that the geometrical shape of the volume should be able to cover all the space without gaps. Perhaps the most trivial, if not most common, such geometry is a rectangular box (or a rectangle in 2D). An obvious feature is that one does not need to transform heading vector of the re–entering particle if Cartesian coordinates are used, and the "opposite" boundary is simply the face parallel to the original one. The periodic boundary fixes the number of particles within the volume, without introducing hard walls, thus the impact on the structure itself is minimal.

At this point, it must be re-mentioned that, in this context we are not interested in the exact mechanism of how the pressure, temperature or any other parameter is maintained within the container, as long as it does not disturb the mechanics of the

system (i.e. the molecular Hamiltonian) significantly, in the same sense thermodynamics is not interested in the intrinsics of bulk matter. This does not mean that this is always the case. In some structures, especially in those that can only exist in solvents, the environment does play an important role in structural mechanics. There exists solvent models for the purpose of explaining such interactions. But majority of Carbon (only) structures may exist in vacuum, and they are inert enough to carry on with the above axiom.

1.6.2   Computational Methods

The ensemble average and the time average presented in the previous section are equivalent in the sense that they both lead to same physical observables. However, there is a big intrinsic difference between them: the time. In general, a propagation, that is, a physical relevance between the consequent members, is not a requirement in an ensemble average. On the other hand, time average is a propagation in phase space by definition. This intrinsic difference results in a branching of calculation methods. There are many different methods in both branches, each unique in its own way. One common thing in all of them is the requirement of computers due to vast number of calculations. In this chapter we will focus on the related computational details. Although each method has its own appeal, remembering our goal, only molecular dynamics method using a canonical ensemble will be presented in detail, along with a brief introduction to Monte–Carlo method, for comparison purposes.

In the realm of computers, the symbolic equations encountered before need to be re-described in a numerical manner, and there are many alternatives for doing so. It will turn out that, in the end, this is a choice between precision and computer time. Lets begin with the canonical Monte Carlo algorithm.

Monte Carlo (MC) and its derivatives rely on ensemble averaging for the observables, therfore there is no propagation in time. The main goal is to find the most

suitable configuration in a given environment, such that its probability of occurrence is significantly higher than the others. Since it is impossible and unsuitable to achieve this by investigating an infinite set of random geometries, a mechanism for selecting more favorable and resemblant is required. Generally, the mechanism involves the deformation of initial geometry in some manner, followed by a decision to keep newly obtained geometry. Although a better configuration in each step (or after a number of steps) is not guaranteed, in the long run the goal should be reached. The exact intrinsics of the deformation and decision mechanisms ultimately define the method at hand, for example in MC, both these mechanisms rely on random numbers, whereas in a genetic algorithm there are other considerations. The major steps a canonical MC are given below:

1. Specify an initial configuration

2. Generate a new configuration x'.

3. Compute the energy change $\Delta\mathcal{H}$.

4. If $\Delta\mathcal{H} < 0$, accept the new configuration and return to step 2

5. Compute $\exp\left(-\Delta\mathcal{H}/\mathrm{k_B T}\right)$.

6. Generate a uniform random number $R \in [0, 1]$.

7. If $\exp\left(-\Delta\mathcal{H}/\mathrm{k_B T}\right)$ is less than R do not apply the change and goto 2

8. Otherwise, apply the changes and goto 2

Algorithm 1: Canonical MC

Notice the propagation in this algorithm, not in phase space but in configuration space. Without the implicit restrictions of such propagation, one will not be examining the structure of interest at all, since there always exists some irrelevant configuration of atoms with finite or better probability of occurrence. Overall, this restricts the ensemble

44

to a collection of "resembling structures". Since such a collection is also huge, this does not break statistical assumptions. When a particular geometry does not change significantly for a significant amount of steps through this propagation, the system is considered to be converged. The PEF is directly involved in the calculation through the Hamiltonian, and numerical calculations involved are pretty straightforward.

Being a stochastic method, MC has its advantages and disadvantages. The algorithm is cheap computer-wise, thus it is very fast and scalable. Furthermore, the motion of atoms are not calculated, and temperature is included through the selection mechanism without effecting the internal energetics of the structure. On the other hand, the method cannot be used for observations of dynamics (which is enough reason for not going into detail in this context), along with the restrictions on the use in non–equilibrium systems. The convergence may take a long time, if the system converges at all[8]. In fact all the derivations of this method try to improve the convergence.

Molecular Dynamics (MD . Instead of a propagation in configuration space, the system is propagated through the phase space, which requires previously introduced equations of motion. This results in a fast convergence rate, since the structure propagates according to its own internal dynamics, and these dynamics of the system can be observed through the process.

The energy of a particular phase space state of the structure is defined through the Hamiltonian

$$\mathcal{H} = \frac{1}{2}\sum_i \frac{1}{m}p_i^2 + \sum_{i \neq j \neq k} \Phi(\vec{r}_{i,j,k}) \tag{1.152}$$

where Φ is the interaction potential. The phase space state is the spatial orientations of the molecules ($\vec{r}_{i,j,k} = \vec{r}_{ij}, \vec{r}_{ik}, \vec{r}_{jk}$) and the momentum ($\vec{p}_i$). We know that momentum in our phase space is not completely independent, due to restrictions on temperature and the interaction potential. Thus, there exists a perpetual propagation mechanism for this system: The spatial coordinates result in a field through interaction potential

---

[8]Classical MC does not guarantee this convergence

giving momentum to atoms, which in turn result in a new set of spatial coordinates. The gears can be started by supplying a set of initial momenta, which is easily done by the use of Maxwell velocity distribution. Some may have considerations on the use of this distribution in a highly interacting system, but in effect, the distribution is active only for an infinitesmall amount of time after which the dynamics of the system take over immediately. After this, rescaling the velocities in order to maintain temperature once in a while will be sufficient. Lets start by the classical solution introduced beforehand:

$$\frac{\mathrm{d}^2 r_i(t)}{\mathrm{d}t^2} = \frac{1}{m} \sum_i F_i \tag{1.153}$$

$$F_i = -\nabla \sum_{j \neq k} \Phi(\vec{r}_{i,j,k}) \tag{1.154}$$

these are simple equations. However, in computational terms, there is a problem: How can this equation be translated into a numerical one? Using the Taylor expansion of course! The expansion for an arbitrary function $u(t + h)$ looks like this

$$u(t + h) = u(t) + \sum_i^{n-1} \frac{h^i}{i!} u^{(i)}(t) \tag{1.155}$$

(in this expansion a dummy variable $x = t + h$ is defined and series are expanded around $x = t$). Lets expand the same function using another dummy variable $x = t - h$.

$$u(t + h) = u(t) + h\frac{\mathrm{d}u(t)}{\mathrm{d}t} + \frac{1}{2}h^2\frac{\mathrm{d}^2u(t)}{\mathrm{d}t^2} + \mathcal{O}(h^3) \tag{1.156}$$

$$u(t - h) = u(t) - h\frac{\mathrm{d}u(t)}{\mathrm{d}t} + \frac{1}{2}h^2\frac{\mathrm{d}^2u(t)}{\mathrm{d}t^2} + \mathcal{O}(h^3) \tag{1.157}$$

here $\mathcal{O}(h^3)$ means that there is an error due to truncation of series in the order of h^3. Assuming all possible $u(x)$ is known but not $\frac{\mathrm{d}^2u(t)}{\mathrm{d}t^2}$ these equations can be solved simultaneously to yield:

$$\frac{\mathrm{d}^2u(t)}{\mathrm{d}t^2} = \frac{1}{h^2}\left[u(t + h) + u(t - h) - 2u(t)\right] + \mathcal{O}(h) \tag{1.158}$$

which is one of the numerical representations of a second order derivative. Please notice that the error in this approximation grows to h! Normally it is assumed that h

is sufficiently small and it can be neglected. There exists representations with smaller error, but they require more points and have a more complex mathematical form, greatly consuming computation time. These equations will be used in a statistical calculation in the end, thus as long as the drift introduced by this error is small, it will be ruled out. Using a similar approach to a first order derivative one obtains:

$$\frac{\mathrm{d}u(t)}{\mathrm{dt}} = \frac{1}{2h}\left[u(t+h) - u(t-h)\right] + \mathcal{O}(h) \tag{1.159}$$

which is considerably better than applying geometrical definition of derivative. After this point, our system is discretized in time in steps of h. The size of this time step is very important both mathematically and physically. This will be discussed later. Applying these equations for discretizing the solution of Newton equations of motion, positions (r_i) and velocities (v_i) of particles are found as (the error is neglected hereafter):

$$r_i^{n+1} = 2r_i^n - r_i^{n-1} + F_i^n h^2/m \tag{1.160}$$

$$v_i^n = \frac{1}{2h}\left(r_i^{n+1} - r_i^{n-1}\right) \tag{1.161}$$

where

$$t_n = nh \tag{1.162}$$

$$r_i^n = r_i(t_n) \tag{1.163}$$

$$F_i^n = F_i(t_n) \tag{1.164}$$

a consequence of this discretization is that velocities calculated belong to coordinates one time step before, so calculated kinetic energy of the system is retarded compared to potential energy! This undesired effect can be eliminated with a neat mathematical trick. Define:

$$z_i^n = (r_i^{n+1} - r_i^n)/h \tag{1.165}$$

using this definition, a mathematically equivalent form of eq. 1.160 can be obtained:

$$r_i^n = r_i^{n-1} + hz_i^{n-1} \tag{1.166}$$

$$z_i^n = z_i^{n-1} + m^{-1}hF_i^n \tag{1.167}$$

eq. 1.167 is obtained using the eq. 1.160 in the following manner:

$$z_i^n = (2r_i^n - r_i^{n-1} + F_i^n h^2/m - r_i^n)/h \tag{1.168}$$

$$= (r_i^n - r_i^{n-1})/h + m^{-1}hF_i^n \tag{1.169}$$

$$= z_i^{n-1} + m^{-1}hF_i^n \tag{1.170}$$

we can use z_i^n in eq. 1.161 to define v_i^n , and obtain two linearly independent equations:

$$v_i^n = (z_i^n + z_i^{n-1})/2 \tag{1.171}$$

$$z_i^n - z_i^{n-1} = m^{-1}hF_i^n \tag{1.172}$$

solving for z_i^n:

$$z_i^n = v_i^n + \frac{1}{2}m^{-1}hF_i^n \tag{1.173}$$

and putting this into previously obtained eq. 1.166 and eq. 1.171:

$$r_i^{n+1} = r_i^n + hv_i^n + \frac{1}{2}m^{-1}h^2F_i^n \tag{1.174}$$

$$v_i^{n+1} = v_i^n + h(F_i^{n+1} + F_i^n)/2m \tag{1.175}$$

a more convenient form is obtained. This form is not only computationally more efficient, since only terms with one previous configuration is present, but also eliminates the nasty problem of retarded kinetic energy. Equations 1.174 and 1.175 together are called Verlett algorithm (velocity form).

Using these numerical equations of motion, an algorithm for canonical molecular dynamics can be devised (Alg.2).

This is one of the most basic algorithms one can follow. Although being so, the numerical calculation is considerably more intense than a Monte Carlo algorithm, and there is an increased set of control parameters. These parameters do not directly depend on the PEF used, their origin is mostly statistical and mathematical considerations on underlying physics. For example, how often does the rescaling of velocities applied?, do we apply it instantaneously or through a time period? Most of them will be omitted since

48

1. Specify the initial positions r_i^1.

2. Specify the initial velocities v_i^1.

3. Compute forces.

4. Compute the positions at $n+1$ using $r_i^{n+1} = r_i^n + hv_i^n + \frac{1}{2}m^{-1}h^2F_i^n$.

5. Compute velocities at $n+1$ using $v_i^{n+1} = v_i^n + h(F_i^{n+1} + F_i^n)/2m$.

6. Compute kinetic energy.

7. Scale the velocities $\alpha v^{n+1} \rightarrow v^{n+1}$ using $\alpha = [(3N)\,k_B T_{\text{ref}}/\sum_i mv_i^2]^{1/2}$ at specific time intervals.

8. Goto 3 until the duration of simulation expires.

<div align="center">Algorithm 2: NVT MD Algorithm</div>

they are highly application specific, but, maybe one of the most important parameter is the length of a single time step, which deserves a little discussion of its own.

A very important consequence of numerical calculation in a MD program is the discretization of time in calculations. The length of a single time step may be considered as a parameter of the system. This time parameter should neither be too large, since error assumptions in the discretization process would lead to wrong results, nor too small, since precious computer time would be lost needlessly. Also, when the time step becomes too small there is machine constant[9] limit which may lead to enormous errors. Value of this parameter depends on the application, and it is decided according to experience. In this particular kind of MD using Verlett algorithm, 1/100th of the oscillation period between two neighboring atoms known to work well. For example, using the two–Body component of the Tersoff potential in Figure 1.4, this parameter

---

[9]machine constant is the number of digits that a computer can store in assigned data memory cell

can be estimated as:

$$r_0 = 1.45\text{Å} \tag{1.176}$$

$$\varepsilon_0 = 2.58\text{Å} \tag{1.177}$$

$$\frac{1}{2}m\left(\frac{\Delta x}{\Delta t}\right)^2 = \varepsilon_0 \tag{1.178}$$

$$\Delta t = \sqrt{\frac{mr_0^2}{2\varepsilon_0}} \tag{1.179}$$

$$\Delta t/100 = h \approx 10^{-16}\text{s} \tag{1.180}$$

where h is the time step in Verlett algorithm. Luckily, this value does not violate the single block machine constant of 32 bit CPU, enabling faster calculations in even home computers of today.
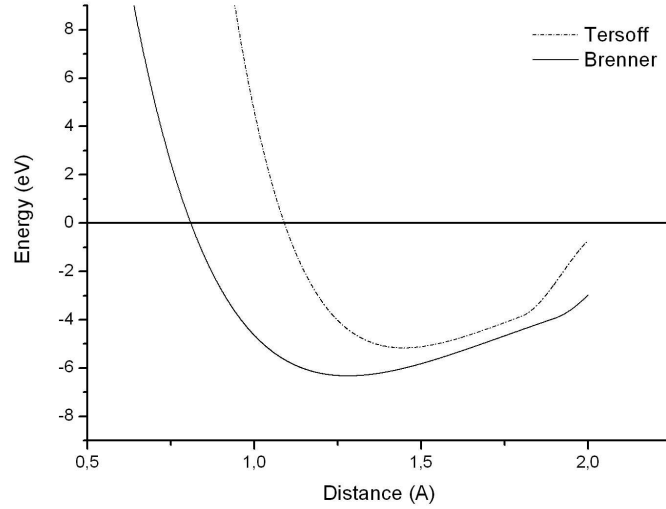
Figure 1.4: Two–body contribution to energy in Tersoff and Brenner potentials.

Another important point in a MD simulation is the decision where to stop. The aim is to reach a stable configuration. Such configuration is most simply explained through

the structural appearance, as the geometry does not evolve any further. Of course, a geometrical approach is quite subjective and hard to decide on. A more fitting way is to use statistical physics definition as the ensemble being in every one of its accessible states with equal probability. The definition may seem obscure, but, in effect, the use of this definition makes the decision job much easier. Remember, the states of our system are defined through configuration energy in PEF, and due to propagation mechanism in MD algorithm, number of accessible states with unrelated geometries is severely limited. In short, when the configuration becomes stable, the energy of the system should be fluctuating around a mean value which corresponds to the desired stable geometry. Using a plot of energy versus time, such behavior can be identified easily.

The intensity of these fluctuations is almost always constant, but there may be some infrequent large fluctuations. Whether these large fluctuations die or carry the system to another stable configuration depends on the actual state of the system. If the system is in the absolute stable configuration, then the fluctuation is certain to die after a certain number of time steps, but the system may have been in a meta stable state, which is not always easy to decide. For example, look at Figure 1.5. The unlikely starting configuration rapidly decays into a meta stable state, which is in effect for about ten thousand MD steps! But pressing on, the system achieves a better configuration. After eighty thousand MD steps, it is highly unlikely that the system is in a yet another metastable state, thus simulation concludes. However, 10000 MD steps is no small value, especially if one is using semi-empirical or ab-initio methods, the metastable state may have easily been misjudged as the stable configuration.

The main advantage of the MD procedure is the rapid decay of unlikely states. Although each step is considerably more expensive than a MC one, with this property, the algorithm is much faster to converge compared to MC in general.
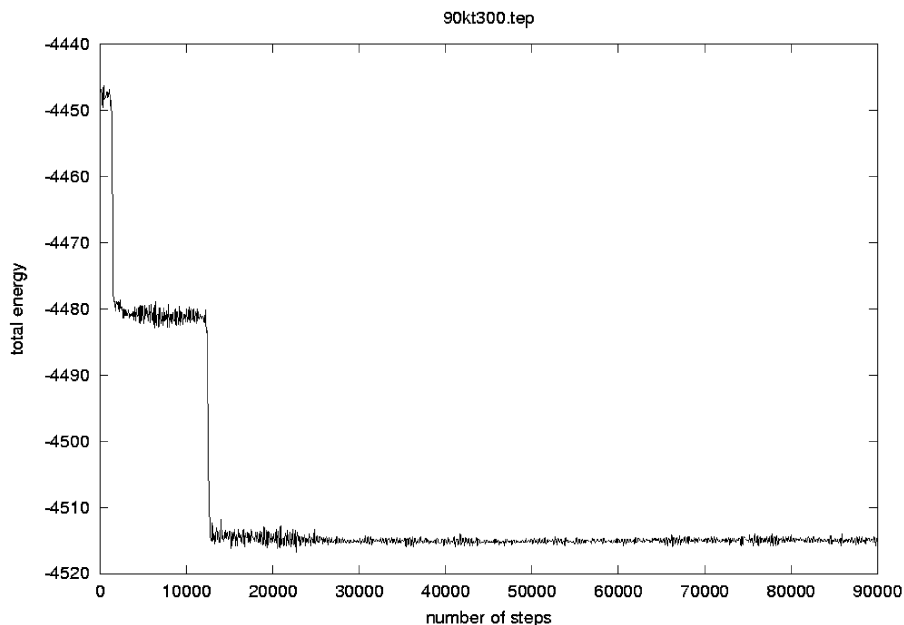
Figure 1.5: Total energy versus MD steps plot of a sample system at 300K. This plot is somewhat extraordinary showing a metastable state.

1.6.3 Further improvements to the speed

A calculation of presented nature, or a simulation as some may prefer to call it, requires a delicate balance between precision and speed. Typically, several thousands of steps are required for each calculation, and if the speed of the computer which calculates each step is slow, then problem at hand becomes insolvable. There are a couple of commonly practiced methods increasing this speed drastically without sacrifying too much precision. For example, in calculating the force exerted on an atom in a MD simulation, it is often unnecessary to consider all atoms in the structure due to cutoffs present in PEFs. A list of close proximity neighbors kept for each atom may save a lot of computer time, since it should only be updated rather infrequently. Using a spatial mesh the idea can be carried on further, improving the method of updating neighbor

list. Ultimately, the structure can be divided to a series of networked computers, to be calculated in parallel processing. There are several different such tweaks, and some of them may even depend on the specific computer architecture. The nature of the tweaks, especially the parallel ones, are beyond this context, a more detailed discussion can be found, for example, in Numerical Recipes series or Parallel programming with MPI [42, 43]. Due to nature of parallel computing, node communication need to be minimalised. This sometimes requires modifications to PEF itself, and specific algorithms including modified forms of PEFs do exist in literature [44, 45].

With this, the discussion on the theoretical nature of the problem is concluded. Of course, this limited text does not cover all the details, but as mentioned above, it is a target specific text, aimed to introduce some nomenclature. The rest of the text is designed in a modular manner, in which each chapter is a self-contained topic. Some further details can be found in each corresponding section, but, as always, the full details are beyond the constraints of this work.

CHAPTER 2

ON THE POSSIBILITY OF A POLYMER-LIKE NANOROD BASED ON STANDALONE BENZENOID CARBON RINGS.

2.1 Introduction

In this chapter, the possibility of existence of a periodic structure consisting of stacked C_6 rings is investigated theoretically. Such a structure is interesting primarily for two reasons: Vertically stacked π-conjugated polymers are interesting both due to self organization properties and their aromatic nature. Phtalocyanine and Hemi-porphyrazine are two examples of such structures [46]. Due to π-conjugation, they are generally expected to be semiconducting or conducting, and due to nature of the coordination, they are expected to be rod-like rigid structures, with properties/advantages of hairy polymers. The minimum cross-section area achievable for such a structure is observed to be limited, too thin structures tend to be radicals. Whether this is due to inherited properties from the polymerized unit, or due to aromaticity leading to instabilities in coordination for certain arrangements is an open question. C_6 ring (a.k.a. benzenoid

ring), without Hydrogens, is a very unstable structure by itself, and extremely hard to realize, if possible at all, as a standalone structure. However, dehydrogenation leads to under-coordination, resulting in a increased p character in the hybridized orbitals, permitting a strained but stronger bond in the stacking direction. The vertically stacked C_6 rings can be considered to be in an intermediate coordination state between sp^2, sp^3 hybridization, maintaining the aromaticity. This may lead to reduced inheritance of radical behavior from the unit cell, resulting in a more stable structure. In this work, two possible schemes for coordination between C_6 rings are considered, with predictions on various physical properties, that can be used in deciding if they are realizable at all.

The importance of C_6 ring stems from the carbon nonstructural with aromatic nature. There are many such 0D nanomaterials in the literature, each with its own set of unique and promising electronic/structural properties. However, how to construct effective networks with such nanostructures interlinked to each other is still an open question. The most important property one has to satisfy is not to disturb the interlinked nanostructures. In order to maintain aberrations due to linking on the perturbative level, one has to devise a method for not only maintaining geometry, but also the electronic configuration. A solution that immediately comes into mind is to use π-conjugation in the C_6 rings that are favored energetically in such structures. This should introduce very little geometrical aberration, and alteration in electronic behavior is generally expected to be on perturbation level, depending on the structure itself. There are a couple of strategies for this purpose, such as Dewar coordination. Other π-conjugated polymers are already used for such purposes. Vertical stacking considered in this work is expected to have two advantages over the planar arrangement often considered: Increased rigidity, and due to aromatic ring-aromatic ring coordination, less impact on the electronic configuration of the connected structure.

The structure investigated will be called the "benzorod" as suggested by the S. Erkoc who proposed it in a recent work [47]. This chapter is segmented into two parts. In

the first part, the structure is investigated as a non-periodic macromolecular entity via empirical potential molecular dynamics calculations. In the second part, a more detailed study using DFT is presented, treating the structure as a 1D periodic nanorod. Various theoretical calculation parameters are established using an abstraction based on molecular properties of benzenoid rings and similarly coordinated bulk systems.

2.2 Molecular Dynamics Investigation

Molecular dynamics method is a very good tool for prototyping a modeled structure which little is known about. Force driven relaxation procedure that is statistical in its nature provide an autonomous mechanism to test the structural stability and thus assert the validity of a given model. Even in some cases such as this one, results can directly be used to predict a better structural model for the system at hand. In this sense, there should be as little predetermined structural constraints on the system as possible. This is best achieved when the system is modeled as a macromolecular entity, getting rid of the restraints imposed by periodic boundary conditions. However, it should be kept in mind that, in the end, we are trying to model a nanorod which is by definition a 1D periodic structure. In order to achieve resemblance, benzorods of varying lengths are prepared. Too long and too short models prone to have various problems that are irrelevant for our purposes.

Conjugation of benzorod with an aromatic structure is modeled via graphene surface (surface interaction) and Buckminsterfullerene (C_{60}) molecule (0D nanostructure interaction) [48].

2.2.1 Method of calculation & Preparation of models

The empirical many–body potential energy function developed for carbon [38, 39] is used in the calculations. This PEF describes the structural properties and energetics of carbon relatively accurately; including diamond crystal as well as the properties of
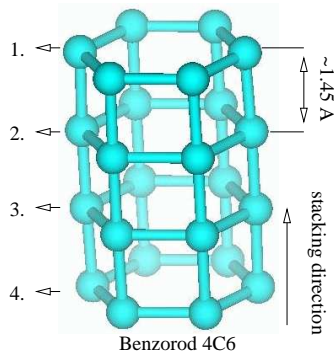
Figure 2.1: The model structure of benzorod 4C6

the individual basal planes of graphite. Furthermore, buckminsterfullerene [48] related structures, such as carbon nanotube and buckyball, can also be simulated, and relatively accurate structural properties and energetics are obtained [49]. There is no explicit "bond" information in the Tersoff PEF and thus carbon atoms may rearrange under external influence without bond conservation restriction, unlike molecular mechanics method [28, 29]. Absence of long range interactions is of no significant importance in this part.

The equations of motion of the particles are solved by considering the Verlet algorithm. The canonical ensemble molecular–dynamics NVT [9] is proceeded. The temperature scaling is taken into account at predetermined MD steps and the temperature of the system is kept constant at a given temperature with direct rescaling of velocities. One time step is taken to be 10^{-16} s in accordance to the two body component of the PEF used.

A pseudo-annealing method is employed in the following manner : Starting at very low temperature (1 K) the initial model is relaxed (as described in Section 1.6.2). Then the temperature of the system is increased to 100 K and relaxation procedure is initiated again. After this, the temperature is increased in steps of 100 K, relaxing the structure at each temperature step, until the system considered distorts. Distortion criteria can

be described as a "non-insignificant deviation from the initial model", such as separation of atoms, geometrical aberrations that change whole the structure, etc. Each system distorts at a different temperature. Relaxation at each temperature step lasts for about 50000 time steps, which is almost always enough to reach equilibrium.

Thanks to this pseudo-annealing method, structural parameters in the initial models, such as inter-layer separation, need not be determined exactly, any under- or over-estimation is corrected through the course of calculations.

Initial benzorod models are generated by stacking dehydrogenated benzene rings together. Each ring, or layer, is in alignment with the others and the inter-layer separation is about1.45 Å. Benzorods are named as nC6 where n is the number of dehydrogenated benzene rings present. As an example, model structure of benzorod 4C6 is shown in Figure 2.1. Notice that, Tersoff PEF is modeled with mostly hybrid orbital bonding in mind, and it is only an assumption that the under-coordination due to missing hydrogen atoms leads to a bonding scheme that is describable using this PEF.
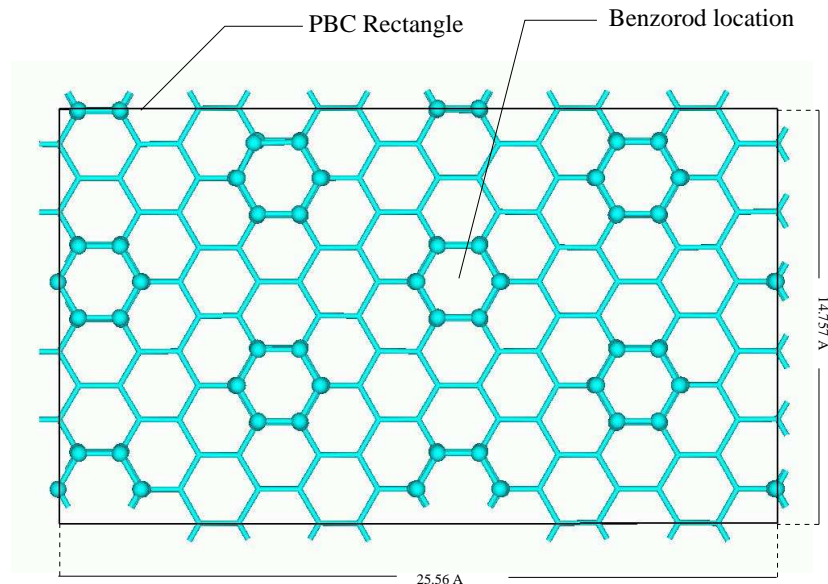

Figure 2.2: A benzorod array. Periodic boundary is shown as the rectangle (along x and y), and locations of benzorods are shown in ball and stick notation.

In order to simulate the graphene surface, periodic boundary conditions (PBC) are applied in lateral directions (x,y). In order to model surface relaxation due to benzorod addition adequately, the size of the periodic rectangle is chosen so that there is a large enough area independent of the restrictions of PBC. Benzorods attached to the graphene surface, or benzorod arrays in short, are structured by adding dehydrogenated benzene rings to selected hexagons of a graphene sheet (Figure 2.2). The site points for benzorods are chosen so that they are beyond interaction distance of each other, which is approximately 1.7 Å in the PEF used.

Benzorod may also act as an interconnecting element for 0D nanostructures. In order to demonstrate this, a chain structure that is composed of C_{60} [48] and interconnecting benzorods is modeled. In this model, there are three C_{60} nanoballs. The benzorods connect C_{60} nanoballs in a linear fashion, using consequent hexagonal faces. By varying the length of two interconnecting benzorods, 9 different structures are obtained. These structures are named as mC60-nC6 where m is the number of buckyballs present and n is the length of the benzorods.

2.2.2 Results & Discussion

Standalone benzorods at various temperatures are shown in Figures 2.3-2.5. The highest temperature indicated for each benzorod is the point where the structure is considered to be distorted. It should be noted that the indicated temperatures are solely for comparison purposes with similar calculations, the system lacks proper environment interaction modeling. The most useful information gained here is the geometrical rearrangement of the structure under stress.

The previously mentioned strain on the structure leads to an interesting geometric reconfiguration. When there are a group of three rings, the middle ring distorts, i.e. it moves outside the bonding radius of the other ring members, and each member becomes a "joint" connecting the other two layers. These "joint" atoms align themselves in a

Benzorods 2-8

2C6				3C6			
	1 K	10800 K	10900 K		1 K	3900 K	4000 K

4C6			
	1 K	6500 K	6600 K

5C6			
	1 K	4800 K	4900 K

6C6			
	1 K	2500 K	2600 K

7C6			
	1 K	3900 K	4000 K

8C6			
	1 K	11600 K	11700 K
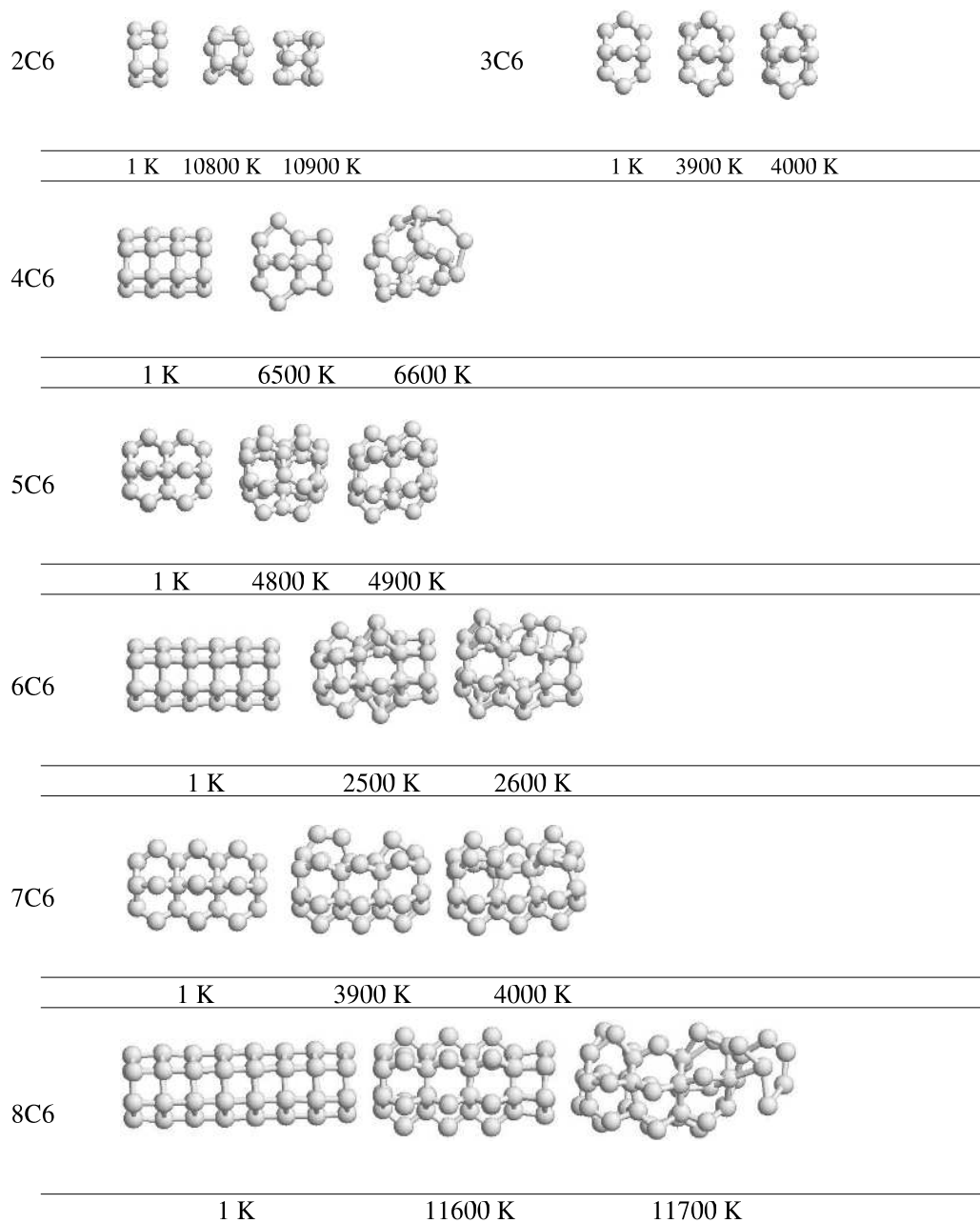
Figure 2.3: Benzorods 2-8C6

Benzorods 9-14

	1 K	2900 K	3000 K
9C6			

	1 K	2900 K	3000 K
10C6			

	1 K	2100 K	2200 K
11C6			

	1 K	2100 K	2200 K
12C6			

	1 K	1600 K	1700 K
13C6			

	1 K	1800 K	1900 K
14C6			
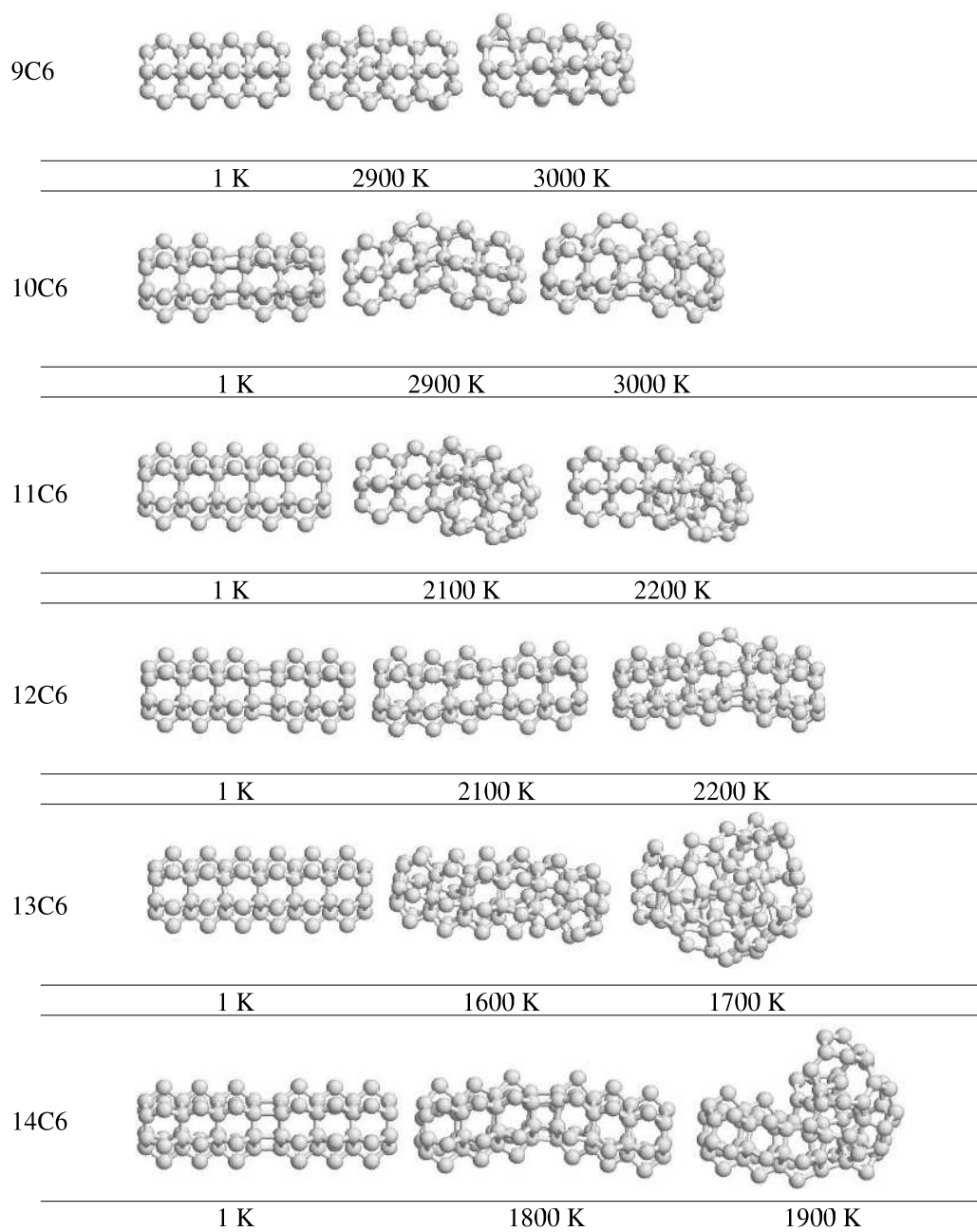
Figure 2.4: Benzorods 9-14C6

Benzorods 15-20

15C6	1 K	1200 K	1300 K

16C6	1 K	1100 K	1200 K

17C6	1 K	1100 K	1200 K

18C6	1 K	100 K

19C6	1 K	1000 K	1100 K

20C6	1 K	100 K

Figure 2.5: Benzorods 15-20C6

Figure 2.6: Dependence of distortion temperature on the number of dehydrogenated benzene rings n.

geometry such that there is an angle of 107° between the "bonds" connecting the two layers. This geometry is most clearly seen in benzorod 3C6. When there are more than three rings, the 3C6 geometry is favored, and the structure aligns itself such that 3C6–like geometry is maximized through the length. When there is an even number of rings however, one of the layers is left–out. This left–out layer maintains the original geometry (2C6–like geometry) with its neighboring layer. The smallest benzorod wit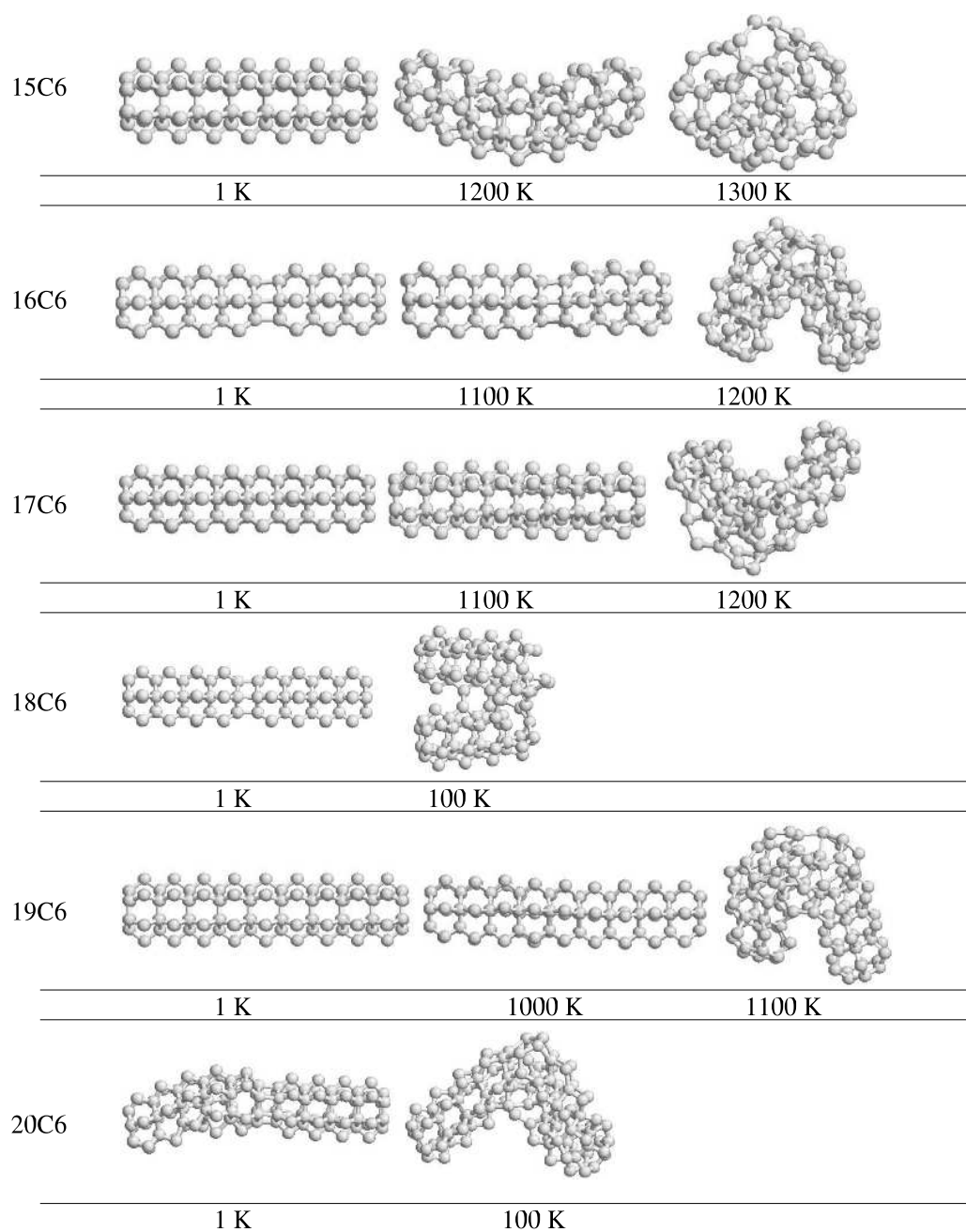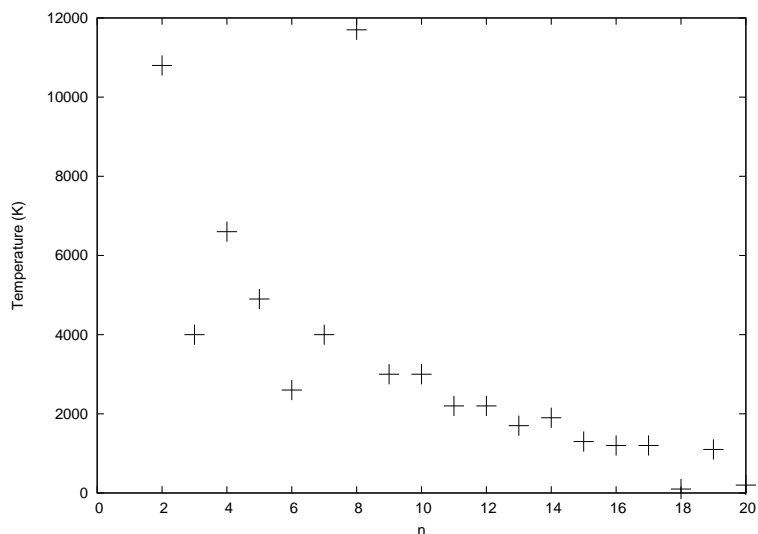h a left–out layer is 4C6. Left–out layer geometry has a preferred location. In most of the cases studied the left–out layer geometry was encountered in the middle of the structure or as close as possible, most probably due to under-coordination at the ends. The exceptions are the 6C6 and 8C6 benzorods. The left–out layer in these two benzorods appear in the ends most probably due to their smaller length. Lastly, the ideal benzorod geometry seems to be stable up to room temperature for lower (and even) number of benzorod rings. When temperature is increased above room temperature , geometry assumes the above described form.

The overall thermal stability of the benzorods studied is length dependent. This is to be expected, as with increasing length, the possibility of a thermal fluctuation leading to

a deformation exceeding the maximum elastically sustainable bending angle increases. In general, when the number of rings increases thermal stability decreases. Distortion temperature versus number of dehydrogenated benzene rings plot is shown in Figure 2.6. The biggest fluctuation in this general trend is 8C6 with distortion temperature of about 11700 K. The peculiar location of the left–out layer seems to increase the stability. This may be interpreted as the re-arranged geometry having a stiffer structure than the initially modeled one. 8C6 is found to be the most stable structure against heat treatment among the models considered. This structure is exceptionally strong and keeps its form up to 11600 K. When the number of rings pass 12, the major structural deformation under heat treatment is bending. The bending occurs at the middle, at the location of left–out layer if present, reinforcing the idea that the initial model has lower modulus of elasticity.
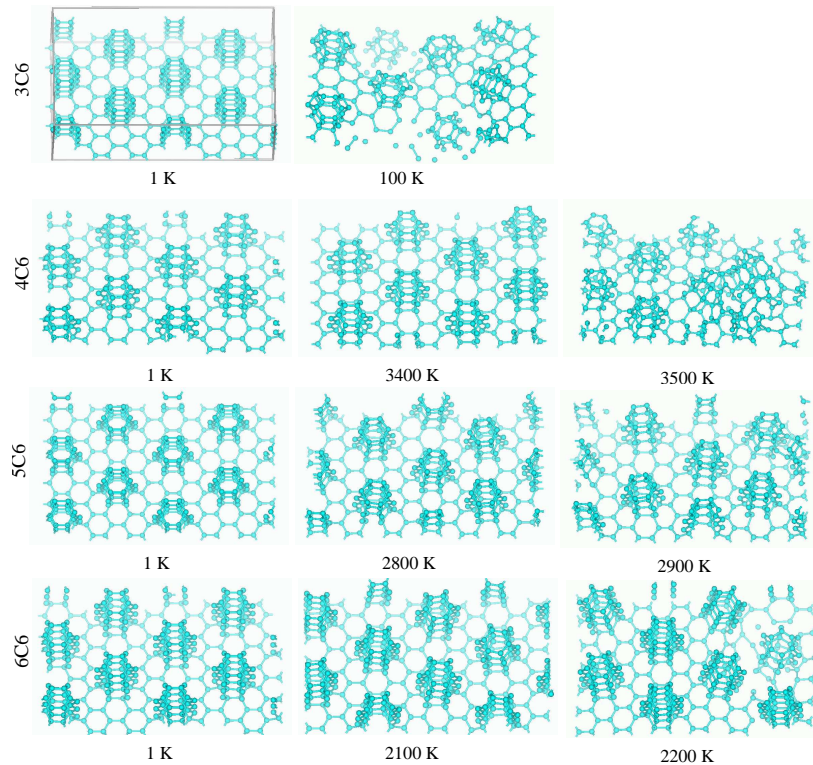
Figure 2.7: Benzorod arrays 3C6 − 6C6
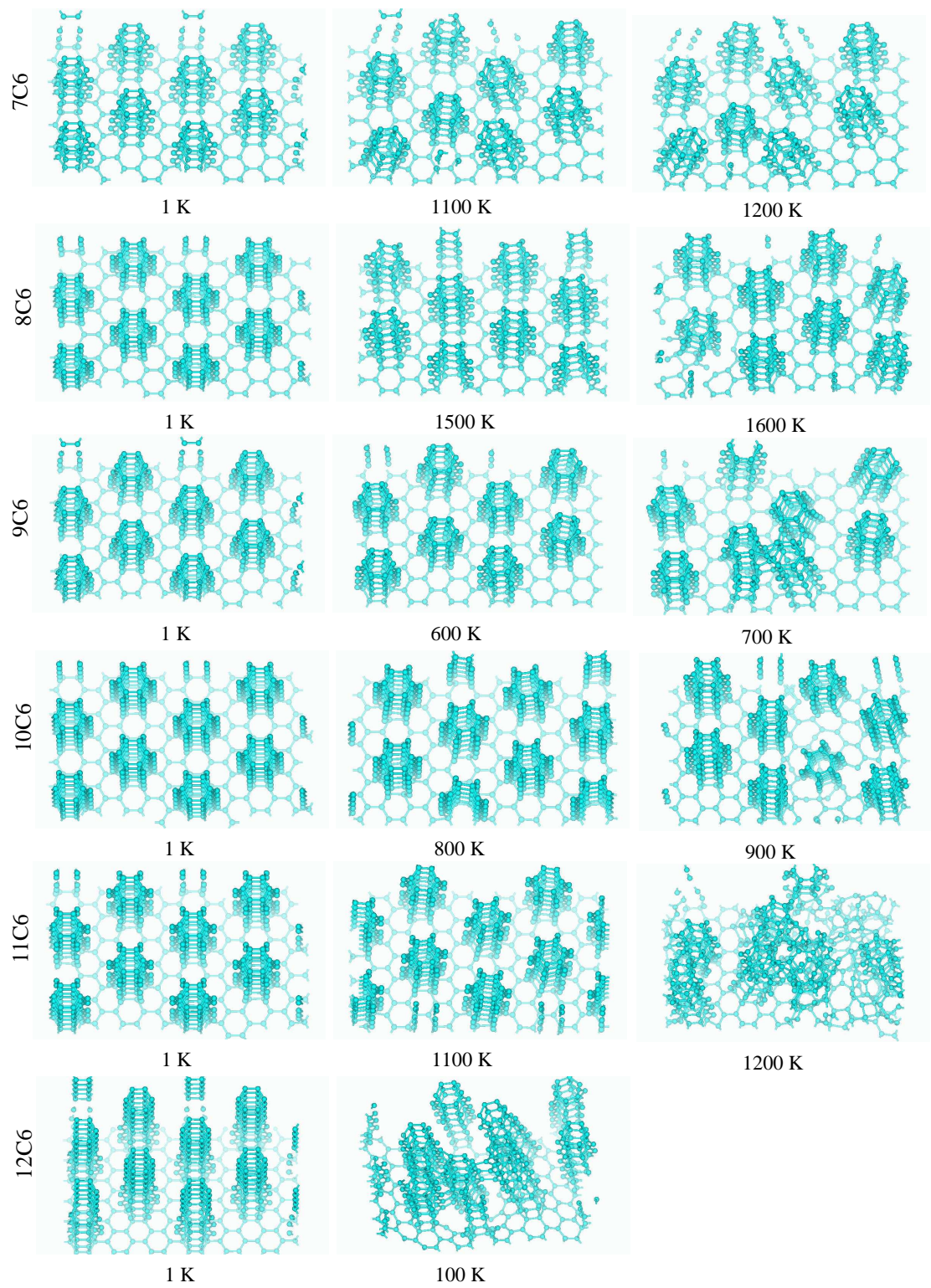
Figure 2.8: Benzorod arrays 7C6 – 12C6

The benzorod arrays at various temperatures are shown in Figures 2.7 -2.9. Even at very low temperatures benzorods deviate from ideal geometry. In the new structure each benzorod assumes a geometrical form similar to isolated benzorods. When the benzorod assumes the above mentioned geometry at elevated temperatures, there is a noticeable geometrical rearrangement in the vicinity of the joint between the benzorod and the graphene sheet. This signs a binding scheme other than sole π-coordination. The most important point is that the graphene–benzorod interconnection seems to be stable up to elevated temperatures.

Figure 2.9: Benzorod arrays $13C6 - 16C6$

Figure 2.10: Nanochains 3C60-1C6 − 3C60-9C6 at various temperatures.

67

Too short and too long benzorod arrays are not favored. In the former, substrate graphene sheet disintegrates, and in the latter, benzorods loose rigidity. Benzorod arrays formed from odd number of benzenoid rings seem to be less stable.

Among the arrays simulated, 4C6 array seems to be the most stable, thus it is the strongest candidate for application, for example as a field-emitter. With the exception of 3C6, arrays shorter than 12C6 are stable up to elevated temperatures.

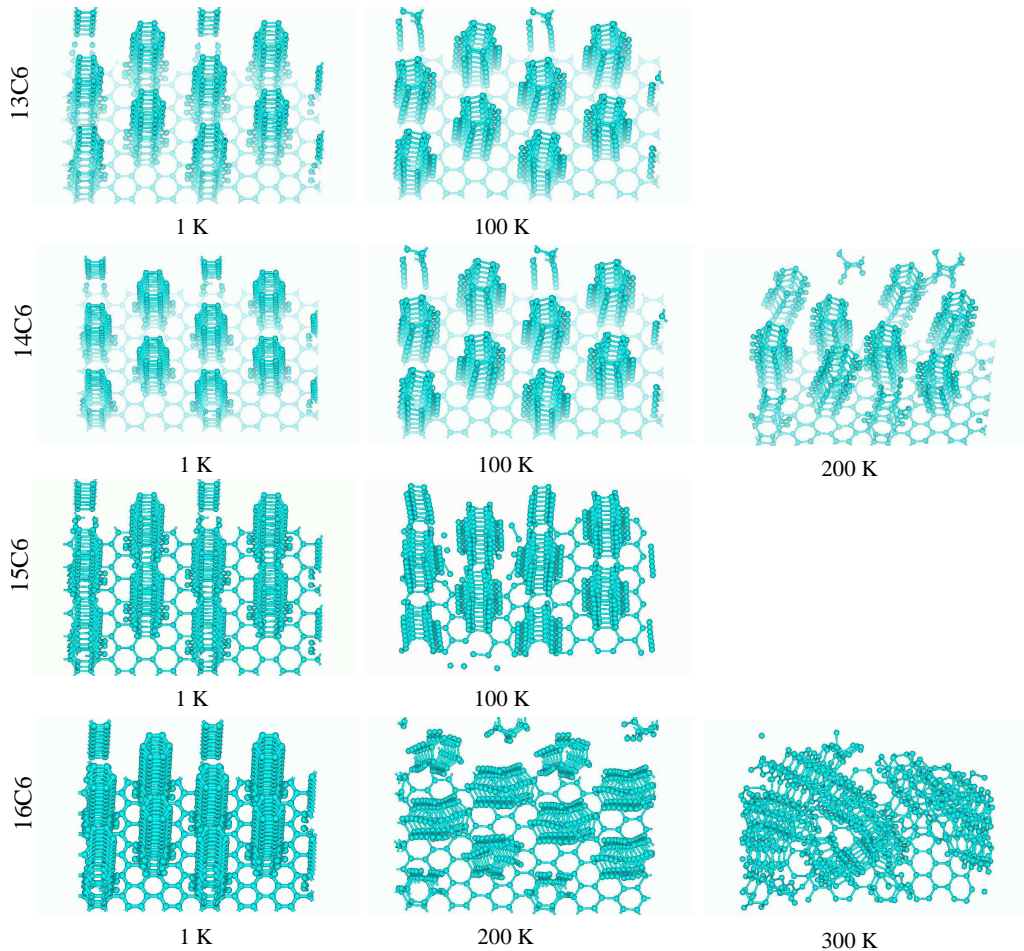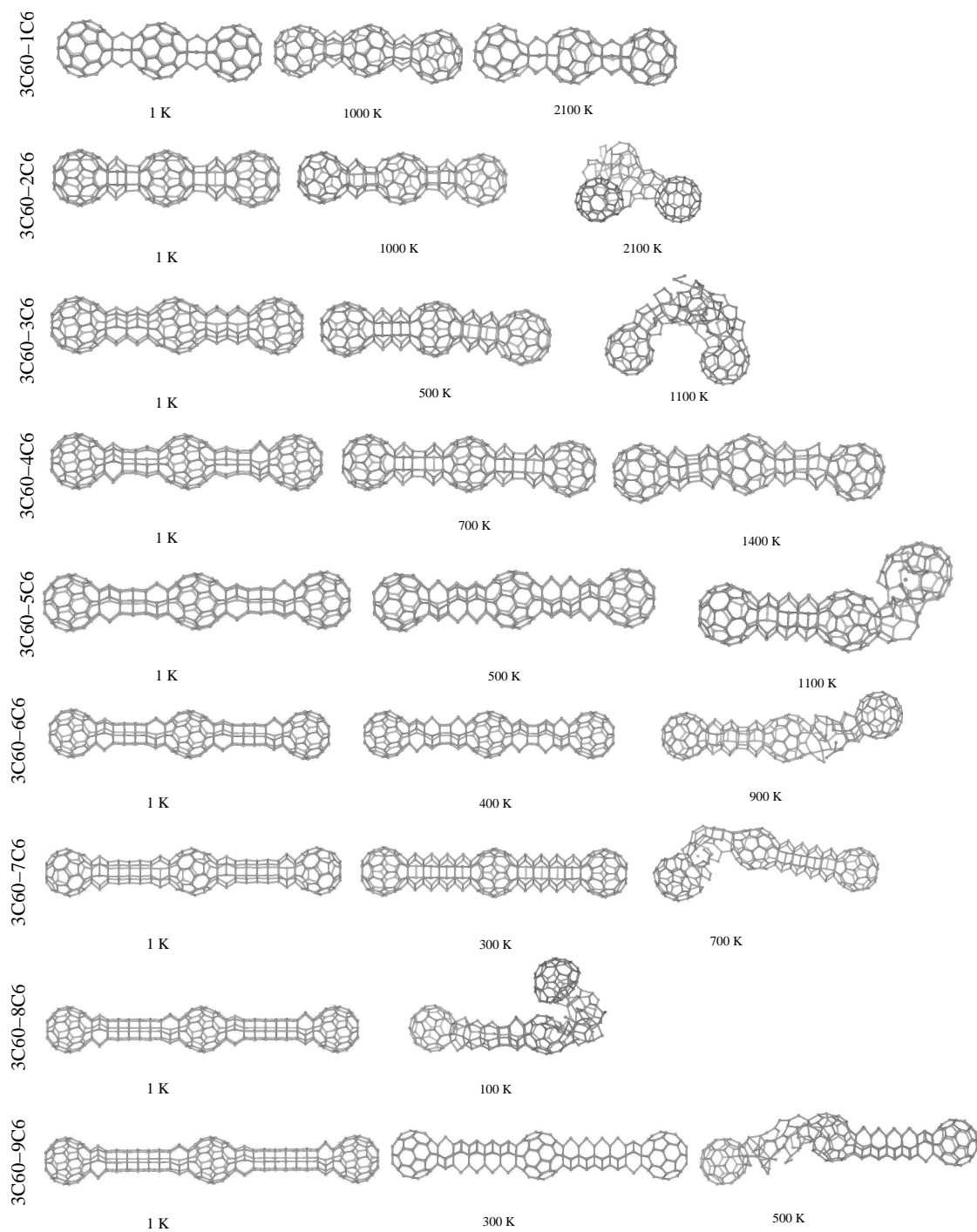The nanochains at various temperatures are shown in Figure 2.10 . Again, benzorods assume above described form even at very low temperatures. There is a slight elongation in C_{60} where the benzorods are connected due to change bonding characteristic. This seems to lower the thermal stability of that section. In chains with shorter benzorods, the decomposition is observed at around these locations. After 3C60-6C6, benzorods seem to be less stable, and decompose before the nanoballs. Starting from 3C60-7C6, length dependent nature of the benzorods surpass the now-disturbed C_{60} in instability.

The structures considered are stable at elevated temperatures, with one exception of 3C60-8C6. Length and ring number dependent nature of benzorod stability is again clearly observable.

These structures are promising in creating aligned rigid nano materials. Chemically more active pentagons are left free for interaction with other material, and separation between C_{60} may be controlled. Thus it may be used in magnetic or photovoltaic applications.

2.3   Periodic Investigation

Molecular dynamics calculations of the previous section demonstrate that there exists stable benzorod geometries at elevated temperatures. This can be interpreted as an indication of the existence and stability of the structure. However, due to nature of the material, a deeper analysis is in order, in order to verify the applicability of Tersoff PEF and to gain insight on the electronic structure.

In this second part, benzorod is investigated as a nanorod, or 1D crystal, using DFT. Both the initially purposed geometry that is seen to be stable only at lower temperatures, and the rearranged (relaxed) geometry is studied. Various observables are calculated for comparison purposes, to be used in the decision whether this structure is viable or not.

2.3.1 Method of calculation & Preparation of models
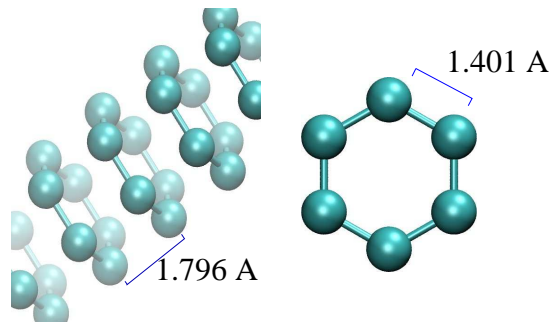
Figure 2.11: Optimized geometrical parameters for the direct coordination stacking scheme

DFT calculations presented in this section are performed using PWSCF [50], a part of the Quantum Espresso package [51].

An ultra-soft pseudo potential using Becke-Lee-Yang-Parr (B3LYP) hybrid exchange correlation generated with Vanderbilt code has been used in the calculations. The pseudo potential is selected due to its smooth behavior in optimizing the lattice parameter of this rather strained system and well description of the geometric properties in the reference carbon structures considered (graphite, diamond and polyethylene). The details for this pseudo can be obtained from the web [52].

Direct stacking scheme for the C_6 ring is presented in Figure 2.11. The C_6 ring of the unit cell is obtained by removing the hydrogen from a geometry optimized benzene

molecule using the same level of approximation. The lattice constant for the system is obtained using a golden search algorithm and cubic spline fit to obtain the energy minimum [42].
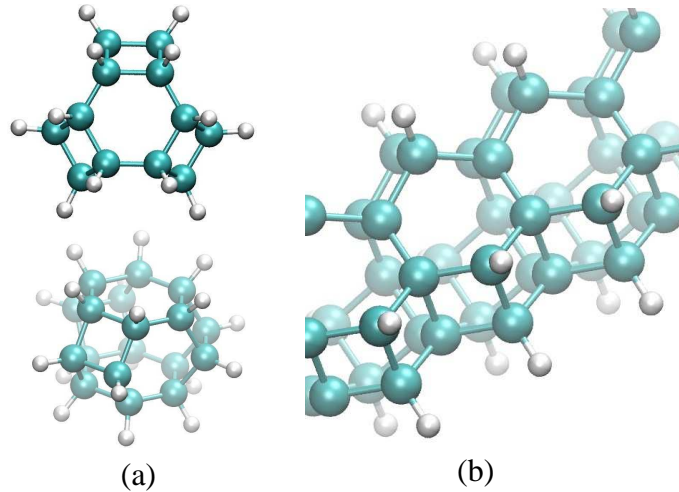
Figure 2.12: Relaxed benzorod. (a) The molecular geometry used in obtaining the unit cell, (b) the relaxed benzorod

In the previous section, it is seen that the direct coordination scheme is observed only at lower temperatures. This indicates that the rearranged benzorod geometry has lower energy than the initial "ideal" geometry. This rearranged geometry should be investigated separately. In modeling this geometry for DFT, it should be kept in mind that in parametrization of Tersoff PEF, hydrogen are treated implicitly, whereas in DFT they should be present explicitly. Since the effect of under-coordination due to lack of hydrogen is crucial in the first form, there was no problem, but in the rearranged form, hydrogenation should be considered manually. In order to obtain rearranged unit cell, a hydrogenated array of three C_6 rings with the middle layer having a slightly enlarged radius is relaxed, using the same level of approximation. The resulting molecular geometry is modified to be a periodic unit, and lattice parameter is calculated by minimizing

the energy via compressing the unit cell in the direction of repetition. The relaxed structure is presented in Figure 2.12.

2.3.2 Results & Discussion

2.3.2.2 The "ideal" benzorod
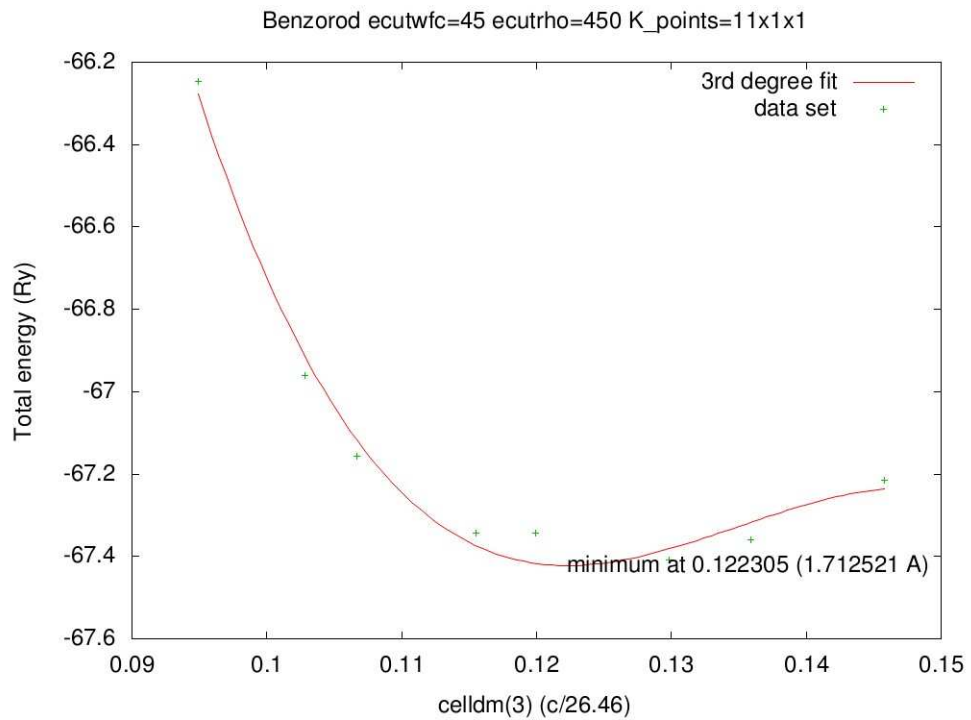
Figure 2.13: Lattice parameter as determined by different calculation parameters. Here, k-point is under sampled

$p - p$ coordination is rather hard to describe in DFT formalism due to its localized nature and steep gradient. Generally, hybrid functionals tend to work better than GGA counterparts. An automatically generated uniform Monkhorst-Pack [53] grid of k-points is used in the calculations. Both due to complexities arising from the delocalized p

orbitals and lattice constant being small, a very precise set sampling the k-point space is required. Under sampling of the k-space leads to an anhormonic splitting as shown in Figure 2.13 due to ill representation of the wave-functions. The convergence for the lattice parameter is achieved using the parameter set in Figure 2.14. Convergence of total energy is achieved much later, in Figure 2.15 . Total energy convergence with respect to parameter set is not mandatory in this calculation, since we will not be investigating related observables such as optical properties. Thus the set shown in (b) is used, in order to save computation time.
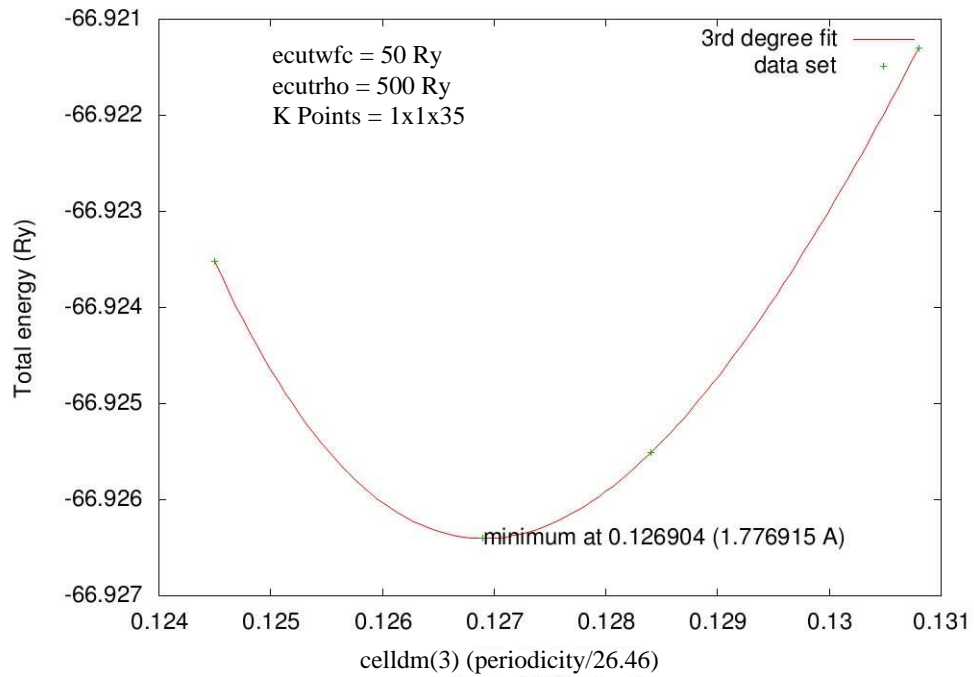
Figure 2.14: Lattice parameter as determined by different calculation parameters. After this point, the change in lattice parameter is negligible
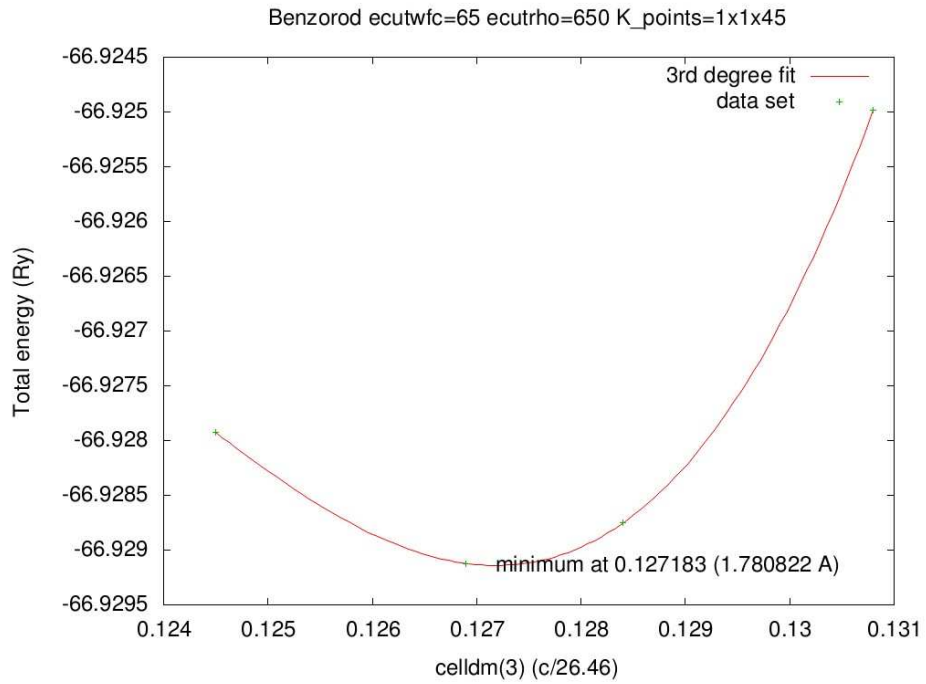
Figure 2.15: Lattice parameter as determined by different calculation parameters. This precise set can be used in calculating relations that require total energy convergence.
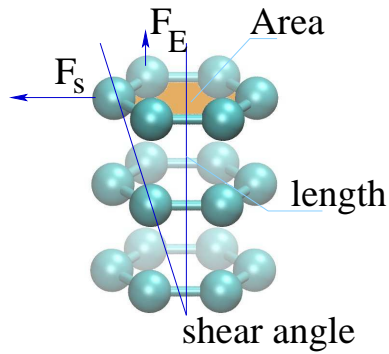
Figure 2.16: The geometrical parameters used in calculating elastic moduli for benzorod. F_s and F_E are the two orthogonal forces applied on one of the layers for creating a shearing stress and elastic stress correspondingly.

The optimized lattice parameter for the system is calculated as 1.765 Å. This value is considerably larger than the initially proposed value of 1.4 Å, but compared to inter layer spacing in graphite (3.34 Å[54]), it is clear that the coordination between the layers is not solely due to plain $\pi - \pi$ conjugation. The pseudo potential employed tends to overestimate bonding length in similar cases, however, length being this close to the cutoff of Tersoff PEF, the reason why structure tends to rearrange into the second form in MD calculations is clear.

In small perturbations, the material can be assumed as isotropic due to symmetry. Then, by applying harmonic approximation all the observable structural properties can be asserted from only two elastic constants. Among the others, Young's modulus and shear modulus are somewhat easier to calculate in our case. In Figure 2.16, parameters used in calculating these constants are shown.
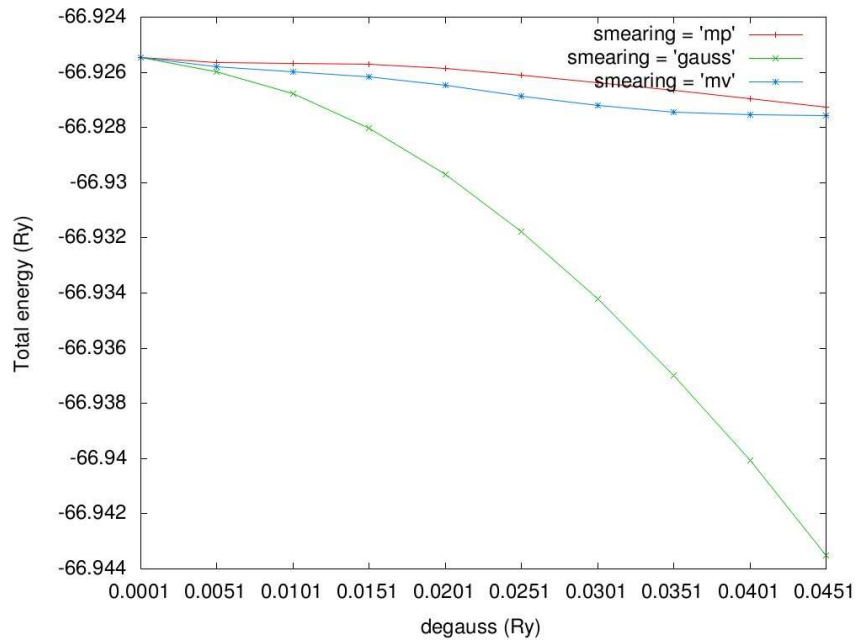
Figure 2.17: Effect of various smearing functions on total energy.

Using the cubic fit functions in Figure 2.14, Young's modulus of the structure can be approximated, for the limited range where harmonic approximation is valid. The cubic function in (b) reads (in Rydberg)

$$E_{EOS,(b)}(x) = -25741.4x^3 + 10236.6x^2 + -1354.47x + -7.28699 \qquad (2.1)$$

Force along the periodic direction, calculated from the gradient of energy at 0.01 Åaway from the minimum ($c/a = 0.1261898$; $a \approx 14$), where harmonic fit is in order, is approximately

$$F_{+0.01} = -\frac{\left(E_{EOS,(b)}(0.1261898) - E_{EOS,(b)}(0.1269040)\right) J}{0.01 \times 10^{-10}m} = 5.1467 \times 10^{-10}N \quad (2.2)$$

Elastic modulus (Young's modulus) can be approximated from [55]

$$E = \frac{\text{stress}}{\text{strain}} = \frac{F_E/A}{dL/L} \qquad (2.3)$$

The cross-sectional surface area, A, for a single benzorod is approximately $5.09951 \times 10^{-20}m^2$. Putting the calculated values in place the elastic modulus is obtained as

$$E = \frac{(5.1467 \times 10^{-10}N)(1.765 \times 10^{-10}m)}{(5.09951 \times 10^{-20}m^2)(0.01 \times 10^{-10}m)} \approx 1781 \times 10^9 \, N/m^2 \qquad (2.4)$$

which is comparable with that of diamond [56]. Although the above result is just a crude approximation, and should be approached skeptically, it may safely be stated that bonding along the stacking direction is much stronger than pure $\pi - \pi$ coordination observed between graphite layers.

Using a similar approximation, shear modulus can also be calculated.

$$G = \frac{\text{shear stress}}{\text{shear strain}} = \frac{F_s/A}{\tan(\theta)} \qquad (2.5)$$

where θ is the shear angle. For a shear angle of $\approx 1°$ [1], the above quantity is calculated as

$$G = \frac{(2.635707 \times 10^{-10} \, N)}{(5.09951 \times 10^{-20}m^2)(0.02)} = 258.3758 \times 10^9 \, N/m^2 \qquad (2.6)$$
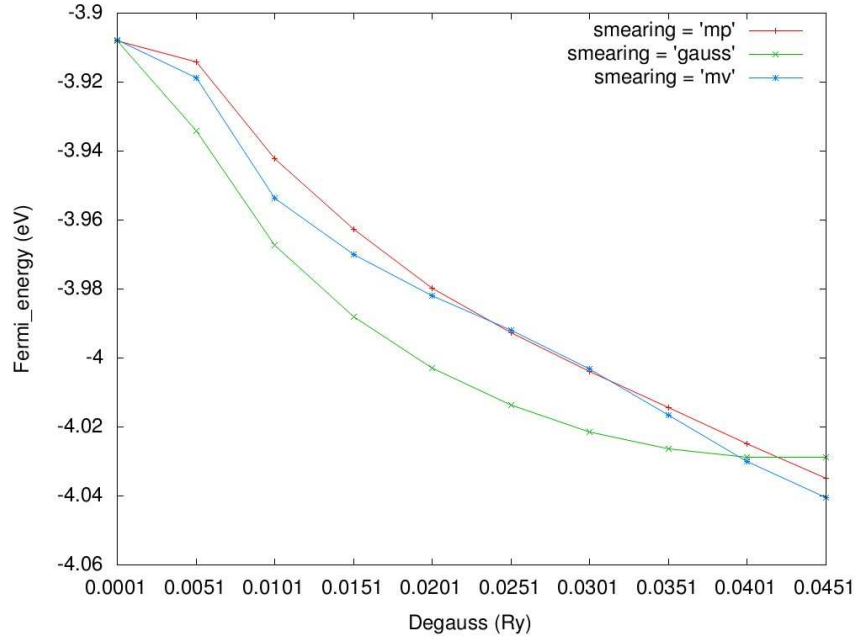
Figure 2.18: Effect of various smearing functions on Fermi level.

which is again in the vicinity of diamond[57].

Before initiating electronic structure calculations, there is another consideration in our system. Since direct conjugated benzorod is expected to be conducting, in order to define density through the Fermi surface adequately, a smearing function should be added. Smearing function allows fractional occupancies for the states crossing the Fermi level, thus continuity of the electron density can be maintained at this boundary. The method can be seen as an artificial temperature acting on the system, but due to numerous considerations, there are a number of choices for the distribution function. In this work, Gaussian spreading [58], Methfessel-Paxton first-order spreading [59] and Marzari-Vanderbilt cold smearing [60] is considered. The effect of smearing on the total energy of the system should be on the perturbative level, whereas monotonous behavior

---

[1]Due to fluctuations, minimum reliable energy difference is observed at this angle.

is expected with increasing spreading in the approximated Fermi level. In Figure 2.17, 2.18 the effect of the considered smearing schemes are shown. Looking at this plot, Methfessel-Paxton first-order spreading with a spread value of 0.01 Ry is decided.

Comparison between projected partial electronic density of states (PDOS) of a single carbon atom in Benzene and Benzorod are presented in Figure 2.19. In both graphs, the values are broadened with a full-width-half-maximum value of 0.03 Ry, for easier comparison. It is clear that the structure is no longer in a pure sp^2 hybridized state. There are two trends observable in the graph, low lying states are dominated by a distorted sp^2 like arrangement, and close to Fermi level, there is a p dominated mixture of orbitals. DOS around Fermi level is non-zero, and most probably the structure has delocalized states leading to conduction.
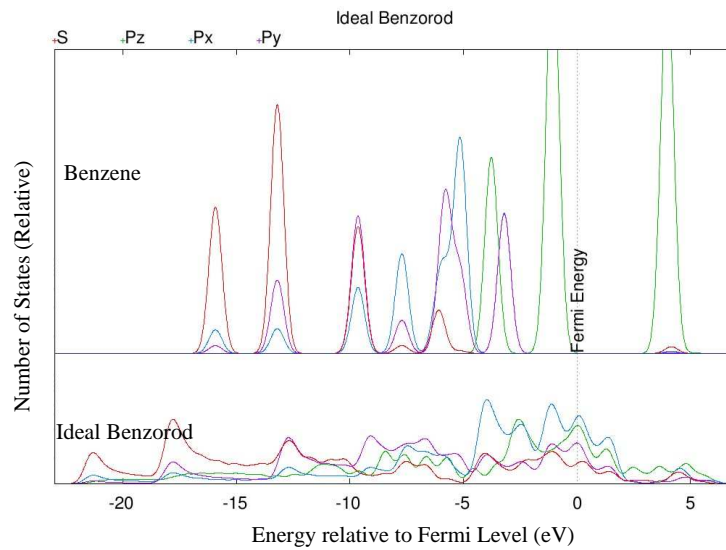
Figure 2.19: Projected partial density of states (PDOS) of carbon in benzene and benzorod.

The conducting characteristic is verified when the band structure is investigated

(Figure 2.20). There are four channels crossing the Fermi level, two directly crossing, two forming a semi-metallic arrangement similar to that observed in basal layers of graphite. This interesting behavior may be attributed to individual layers in benzorod maintaining their aromaticity. Comparing with PDOS, it may be argued that the direct crossing band is most probably due to p-p coordination , whereas the semi-metallic state is due to conjugation between the two aromatic states.
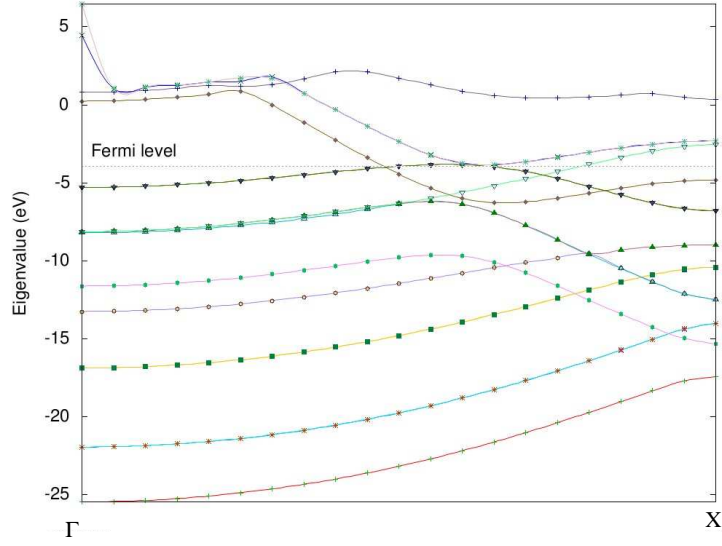
Figure 2.20: Band structure of the ideal benzorod

Charge density plot for the direct coordination scheme is shown in Figure 2.21. Each carbon contributes to the coordination in the lateral direction. These are the non-localized states encountered in the previous section.

Binding energy per atom can be calculated from

$$E_b = \frac{(E_{\text{cell}} - \sum_i^n E_{\text{atom},i})}{n} \tag{2.7}$$

where n is the number of atoms, E_{cell} is the total energy per unit cell and $E_{\text{atom},i}$ is
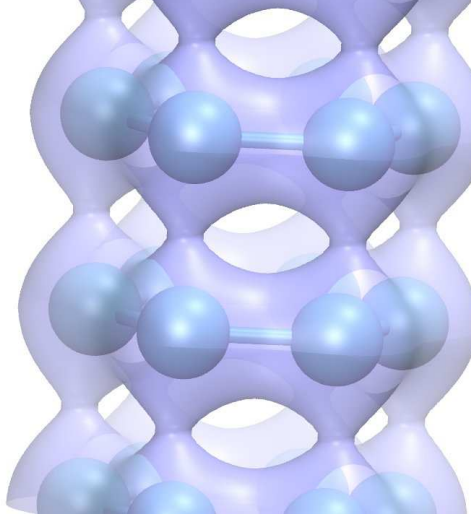
Figure 2.21: Charge density in the direct coordination scheme.

the self energy of ith atom calculated at the same level of approximation as the E_{cell}. For directly conjugated geometry the binding energy comes out to be $E_b = -6.04$ eV. Being negative, the structure can be considered as stable energetically.

2.3.3 Relaxed Benzorod

One interesting trend in the rearranged unit cell geometry is that the number of hexagons is maximized. Although this leads to highly uncommon rectangular arrangement of carbon, the binding energy per atom is $E_b = -6.39$ eV in the rearranged cell, noticeably lower than the previous model. Interestingly, removing hydrogen and re-relaxing the unit-cell leads to the unit cell of an armchair carbon nanotube [61] (which has considerably lesser binding energy per atom $E_b \approx 7.9$ eV)! Carbon nanotube are discussed extensively in the literature, and will not be further discussed here.

Convergence of the lattice parameter is achieved at 2.669 Åusing the parameter set
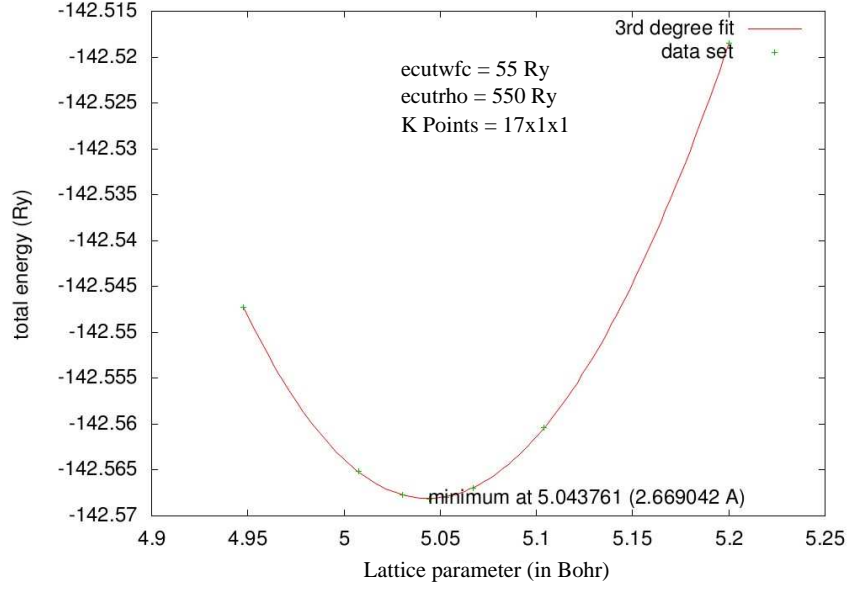
Figure 2.22: Relaxed benzorod, parameter optimization

seen in Figure 2.22. The cubic fit presented in the Figure reads

$$E_{fit}(x) = -0.961718x^3 + 16.731x^2 - 95.3771x + 36.262 \qquad (2.8)$$

using this function, force required to compress structure 0.01 Åis calculated as

$$F_{+0.01} = -1.693026 \times 10^{-9} \, N \qquad (2.9)$$

in turn, Young's modulus comes out to be

$$E = \frac{(-1.693026 \times 10^{-9} \, N)(2.669 \times 10^{-10} m)}{(6.0716 \times 10^{-20} m^2)(0.01 \times 10^{-10} m)} \approx 7442 \times 10^9 \, N/m^2 \qquad (2.10)$$

which is again on par with diamond. However, calculating the Shear modulus for a displacement of $\sim 1°$

$$G = \frac{(8.288844 \times 10^{-12} \, N)}{(6.0716 \times 10^{-20} m^2)(0.02)} = 6.8245 \times 10^9 \, N/m^2 \qquad (2.11)$$

80

it turns out that the rearranged geometry is much more elastic than the previous one. The value is in the vicinity of soft metals such as lead [62].

In the rearranged form, benzorods are not expected to be conductors, trying the place a smearing function proves this (Figure 2.24,2.25).
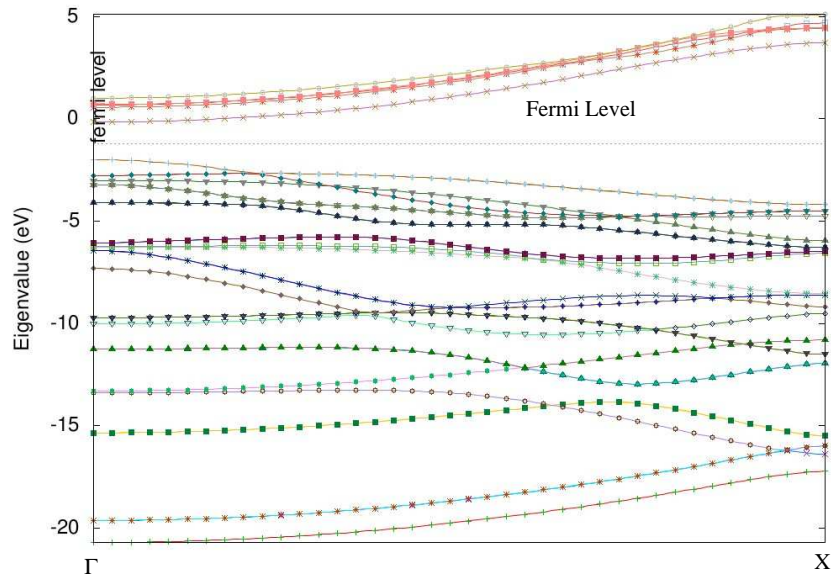
Figure 2.23: Relaxed benzorod, band graph

Band graph in Figure 2.23 proves this fact. The exact value of band gaps in DFT are not always reliable, a different methodology than what is used is required for more precise results. However in rearranged form, benzorod can be considered as a direct gap semiconductor.

There are two distinct atoms in the unit cell, the interconnecting layer atom (atom 2), and the rearranged layer atom (atom 11). Investigating Figure 2.26, it is seen that both atoms are in a state resembling sp^3 hybridization, with a slightly stronger
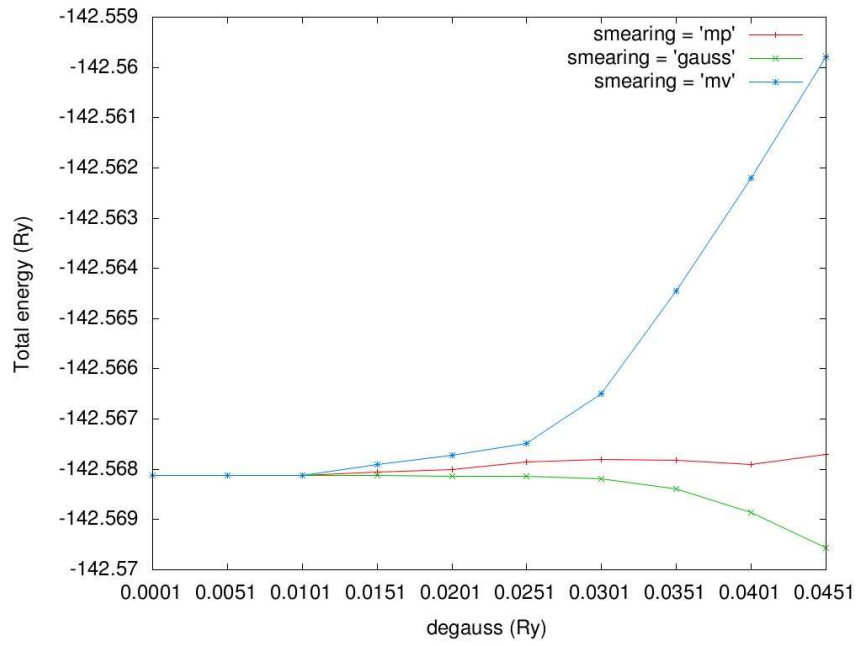
Figure 2.24: Relaxed benzorod, effect of smearing on total energy.
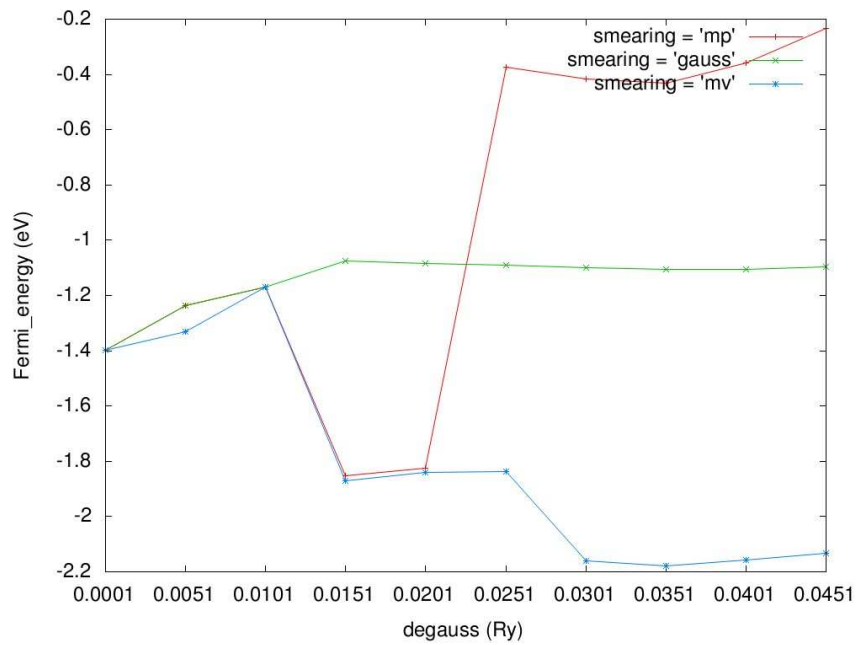
Figure 2.25: Relaxed benzorod, effect of smearing on Fermi level

p character (like in sp^2 hybridization) in interconnecting layer atom. The separation of levels at the vicinity of Fermi level is large, and it is outside the limits of covalent splitting of channels.
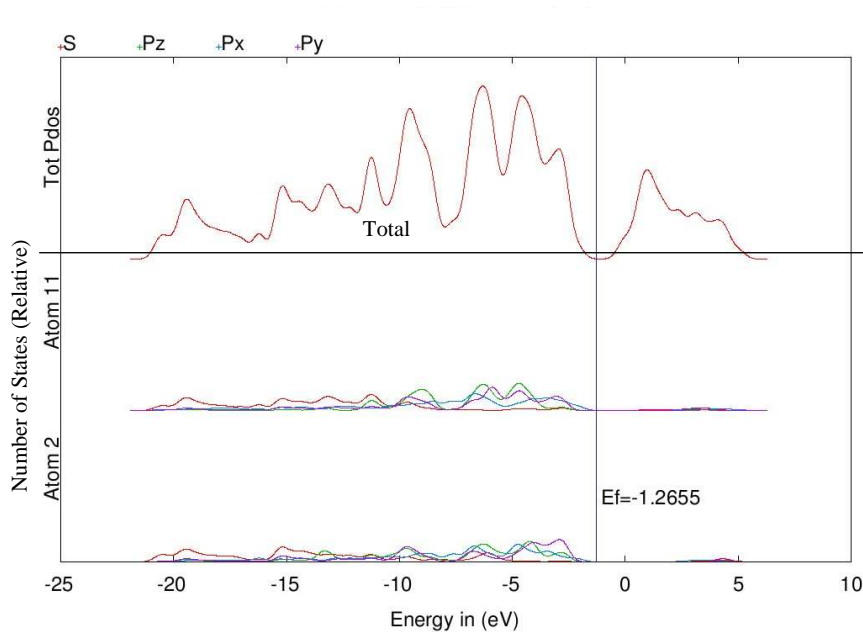
Figure 2.26: Relaxed benzorod, PDOS

Charge density is shown in Figure 2.27. As expected, the inter layer coordination is purely due to covalent bonding.

2.4 Conclusion

MD calculation presented in the first part predict that benzorod is thermally stable, with a rearrangement of geometry at elevated temperatures. Furthermore, coordination with aromatic surfaces and nanocages are predicted to be possible, with little impact on the coordinated species at lower temperatures. As a macromolecular entity, benzorod

has a length limit, the structure is eventually prone to bending.
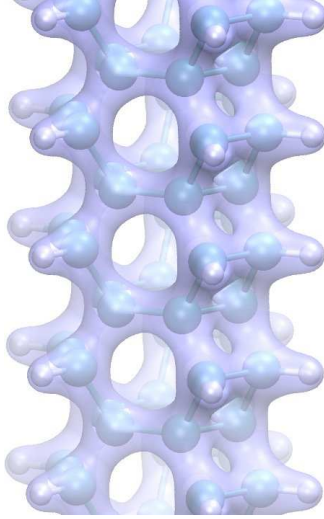
Figure 2.27: Relaxed benzorod, charge density

DFT calculations show that the structure is energetically stable as well. Binding energy per atom in the ideal benzorod is $E_b = -6.0$ eV. The rearranged geometry has slightly lower binding energy $E_b = -6.3$ eV, but without the presence of hydrogen the unit cell transforms into that of an armchair nanotube which has considerably lower binding energy $E_b = -7.9$ eV. This is an interesting transformation, it may indicate that hydrogenation of a carbon nanotube results in cubane like formations on the surface and rearranges the nanotube into the relaxed benzorod geometry via an endothermic reaction. Noting the significant difference of elastic constants and band structure between the two geometries, this transformation may be utilized in tuning the properties carbon nanomaterials.

The ideal benzorod geometry is conducting, with more than one channel, and calculated elastic properties are comparable with that of diamond. Adding this the small cross-section area, this structure is quite promising for field emission applications such

84

as STM tips.

The rearranged form is quite resistant to compression, however, unlike the ideal geometry, very susceptible to shearing forces. The rearranged form is also a direct band semi-conductor instead of being a conductor.

Note: This chapter is based on published works [63, 64, 65]

CHAPTER 3

BAMBOO SHAPED SINGLE WALL CARBON

NANOTUBES

3.1 Carbon nanotubes

Carbon nanotube (CNT) [61] is probably the most reknown and popular nanostructure within this context.

The carbon nanotubes have many varieties, and all these various forms have their own subgroups, resulting in a huge family of materials. However, generally, majority of attributes common in members are due to properties of single wall carbon nanotube (SWCNT). Thus, a solid understanding of the intrinsics of this particular one is a necessity for studying carbon nanotubes in general. The discussion in this section is intended to be a short introduction limited, but the reader is encouraged to proceed further (For example see [66]).

Single wall carbon nanotube structure consists of sp^2 hybridized carbon atoms. The corresponding wavefunction for this hybridization scheme is:

$$\left| sp_a^2 \right\rangle = C_1 \left| 2s \right\rangle - \sqrt{1 - C_1{}^2} \left| 2p_y \right\rangle \tag{3.1}$$

$$\left| sp_b^2 \right\rangle = C_2 \left| 2s \right\rangle - \sqrt{1 - C_2{}^2} \left\{ \frac{\sqrt{3}}{2} \left| 2p_x \right\rangle + \frac{1}{2} \left| 2p_y \right\rangle \right\} \tag{3.2}$$

$$\left| sp_c^2 \right\rangle = C_1 \left| 2s \right\rangle - \sqrt{1 - C_1{}^2} \left\{ -\frac{\sqrt{3}}{2} \left| 2p_x \right\rangle + \frac{1}{2} \left| 2p_y \right\rangle \right\} \tag{3.3}$$

the three unknown coefficients are solved using the already known orthogonality relations of the $\left| sp^2{}_i \right\rangle$, $\left| 2s \right\rangle$, and $\left| 2p_{x,y} \right\rangle$:

$$C_1{}^2 + C_2{}^2 + C_3{}^2 = 1 \tag{3.4}$$

$$C_1 C_2 - \frac{1}{2}\sqrt{1 - C_1{}^2}\sqrt{1 - C_2{}^2} = 0 \tag{3.5}$$

$$C_1 C_3 + \frac{1}{2}\sqrt{1 - C_1{}^2}\sqrt{1 - C_3{}^2} = 0 \tag{3.6}$$

yielding $C_1 = C_2 = 1/\sqrt{3}$ and $C_3 = -1/\sqrt{3}$. The resultant geometry for the combined orbitals is the co-planar equidistant angular-wise configuration we see.

Due to common hybridization scheme, it is no surprise that in defining the geometry and electronic properties of a single wall carbon nanotube, graphene layer is often used as a starting point. Geometrical details of graphitic lattice are presented in Figure 3.1.
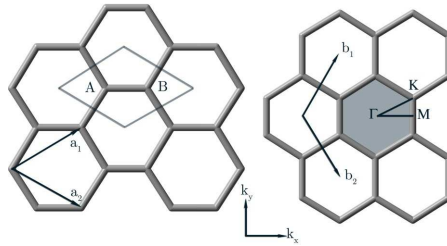
Figure 3.1: Graphene sheet. (a) the unit cell. (b) Brillouin zone. Points Γ, K, and M are used for obtaining dispersion relations. Points A and B are the two dissimilar carbon atoms in the unit cell [66]. $\vec{a}_1 = \left(\frac{\sqrt{3}}{2}a, \frac{a}{2} \right)$, $\vec{a}_2 = \left(\frac{\sqrt{3}}{2}a, -\frac{a}{2} \right)$

One of the most interesting points in a graphene sheet is its electronic configuration. The non hybridized p orbitals of carbon lead to a behavior called aromaticity, which result in the mobility of electrons in this particular geometry. The lattice is conducting due to continuous overlap of phase space electronic wavefunction at consequent cells, but not quite like the mobility of electrons encountered in metals. In fact, the graphene layer is called a "zero band semiconductor" for this property. The mobility, as mentioned before, is geometry related, and should the lattice geometry be distorted, a band gap could be observed.

This is exactly what happens in a single wall carbon nanotube. The bulk of the structure is analogous to a graphene sheet rolled into a cylindrical shape. This is a direct intervention to unit cell periodicity without disturbing sp^2 nature significantly, thus, there is a relation between the bulk geometry and band gap. Term "bulk" is used here, since the resultant structure can be considered as a one dimensional crystal. Consequently, it is possible to name a single carbon nanotube after its unit cell (however, such a name will not cover any information about the "caps"). The vectors used to define a single wall carbon nanotube unit-cell from graphene are shown and described in Figure 3.2, and Table 3.1 respectively.

It is clearly seen that these vectors are interrelated, making most of them redundant in naming a structure. In fact, the unit-cell can be uniquely identified by choosing only one of them. A common practice is to use the chiral vector C_h. In this naming scheme the composition of C_h in terms of graphene plane unit vectors is used, in the form of C(n,m), where n and m are integers corresponding to this composition. Since the electronic behavior directly depends on the geometry, this name also serves in identifying the conduction characteristics .

The primary symmetry classification of a SWCNT is either being chiral or achiral. There are only two distinct cross–sectional geometries that the structure can be oriented in achiral form, namely the armchair and the zigzag configurations. Nomenclature arises
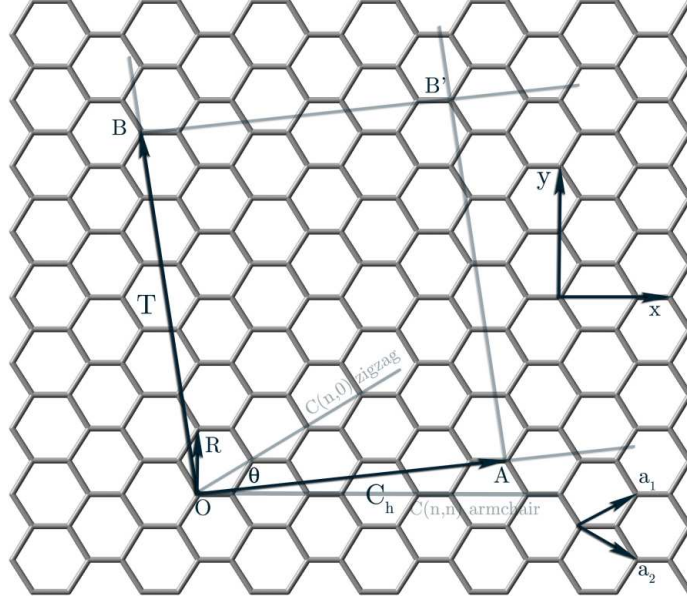
Figure 3.2: The unrolled honeycomb lattice of a SWCNT [66] . In short, the unit-cell is formed when the sheet is rolled such that points O and A coincide, rest follows from the definitions.

from the shape of the cross section (Figure 3.4). All the other possible orientations are called chiral, having non–superposable axial mirror images.

Length of the chiral vector gives the circumference of cross section by definition. Since $\vec{a}_1$ and $\vec{a}_2$ are not orthogonal to each other in Cartesian coordinate system length of the chiral vector is found using:

$$\vec{a}_1.\vec{a}_1 = \vec{a}_2.\vec{a}_2 = a^2, \ \vec{a}_1.\vec{a}_2 = \frac{a^2}{2} \tag{3.7}$$

$$\left|\vec{C}_h\right| = \sqrt{\vec{C}_h.\vec{C}_h} = a\sqrt{n^2 + m^2 + nm} \tag{3.8}$$

using this length, diameter of the tube can be found as :

$$d_t = \frac{\left|\vec{C}_h\right|}{\pi} \tag{3.9}$$

the diameters of some selected tubules are presented in Table 3.2.

Table 3.1: Parameters for Carbon Nanotubes[a] (adapted from [66]).

symbol	name	formula	value
$\vec{C}_h$	chiral vector	$\vec{C}_h = n\vec{a}_1 + m\vec{a}_2$	$0 \leq |m| \leq n$
θ	chiral angle	$\sin\theta = \frac{\sqrt{3}m}{2\sqrt{n+m+nm}}$	
		$\cos\theta = \frac{2n+m}{2\sqrt{n+m+nm}}$	$0 \leq |\theta| \leq \frac{\pi}{6}$
		$\tan\theta = \frac{\sqrt{3}m}{2n+m}$	
a	length of unit vector	$a = \sqrt{3}a_{\text{C-C}} = 2.49\text{Å}$	$a_{\text{C-C}} = 1.44\text{Å}$
$\vec{a}_1, \vec{a}_2$	unit vectors	$\left(\frac{\sqrt{3}}{2}, \frac{1}{2}\right)a, \left(\frac{\sqrt{3}}{2}, -\frac{1}{2}\right)a$	x, y coordinate
$\vec{b}_1, \vec{b}_2$	reciprocal lattice vectors	$\left(\frac{1}{\sqrt{3}}, 1\right)\frac{2\pi}{a}, \left(\frac{1}{\sqrt{3}}, -1\right)\frac{2\pi}{a}$	x, y coordinate
d	$\gcd(n, m)$[b]		
d_r	$\gcd(2n+m, 2m+n)$[b]	$d_R = \begin{cases} d & \text{if } (n-m) \text{ is a multiple of } 3d \\ 3d & \text{if } (n-m) \text{ is not a multiple of } 3d \end{cases}$	
$\vec{T}$	translational vector	$\vec{T} = t_1\vec{a}_1 + t_2\vec{a}_2$	
	$\gcd(t_1, t_2) = 1$	$t_1 = \frac{2m+n}{d_R}, t_2 = -\frac{2n+m}{d_R}$	
T	length of $\vec{T}$	$T = \frac{\sqrt{3}L}{d_R}$	
N	Number of hexagons in unit cell	$N = \frac{2(n+m+nm)}{d_R}$	
$\vec{R}$	symmetry vector	$\vec{R} = p\vec{a}_1 + q\vec{a}_2$	$\gcd(t_1, t_2) = 1$
τ	pitch of $\vec{R}$	$\tau = \frac{(mp-nq)T}{N} = \frac{MT}{N}$	
ψ	rotation angle of $\vec{R}$	$\psi = \frac{2\pi}{N}$	in radians
M	number of $\vec{T}$ in $N\vec{R}$	$N\vec{R} = \vec{C}_h + M\vec{T}$	

[a] In this Table n, m, t_1, t_2, p, q are integers and d, d_R N and M are integer functions of these
[b] $\gcd(n, m)$ is the greatest common divisor of integers n and m

3.2 Bamboo shaped carbon nanotubes

The cylindrical geometry of carbon nanotube arises an interesting question: What is the source of the curvature? Knowing that the ground state of such graphitic carbon is planar, there has to be a process causing this (stress inducing) curvature somewhere at the synthesis. One of the first among the numerous mechanisms that come into mind is a pentagon "defect". Looking at the orbital composition of carbon sp^2 hybrid discussed in the previous section, and putting the corresponding atomic wavefunctions in place,
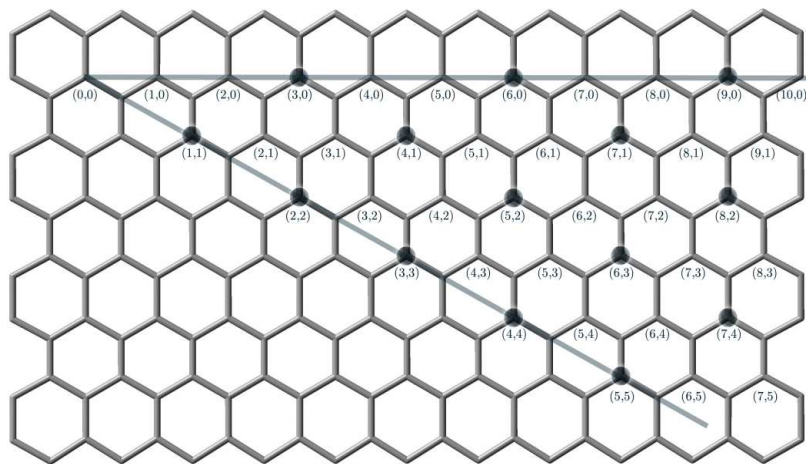
Figure 3.3: Electronic structure of carbon nanotubes as a function of chiral vector, Indicated dots represent metallic nanotubes.

the geometry of "bonds" turn out to be arranged in a planar fashion 120° apart, which is clearly the reason of the hexagonal appearance of graphene layer. Even by simple deduction, it is easy to predict that any other polygonal arrangement is in conjunction with a disturbance in the overall geometry, especially the planar nature (along with other changes, of course, [68]). Consequently, these "other" polygonal arrangements can be labeled as defects, and some molecules can be considered as the carrier of these defects[1]. The pentagon defect is particularly important, due to its common appearance as the source of curvature in organic or graphitic carbon. It is now known that such curvature inducing elements play an important role in single wall carbon nanotube formation [69, 70].

In this chapter, a relatively recent addition to carbon nanotube related structure

---

[1]The label "defect" is meaningless in a macromolecular point of view. The label just points out the presence of curvature inducing elements.
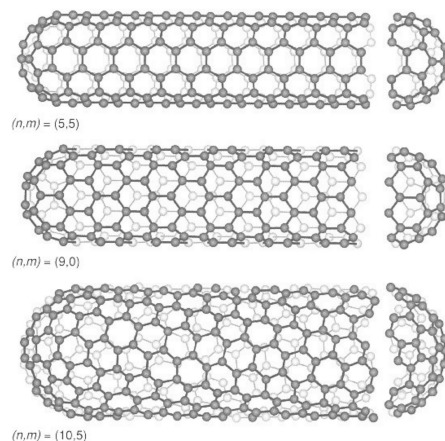
Figure 3.4: Cross sectional geometries of a SWCNT. Top: Armchair; Middle: Zigzag; Bottom: Chiral. Here (n,m) correspond to integers forming the chiral vector [67].

family is examined: The bamboo shaped carbon nanotubes [71, 72, 73, 74, 75]. Nomenclature comes from the overall appearance, geometrical abberations of these (periodically) compartmented multi wall carbon nanotubes resemble a bamboo plant. Experimental work suggest that intersecting layers forming the compartments are either precipitation of the catalyst material, or a graphitic interlayer. A single wall bamboo shaped carbon nanotube is not experimentally observed yet, but this example demonstrates that it may very well be feasible with the help of an organic molecule called coronene.

Assume that in the above mentioned non-catalytic growth process, the triggering effect of folding in a specimen of graphite was not the single pentagon in the center of corannulane, but a series of pentagons at the circumference of coronene. This is energetically less probable, but nevertheless possible. Resultant structure would be a carbon nanotube with dictated diameter. Furthermore, the structure of coronene permits periodic compartmenting similar to graphitic inter-layers observed in multi-walled

Table 3.2: Diameters, d (in Å), of ideal carbon nanotubes in zigzag, C(n,0); armchair, C(n,n); and chiral, C(n,m), m<n, m≠0, models ($a_{c-c} = 1.42$ Å for this case).

C(n,m)	d	C(n,m)	d	C(n,m)	d	C(n,m)	d
C(2,0)	1.5669	C(2,1)	2.0728	C(7,1)	5.9148	C(9,3)	8.4742
C(3,0)	2.3503	C(3,1)	2.8247	C(7,2)	6.4127	C(9,4)	9.0351
C(4,0)	3.1338	C(3,2)	3.4149	C(7.3)	6.9634	C(9.5)	9.6271
C(5,0)	3.9172	C(4,1)	3.5902	C(7,4)	7.5552	C(9,6)	10.2448
C(6,0)	4.7006	C(4,2)	4.1456	C(7,5)	8.1793	C(9,7)	10.8839
C(7,0)	5.4841	C(4,3)	4.7655	C(7,6)	8.8289	C(9,8)	11.5408
C(8,0)	6.2675	C(5,1)	4.3620	C(8,1)	6.6937	C(10,1)	8.2540
C(9,0)	7.0510	C(5,2)	4.8926	C(8,2)	7.1803	C(10,2)	8.7240
C(10,0)	7.8344	C(5,3)	5.4841	C(8,3)	7.7160	C(10,3)	9.2366
C(2,2)	2.7139	C(5,4)	6.1189	C(8,4)	8.2911	C(10,4)	9.7851
C(3,3)	4.0709	C(6,1)	5.1374	C(8,5)	8.8982	C(10,5)	10.3639
C(4,4)	5.4278	C(6,2)	5.6495	C(8,6)	9.5309	C(10,6)	10.9681
C(5,5)	6.7848	C(6,3)	6.2184	C(8,7)	10.1847	C(10,7)	11.5938
C(6,6)	8.1417	C(6,4)	6.8299	C(9,1)	7.4735	C(10,8)	12.2377
C(7,7)	9.4987	C(6,5)	7.4735	C(9,2)	7.9510	C(10,9)	12.8970
C(8,8)	10.8556						
C(9,9)	12.2126						
C(10,10)	13.5696						

counterparts. Symmetry will hopefully manage the high stress in such a compartmented structure, and the idea may be carried on further, for bigger single wall bamboo shaped nanotubes, although they would be less and less viable.

The dictated nanotube geometry by the coronene in this scheme is C(12,0). Resultant structure is shown in Figure 3.5. Bamboo shape of the structure results from the different diameters of the C(12,0) nanotube and the coronene. There are 6 pentagons in the C(12,0) - coronene connection, along with 6 distorted hexagons. These pentagons and highly bent hexagons are the major source of stress, but the forces are perfectly balanced out due to symmetry. In a sense, the structure is "locked" to be in this geometry due to symmetry. There is no physical argument requiring the periodicity of the structure at this point, however, this example will serve good in experimenting with PBC for periodic structures. It should be restated at this point that a periodic boundary condition is always in effect in a molecular dynamics study employing NVT criteria. What is meant by "with PBC" is that the periodic boundary condition is used for periodic repetition of the structure at hand, rather than placing the boundary at
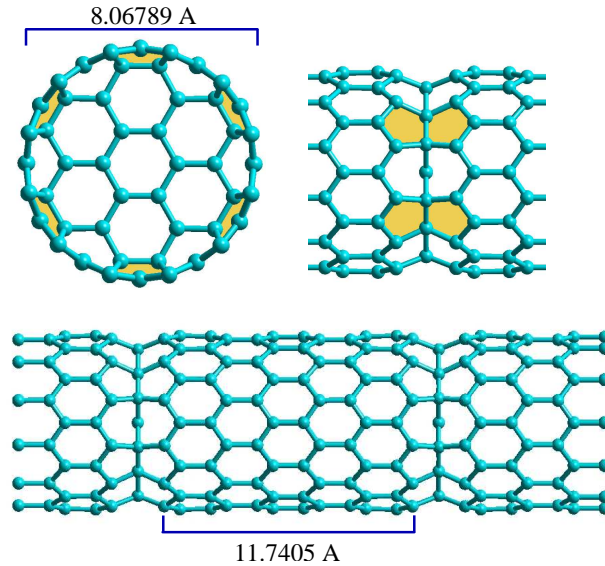
Figure 3.5: Structural details of the Single–walled carbon bamboo nanotube. The pentagons in the bamboo region are shown in the upper part. The length of the tubular section in the initial structure is shown in the bottom.

an abstract distance. With a simple arrangement at both ends, the structure may be prepared for repetition. This is similar to unit cell concept in solid state physics, the geometry should be such that with consequent repetitions, a continuous and periodic body should be obtained. However, there is no explicit restriction on size, the particular unit may as well contain many sub-units itself. A one dimensional periodicity is planned in this example, so the only consideration is, when the geometry is repeated on the left or right several times, do we obtain a continuous structure? By arranging the length of tubular sections after compartment in the left end right, this can be taken care of. The unit is big enough to observe behavior in the vicinity of compartmenting layers, and the compartment itself, smaller units risk too much intervention of periodicity criteria.

The results of molecular dynamics are shown in Figure 3.6. There is a slight, nonetheless noticeable, difference in results with and without PBC. Both results agree
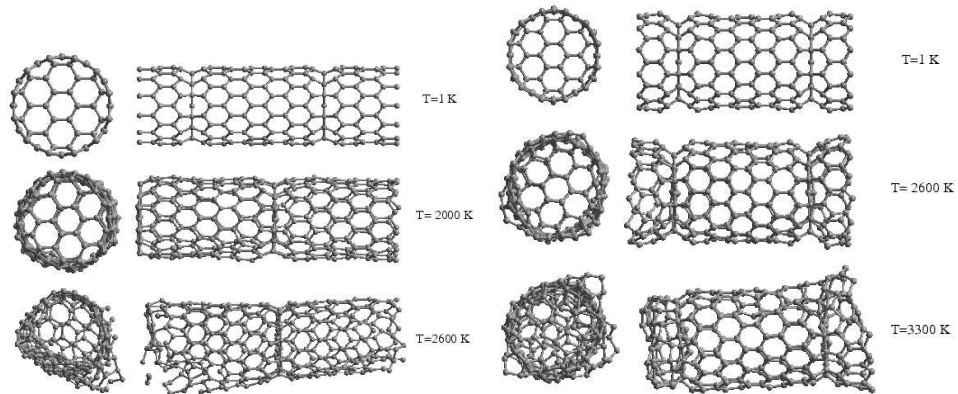
Figure 3.6: Molecular dynamics results at various temperatures, with and without PBC respectively.

that the structure is stable up to elevated temperatures, in agreement with the symmetry balancing force hypothesis. However, the structure without periodicity seems to be slightly more stable. Furthermore, the weakest point in periodic structure turns out to be the vicinity of bamboo region, whereas in the non periodic structure the tubular section collapses. Why is it so? First of all, lets begin by comparing the non periodic result with Figure 3.5. Without the periodicity, the length of the tubular section between the intersections shrink to 8.55 Å. This is due to a small re-alignment of the pentagon hexagon pairs in the bamboo region (Figure 3.7). There is a significant kink close to bamboo region due to this re-alignment. In the re-aligned shape, pentagons are more planar, and it turns out that this increases stability. This is a typical example how the structure re-aligns in a dynamical situation. The periodicity for PBC is calculated using an energy optimal geometry, which is not necessarily same in a dynamical state with finite temperature. Thus, in this particular example the periodic structure is slightly elongated, as if something is pulling it from both sides. This is due to number of particles in the periodic box being constant.

Electronic properties of the structure is calculated at the Extended Huckel level [76]. This is a semi emprical method useful for predicting chemical properties such as
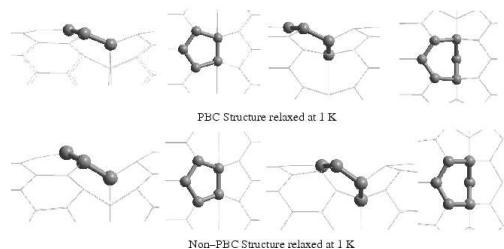
Figure 3.7: Pentagon and Hexagon geometry in the relaxed structures with and without PBC.

molecular orbitals and electronic configuration of very large systems. Structural geometry related calculations using this method are unreliable, thus the results of molecular dynamics at 1 K are used directly. Charge distribution and charge density on the structure are shown in Figure 3.8. There are no significant abberations in the charge density. Charge distribution at the vicinity of the bamboo regions is uneven. This is expected due to lack of PBC and asymmetry of the region, but it is seen that Coronene acts as a barrier effecting the overall distribution. A band study of the structure may yield
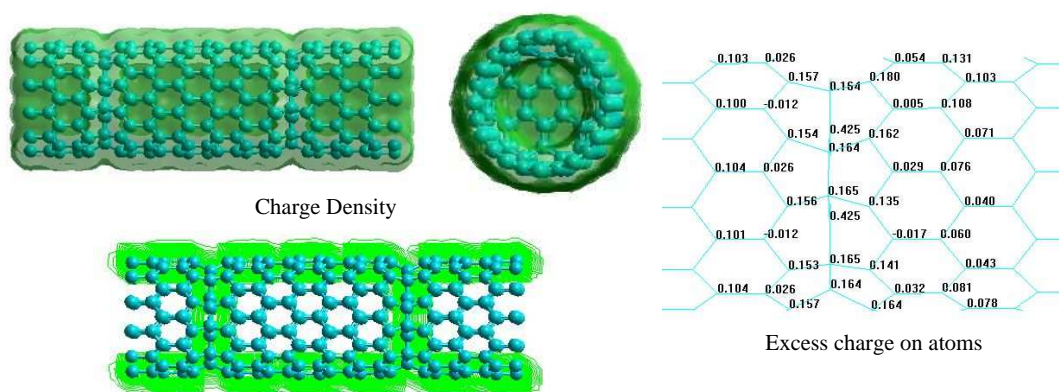
Figure 3.8: Charge Density and charge distribution of the structure.

interesting behavior.

Molecular orbital graphs are presented in Figure 3.9. It is seen that because of Coronene spacers, most of the molecular orbitals are not continuous through the structure. This is also the case for the highest occupied and lowest unoccupied (HOMO, LUMO) orbitals. This may indicate an effective barrier in band structure. Apart from that, HOMO and LUMO orbitals are placed very close in the energy spectrum, and frontier band gap is negligible. The spectrum is continuous upto and above Fermi level. Continuity is maintained upto slightly above the 0 eV level. Although this spectrum corresponds only to zero momentum point in a band graph, due to localization of molecular orbitals and continuous behavior of the eigenvalue spectrum, it is highly probable that the conducting behavior of the tubular section is unaltered.
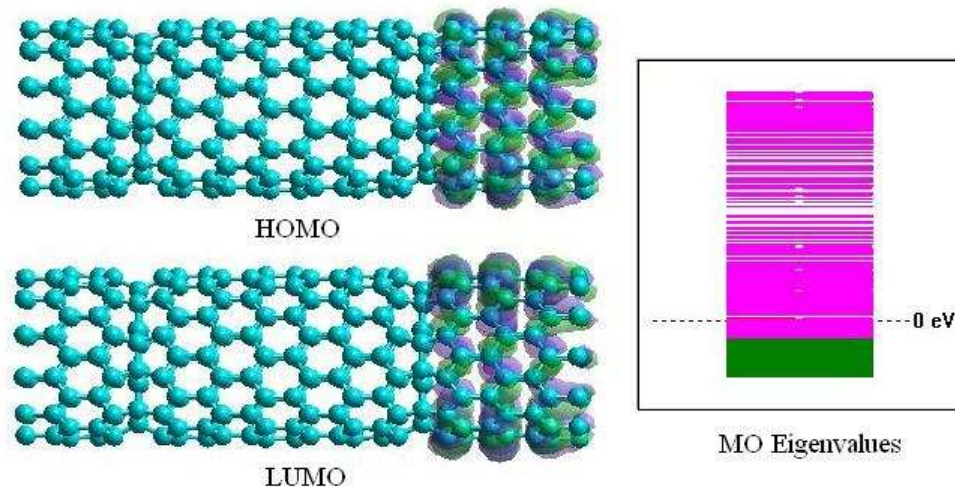
Figure 3.9: Plots of the highest occupied and lowest unoccupied molecular orbitals (HOMO-LUMO) and eigenvalue spectrum.

Note: This chapter is based on published work[77]

CHAPTER 4

FUNCTIONALITY OF C(4,4) CARBON NANOTUBE

AS MOLECULAR DETECTOR

4.1   Introduction

One application of carbon nanotubes is functionalization as a high precision detector for chemicals at the molecular level [78]. Detectors of this kind are highly anticipated in industry and commercial applications, mostly in security. Due to cylindrical symmetry, the carbon nanotube has a large surface area, and electronic properties are drastically altered with disruption of the surface configuration. In this respect, it is an ideal receptor for a detector. However, there are a couple of problems in realization of such a detector.

Geometry and hybridization dependence of the Carbon nanotube translate into alterations in electronic conductance with the disruption of the surface. However, due to chemically inert nature, not all elements can interact with a carbon nanotube. This drawback is most commonly overcome by using intermediate receptors, organic or otherwise [79]. Although the number of chemicals that can be detected is drastically

increased, the effective surface area is reduced, and additional problem of interaction of intermediate material with nanotube is introduced. In some of the rare cases, especially in highly reactive chemicals, the intermediate material can be bypassed [80, 81, 82, 83]. High surface area and detection even at single molecular level features may be exploited in a potential application in this case. Increasing the surface curvature increases the tension on the sp^2 hybridized carbon, thus a carbon nanotube with smaller diameter should be more susceptible to surface intrusion.

Another problem in realization of a detector is the ever-present environmental fluctuations. Carbon nanotubes are quite flexible, thus in a typical exposed environment, significant vibrational modes are present, thermal or otherwise. These geometrical vibrations show as fluctuations in the conductance. Any detectable alteration in conductance thus should be significant enough to be observable among these, or alter the structural behavior itself. Use of smaller diameter nanotubes increases the stiffness and alterations in the conductance become more significant.

Electron transport at nano scale is a quantum concept [84, 85]. This is due to mean free path of electrons being comparable or larger than the characteristic length of the structure of interest. In this case, quantum coherence effects become significant and classical approaches are mostly inadequate. Thus, a more delicate approach is required. Calculation of electron distribution is a requirement for most general cases. Once the distribution is established, one of the available non-equilibrium techniques is employed to solve transport equations. In addition to fundamental limits imposed by quantum transport theory, the overall conductance behavior is determined by quantum effects at the interfaces, the most dominant of which are being the overlap of consequent orbitals and broadening of levels. Any realistic model for transport calculation should at least incorporate these factors. Since conductance is calculated at the quantum level, each problem is quite specific to its geometry and electronic configuration. The question of identifying chemical by the features of I-V trace is an open question.

4.2 Method of Calculation

Single wall Carbon nanotube (SWCNT) C(4,4) is used as the medium in this calculation. In the common nomenclature, which is also used in this work, integers n and m in C(n,m) represent the composition of chiral vector in terms of graphitic unit vectors. This uniquely defines the unit cell of SWCNT, and thus its general electronic behavior. Like all armchair nanotubes, C(4,4) exhibit metallic conductance behavior.

The first step in the calculation is to obtain a stable geometry for the activated carbon nanotube. Gaussian package is used in this part of the calculation [86]. Various toxic and/or corrosive chemical agents are investigated for the possible activation of C(4,4). Each agent is placed in all of the typical sites over one of the hexagons towards the center of the nanotube, with various orientations, and a geometry relaxation procedure is invoked at PM3 level. Without the bond conservation restriction, this procedure serves as a method for both finding/testing a stable orientation for the tested agent and obtaining a relaxed geometry for the activated SWCNT. The atoms at both ends of the C(4,4) segment used in this part are held fixed, in order to maintain geometrical consistency with the ideal unit cell geometry used in electrode regions. Several chemicals were unable to form a stable bond with the surface in all of the tested setups, and these molecules are omitted in this context. The discussed activations of the C(4,4) surface are due to HCN, Cl_2 and CNCl molecules individually.

Transiesta-C package is used in the calculation of transport properties [88]. The package is based on and developed from the McDCal, Siesta and TranSiesta programs [90, 91, 92, 93]. The unique feature of this package is the ability to simulate open systems, in which an applied bias difference drives a current. The system is treated in three parts, right electrode, scattering region, and left electrode. The "electrodes" are treated as bulk, and in a separate calculation effective potential is calculated. Non - equilibrium Greens function (NEGF) technique is then employed in a self consistent fashion to solve corresponding effective potential in the scattering region [89]. The

procedure used in the package is as follows: First, using an initial guess for the potential, Hamiltonian Matrix is formed using localized basis sets. The Hamiltonian matrix is used to setup the NEGF of the system. In the next step the non-equilibrium density matrix is calculated from the NEGF. The density matrix defines the effective potential in the scattering region, and thereby new set of Hamiltonian parameters. The steps are repeated until a self-consistent solution is found.

In a typical case, electrodes are chosen to be metal crystals, and act as electron reservoirs. However, in this case, the point of interest is the change in the transport behavior of carbon nanotube, and use of metal electrodes complicates the results with non-trivial surface overlap matrices and consequent non-linear effects. C(4,4) ideal geometry has a nearly constant density of states (DOS) spectrum in a wide range and it is quite suitable for an electrode. In this way, an infinite carbon nanotube with a single molecule attached is simulated with an assumption of contacts at infinity.

The procedure of calculation of surface matrices and non-equilibrium electron density are handled intrinsically in Transiesta-C. Control of the procedure is mainly limited to defining cutoffs and ranges. Due to number of atoms involved, Single-Zeta type orbitals, and LDA exchange correlation functional of Perdew and Zunger is employed.

After calculating the relaxed geometry for the scattering region, the electrodes are attached to suitable sites, and Transiesta-C electronic calculation described above is invoked. Next, by increasing chemical potential of either the left or right electrode correspondingly, a bias is created. In steps of 0.1 eV, calculation is performed up to 1 eV, for both negative and positive bias. This energy is quite lower than the binding energy of the species considered, and it is seen that the changes in the DOS (MPSH) of the scattering region is insignificant, thus the perturbative approach mentioned above holds. Since the system is a conductor, Fermi-Dirac smearing at a temperature of 300 K is considered in all of the calculations.

4.3 Results and Discussion

There are three activated C(4,4) models in the context of this calculation. The models are named according to the molecule attached to the surface of the carbon nanotube, Cl_2, CNCl, and HCN. For comparison purposes, a limited calculation on clean C(4,4) geometry is also performed. Figures 4.1-4.9 show different volumetric graphs, and representations of the optimized geometry of scattering regions . There are three figures for each model considered. Two volumetric graphs presented along with the geometry in the first Figure of each model are the maximum intensity projection of the effective potential and the difference between the atomic electronic density and the self-consistent one (referred as V_{eff} and ρ henceforth) at zero bias. Next two figures contain a series of graphs showing differences in effective potential (ΔV_{eff}), and differences in ρ ($\Delta \rho$) with respect to zero bias result, under potential difference. Darker shades of blue represent more negative values in both types of volumetric graphs, and, if used, darker shades of red correspond to larger values. DOS, molecular projected self consistent eigenvalues (MPSH) spectrum for all the models considered are given in Figure 4.10. Transmission spectrum and I-V trace are presented in Figures 4.11 and 4.12 respectively.

The geometry optimized result of the Cl_2 model is shown in Figure 4.1. After the geometry optimization procedure, Cl_2 disassociate, and two chlorine atoms attach separately to two carbon atoms (at top position) on the surface. With the change in coordination number, the geometry and aromaticity in the immediate vicinity of the activation site is altered. Although the geometrical aberrations seems not extravagant, the electronic structure is altered significantly due to high electronegativity introduced by the Chlorine atoms. In both V_{eff} and ρ graphs, electronegativity of chlorine atoms is visible. An effective potential barrier is observable in V_{eff} graph. V_{eff} is interlinked with the Fermi level, thus this graph is a measure of how much the internal electronic structure, especially the DOS, alters in the middle region. In all the models considered, the barrier due to scattering region manifests itself as a hourglass like spatial geometry
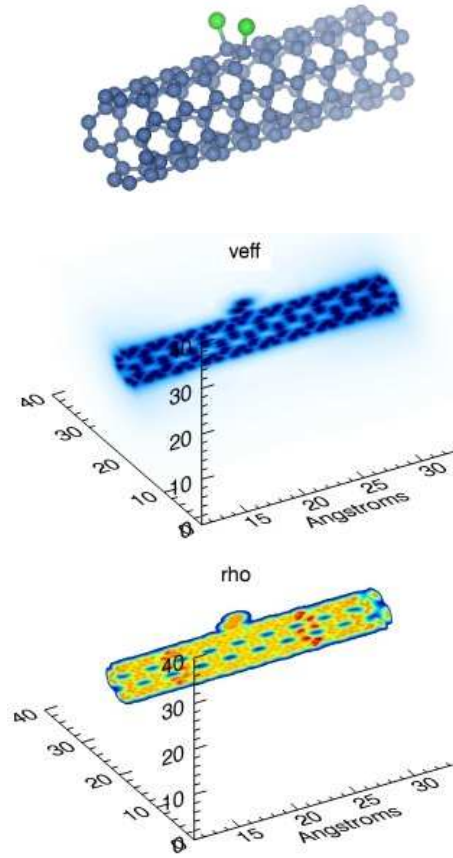
Figure 4.1: Cl_2 model, and maximum intensity projections for effective potential and electron density.

in V_{eff} distribution, around the footprints of atoms. The strength of barrier can be interpreted from the change in intensity along the body. In this respect, the Cl_2 model has a less stronger barrier compared to the CNCl model. Although, under increased bias the barrier may alter drastically, it is seen that V_{eff} graphs at zero bias give a good estimate on drop of conduction in the I-V trace.

The most significant observation in ρ graph is the buildup of electrons at the electrode interface surfaces. This is inevitable due to high electronegativity of the Chlorine. The saturation tendency in the IV graph can be attributed to this accumulation. It may be argued that this charge accumulation is purely due to method of calculation,

and in an ideal case it should disappear. However, when a highly electronegative species is present, charging of the contact region is inevitable in a realistic case, and the accumulation encountered here can be considered as a crude approximation of it. Also, as expected, chlorine atoms have a large electron density around them, and under certain conditions, this charged region may act as the capacitor region in a field effect device (FET).
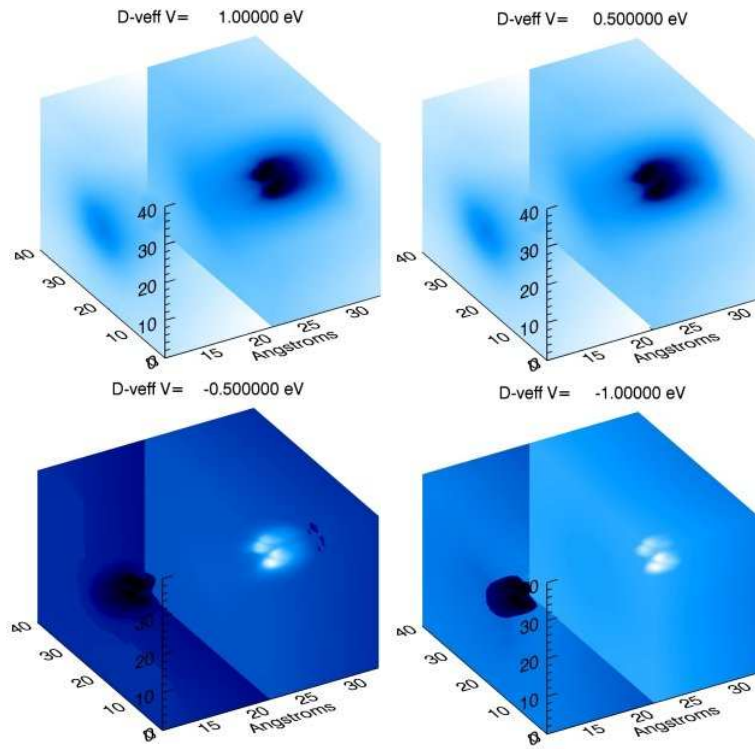
Figure 4.2: Difference effective potential maximum intensity projections for Cl_2 model (relative to 0 eV).

Figures 4.2 and 4.3 contain ΔV_{eff} and $\Delta\rho$ series. The graphs are prepared such that the scattering region is centered at $x = 0$, for easier distinction of behavior at left and right electrodes. In the ΔV_{eff} series, a strong energy barrier is observed at the
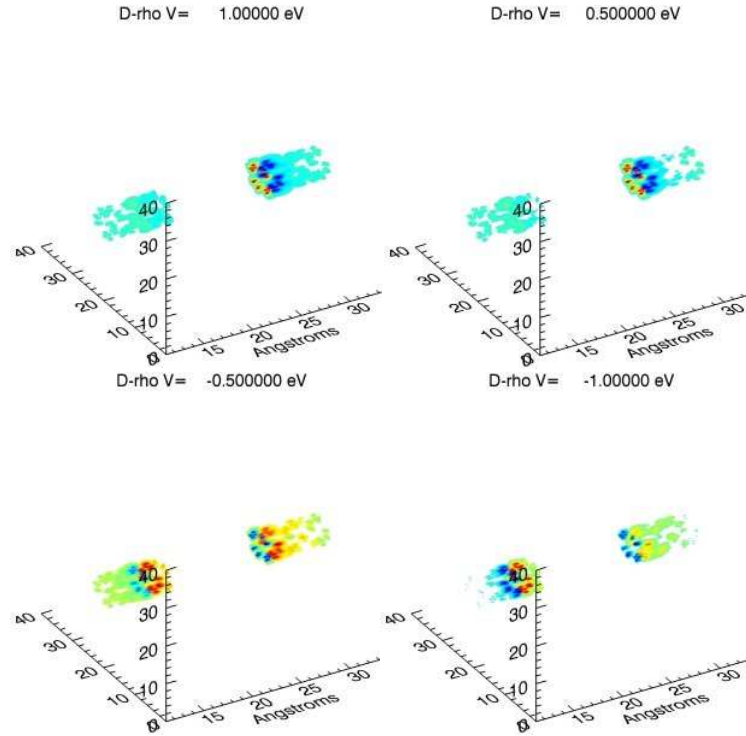
Figure 4.3: Difference electron density maximum intensity projections for Cl_2 model (relative to 0 eV).

vicinity of Chlorine. This indicates an interruption of conduction channels, as for an uninterrupted channel, the variation should be homogeneous through all the scattering region. There is a clear distinction in negative and positive bias, which manifests itself as asymmetric I-V trace. The underlying reason for this is the asymmetry in the position of chlorine atoms, and the resultant unidirectional field at the center. There is a saturation behavior observed in the I-V graph, as expected, and the structure is saturated more readily in positive bias. In the $\Delta\rho$ series, it is seen that the charge accumulation on the electrode region boundary increase with applied bias. The surface closer to the Chlorine atoms tends to accumulate charge more, and in reverse bias, the structure is more hesitant to deplete this charge, which explains the behavior at I-V trace. In a more realistic case, this asymmetric behavior is most likely to disappear. Overall, the
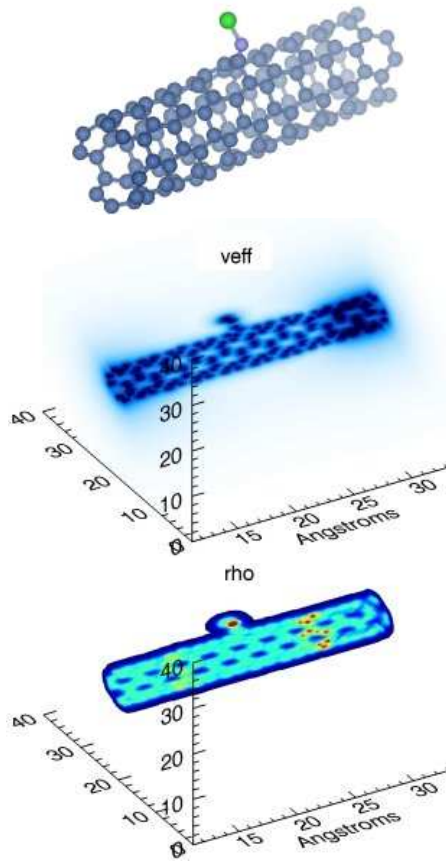
Figure 4.4: CNCl model, and maximum intensity projections for effective potential and electron density.

structure can be modeled as a leaky capacitor, with ohmic behavior under certain bias.

Looking at the CNCl model in Figure 4.4, the first thing to note is the orientation of molecule. In fact, a stable orientation with molecule oriented parallel to the surface can not be found using the method at hand. Even at 0 bias, there is a buildup of electrons on the surface, meaning a significant repulsion from the middle region. In overall, the weakest conductance is observed in this model. Also, this model has the strongest V_{eff} barrier using the considerations presented above. The electron density in ρ graph peaks slightly above the nanotube, approximately at N-Cl bond. Chlorine again has a significant footprint observed in V_{eff} graph.
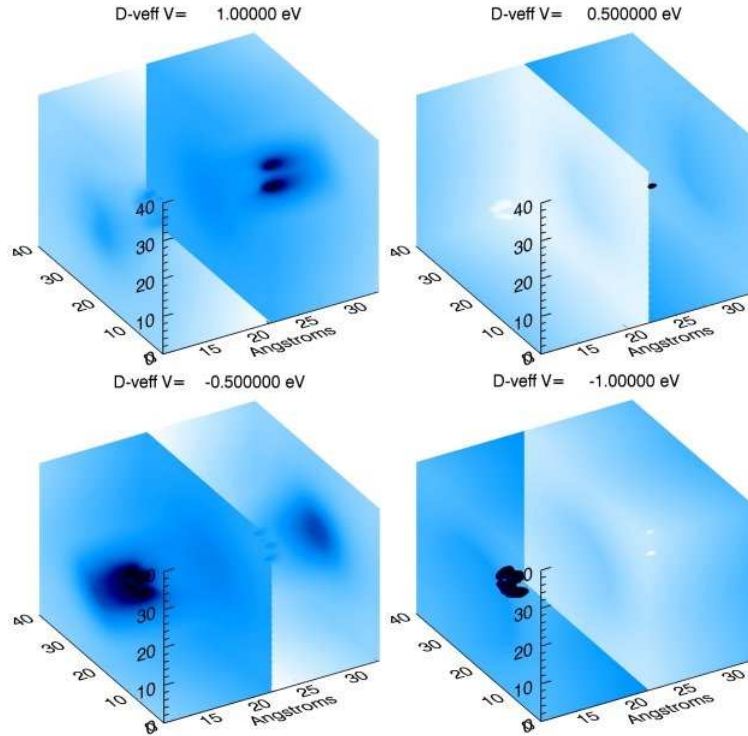
Figure 4.5: Difference effective potential maximum intensity projections for CNCl model (relative to 0 eV).

Looking at ΔV_{eff} series in Figure 4.5, it may be inferred that number of channels contributing to the current is low, although a barrier is present at lower bias, the distribution is mostly homogeneous. The effect of lower conductance is also observable in the $\Delta \rho$ series (Figure 4.6), where an homogeneous change is observed, and the impact of the applied bias is mostly seen as the charging of contact regions. In the end, despite the impact of electronegativity is not as drastic as the case of Cl_2, the effect of CNCl on the scattering region runs deeper, decreasing the number of conduction channels significantly. This case can be modeled as an ohmic resistance of very high value.

The last model considered in this study, the HCN model, is presented in Figure 4.7. This molecule also has a electronegative nature. There is an observed buildup of electrons close to Nitrogen atom. The footprint of atoms in attached molecule is
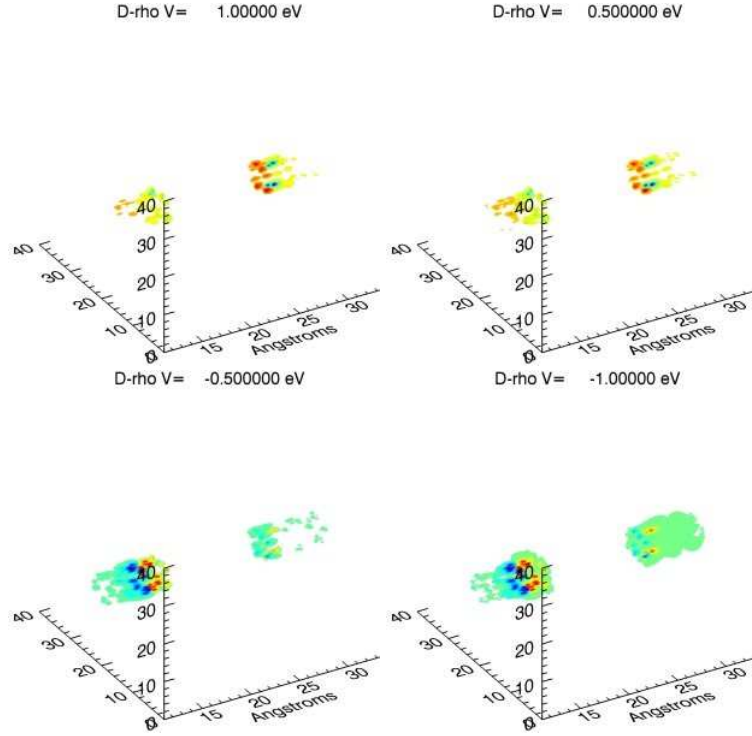
Figure 4.6: Difference ρ maximum intensity projections for CNCl model (relative to 0 eV).

significantly lower than chlorine containing models. Also at zero bias graph, the buildup of electrons at the contact surfaces are significantly less compared to other models. The strength of barrier is comparable to that of the Cl_2 model.

ΔV_{eff} series presented in Figure 4.8 show a behavior that is in between the Cl_2 model and the CNCl model. A barrier is present at all times, but it is overlaid on a general trend of homogeneous change in effective potential. $\Delta \rho$ series also indicate an homogeneous behavior under increased bias. Overall, the linear character of this model is stronger, and can be modeled as an ohmic resistance of lower value than the CNCl case.

DOS and MPSH spectrum are presented in Figure 4.10. Bare C(4,4) contains a
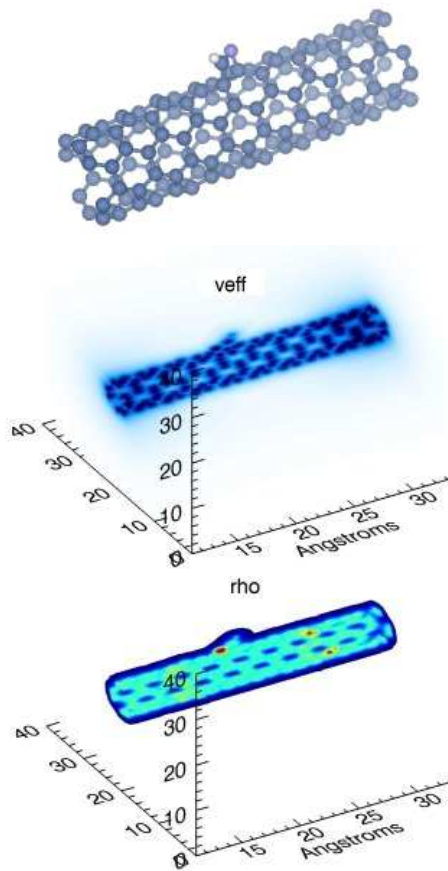
Figure 4.7: HCN model, and maximum intensity projections for effective potential and electron density.

rather wide constant DOS range, which is in direct correspondence with metallic behavior. In all the other models considered, there is a strong presence of singular peaks in this range, hinting how much the aromatic nature is altered when something attaches to the surface. The depletion of channels emerges as a decrease of states around the Fermi level in DOS graph. Being on the perturbative level, the effect of applied bias manifests itself as a translation of Fermi energy mostly, thus the depletion bias can be predicted from this graph. Frontier molecular orbital gap seen in MPSH is also altered, which indicates an altered optical behavior. The change in level separation in some
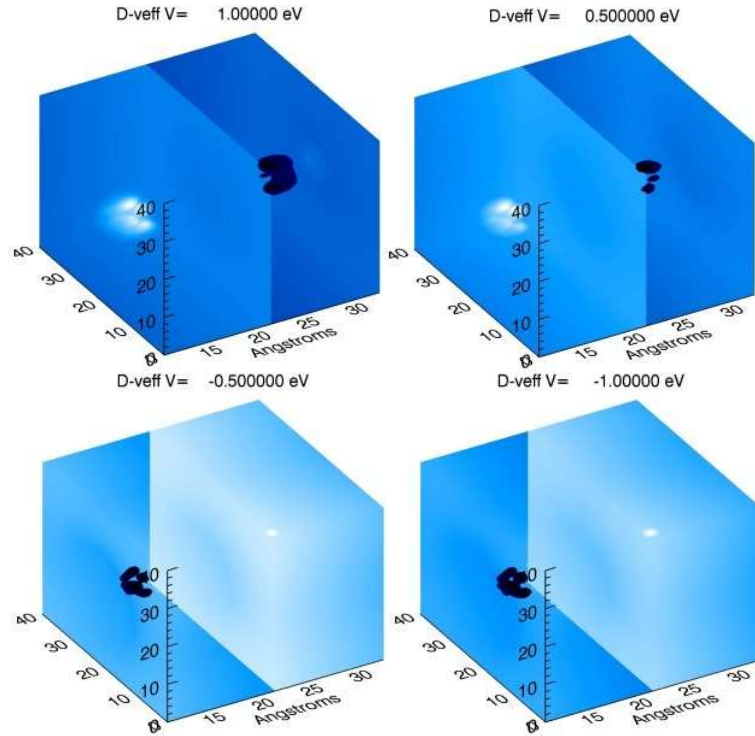
Figure 4.8: Difference effective potential maximum intensity projections for HCN model (relative to 0 eV).

cases can be attributed to the energy grid used in calculating the MPSH, otherwise, the impact of applied bias is mostly negligible.

Transmission spectrum is another heavily altered quantity. Instead of rather monotonous, even ohmic conductor like transmission spectrum of C(4,4), there are a number of high peaks and deep recessions through the spectrum for all models. At this point it must be stated that this graph is not normalized, and is not a substitute for transmission eigenvalues which are used in calculating the current. However, this graph gives an insight on how many channels could contribute to current, and what energies of incoming distribution of electrons are more likely to be transmitted under given bias. It is seen that, except the CNCl model, all the models should have more than one channel contributing to the current, consistent with what observed in previous graphs. For both
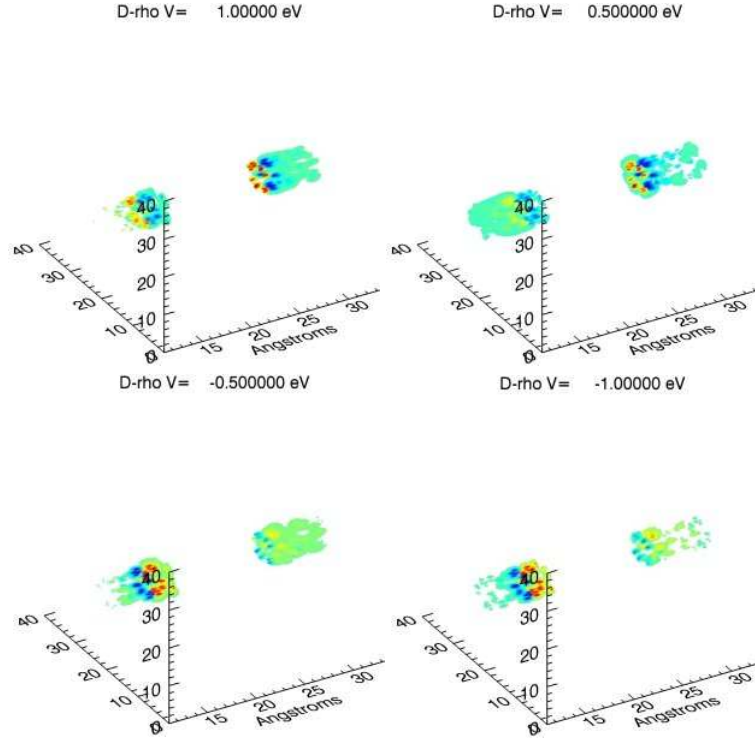
Figure 4.9: Difference ρ maximum intensity projections for HCN model (relative to 0 eV).

Cl$_2$ and HCN model, the transmission spectrum distribution close to Fermi level tends to increase under negative bias. Saturation behavior in Cl$_2$ is clearly observable, as the distribution tends to flatten around Fermi level under increased bias, but higher bias may result in increased conductance looking at the upcoming peaks. The larger recession observed in CNCl suggests that majority of electrons are not transmitted directly, only indirect conduction seems to be possible. It is curious how this happens, since looking at transmission spectrum at zero bias, one may expect increased conductance under negative bias, but as the Fermi level changes, transmission spectrum tends to flatten instead of translating itself.

The most notable results from the I-V trace are the significant loss in conductivity and localized non-linear behavior for activated models. Metallic behavior of C(4,4) and
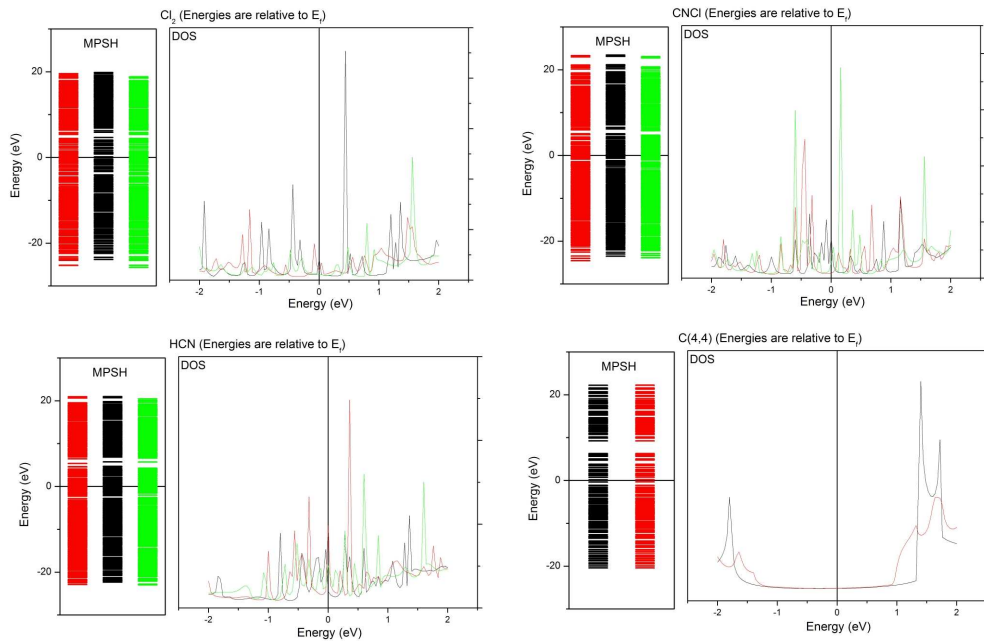
Figure 4.10: MPSH Eigenvalues and DOS distributions for the models considered (Red: +1 eV Black: 0 eV Green: -1 eV Bias), for comparison purposes, C(4,4) results are also presented

ideal overlap shows as a perfectly linear I-V trace for the range considered. Cl_2 model exhibit a saturation behavior for increased bias. The conductance in CNCl model drops drastically. There are a number of jumps in conductance, and position of these kinks are different for each model, indicating different splitting of conductance channels. However, it remains indeterminate whether this is a result of the molecule used in activation, or the geometrical location of the activation itself. A larger model is required to study this effect, which is sadly beyond the limitations of the package used. Another interesting result is the non-symmetric behavior under negative and positive bias. Negative bias results in a less resistive structure if averaged. As mentioned above, this effect should be geometrical in nature. If to be modeled ohmically ignoring the non-linear behavior, it is observed that each model has a different resistance. Not surprisingly, the molecules
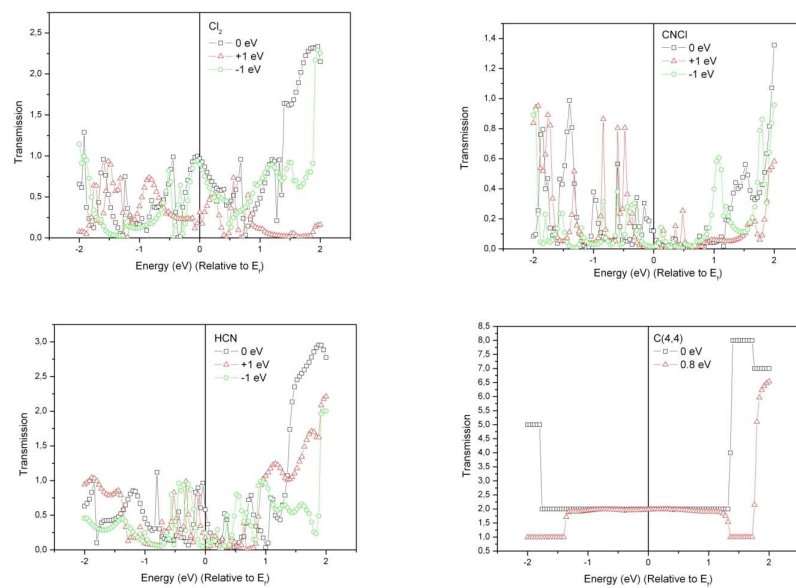
Figure 4.11: Transmission values for the models considered, for comparison purposes C(4,4) results are also presented
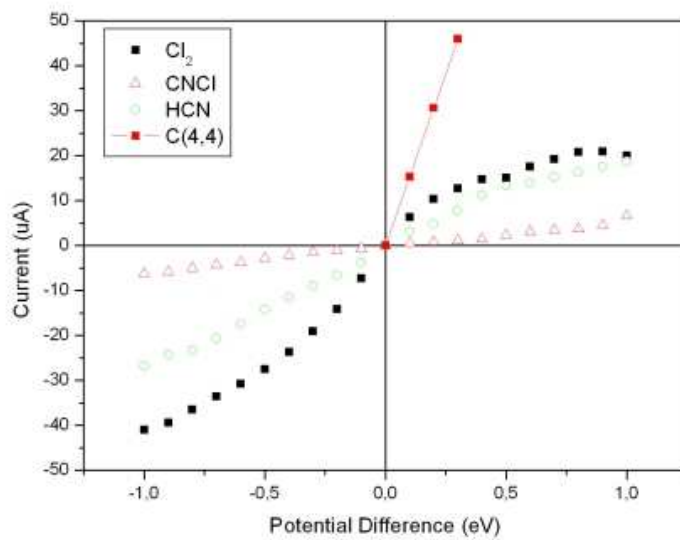
Figure 4.12: Comparison of I-V characteristics.

that are able to attach C(4,4) exhibit high electron activity.

Although this is an approximate calculation in order to observe general behavior, significant prospects are observed. In the use of detecting active chemicals even at molecular level, the structure is promising. There are stable geometrical configurations for various chemicals attached to the surface, nanotube is rather small in diameter, and thermally stable by itself. The alteration in electronic behavior may also be used in a different fashion, for example in electronics, or optronics. There are a number of points left uncovered at this preliminary work, such as the effect of applied current on the geometry, thermal vibration issues, and reversibility. Even at this level the results indicate a realizable application in the future.

Note: This chapter is based on published work [94]

CHAPTER 5

STRUCTURAL AND MOLECULAR ELECTRONIC PROPERTIES OF BN RING DOPED SINGLE–WALL CARBON NANOTUBES

5.1   Introduction

Electronic behaviour of Carbon nanotubes is decided by geometrical parameters [66]. This arises from the peculiar 0-band semi conductor configuration of graphene plane. Depending on the chiral vector, which is a measure of how the graphene plane is folded to form the carbon nanotube, band gap of the material varies. One result of this geometrical dependence is that the electronic structure of carbon nanotube can be varied, even after the synthesis, by mechanical distortions.

The decision whether this is good or bad relies on the application. Potential applications suggest that by connecting tubes with different geometry, or by mechanically deforming a particular carbon nanotube, one may obtain various electronic devices [110]. But such precision in synthesis of carbon nanotubes is not yet achieved, and dependence of electronic properties on mechanical deformations prove to be more of a problem than

an advantage [111].

So in order to realize devices using nanotubes, different approaches to the problem suiting the needs are required, at least in the short term. Boron-Nitride nanotubes (BNNTs), for example, are large band semiconductors independent of the geometry and wall composition [112, 113]. Furthermore, they are more rigid, more prone to oxidation [114], and can be produced nearly defect-free. However, by themselves, they do not offer the flexibility of carbon nanotubes, and they are often more expensive to synthesise.

At this point, the question of "Are these doping techniques are applicable to this problem?" arises. In general, theoretical calculations suggest that CBN heterofullerenes are possible [115]. In literature it is suggested that by introducing dopants [116], or by creating heterojunctions between nanotubes [111], chemically and electronically more stable electronic devices may be realized.

When one looks at the synthesis methods of BNNTs, chemical vapor deposition, laser evaporation and carbon nanotube substitution mechanisms are encountered. Among these, carbon substitution methods are of interest [95, 96], since if a controlled exposure technique may be realised, carbon nanotube-boron nitride nanotube heterojunction devices may be produced. There are other methods in producing a CBN heterojunction from scratch [97], but geometrical yield control is often not possible.

Effect of Boron, Nitride [98, 99, 100] and Boron-Nitride [101] dopants on fullerene, carbon dopants on BNNTs [102], also CBN nanotube heterojunctions [111] are discussed in a number of works. For example, addition of Boron is reported to increase conductivity of the material [116].

Usually, CBN nanotube heterojunctions are considered to be a junction between BNNT and CNT, a domain region of hexagonal B-N on carbon nanotube surface, or a single B-N ring. Since nanotubes are considered to be one dimensional structures theoretically, it is feasible to consider a B-N dopant that does not alter this feature, yet maintain interesting features of a BNNT. In this work, a single BNNT unit cell

replacing that of a corresponding carbon nanotube is studied. The ring is composed of B-N hexagons, and replaces one ring of Carbon nanotube.

Since BNNTs are always semiconducting independent of the geometry, the introduced ring would also be a semiconductor. One of our aims is to discuss molecular electronic properties of a possible metallic carbon nanotube - semiconducting B-N nanotube dopant - metallic carbon nanotube device. This device should be a Schottky diode by definition, although this may not be the case due to presence of nearly free electron orbital inside the B-N nanotubes, and the polar nature of the B-N bond.

The polar nature of the B-N bond leads to some interesting behaviour, such as the proposed self-polarization effect [103]. This self-polarization is maximised in some particular geometries, when the polar bonds align along the tube axis. As a result some interesting field emission properties are predicted and observed in BNNTs [104, 105, 106]. Some interesting results in the present work are due to this effect.

Carbon nanotubes are customarily identified by their chiral vector. The nomenclature is "C(n,m)" where n and m are integers identifying the composition of chiral vector in terms of graphitic plane base vectors. The usual nomenclature is also continued in this work, with C(n,m) identifying carbon nanotubes and CBN(n,m) identifying Boron-Nitride doped carbon nanotubes.

5.2 Calculation

In order to compare the electronic properties of C(n,m) and CBN(n,m) both Carbon nanotube and doped Carbon nanotube structures were prepared. Four geometries were considered, which sum up to eight different structures. First four of these structures are Hydrogen terminated Carbon nanotubes. Remaining four structures are obtained by replacing the middle ring of the corresponding Carbon nanotube by a BNNT ring. Considered structures are C(4,0), C(4,4), C(5,0), C(5,5) and their CBN(n,m) counterparts. All eight structures are shown in Figures 5.1-5.2.
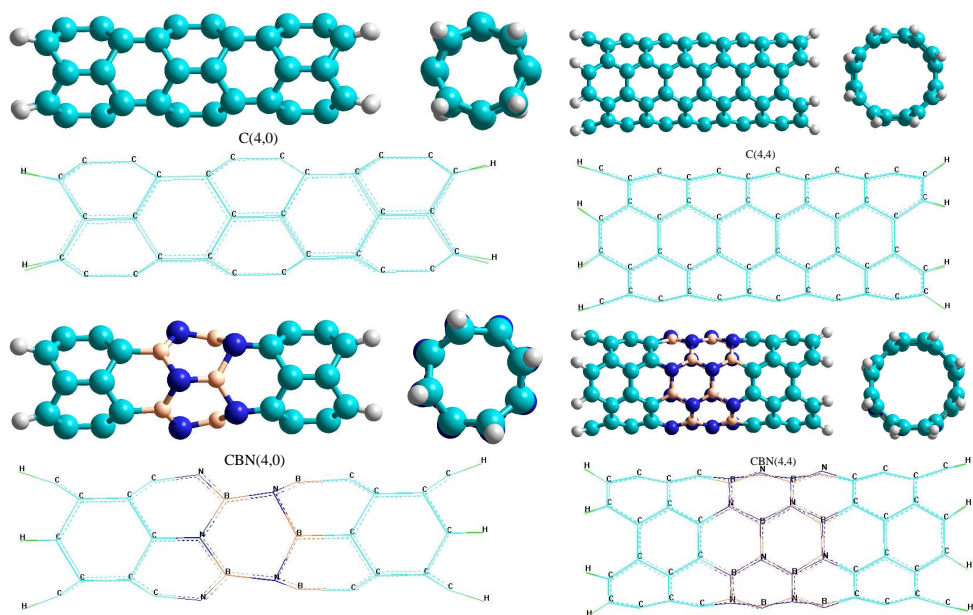
Figure 5.1: AM1 optimized geometries of CBN(4,0) and CBN(4,4) in comparison with the ideal tubes.
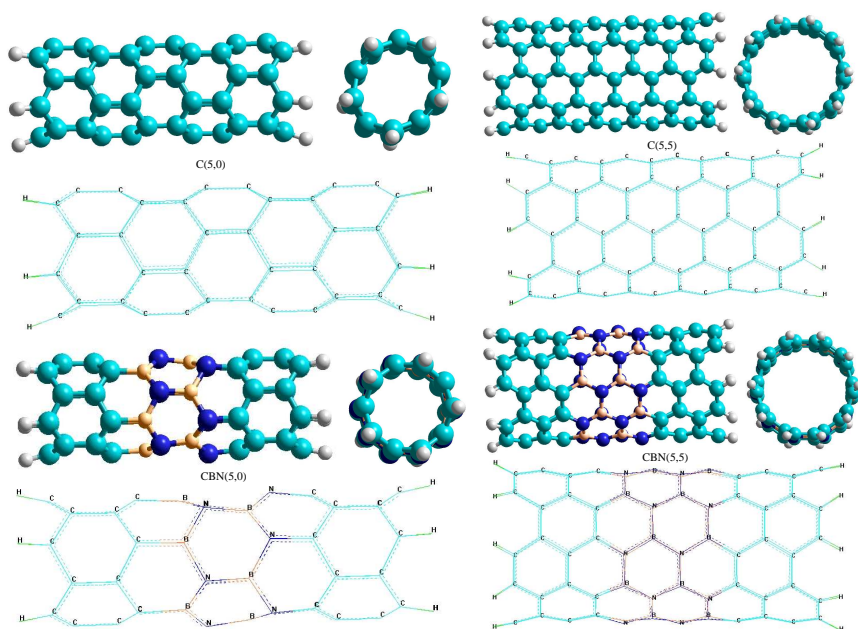
Figure 5.2: AM1 optimized geometries of CBN(5,0) and CBN(5,5) in comparison with the ideal tubes.

	C(4,0)	CBN(4,0)
Charge Density		
Electrostatic Potential		
HOMO		
LUMO		
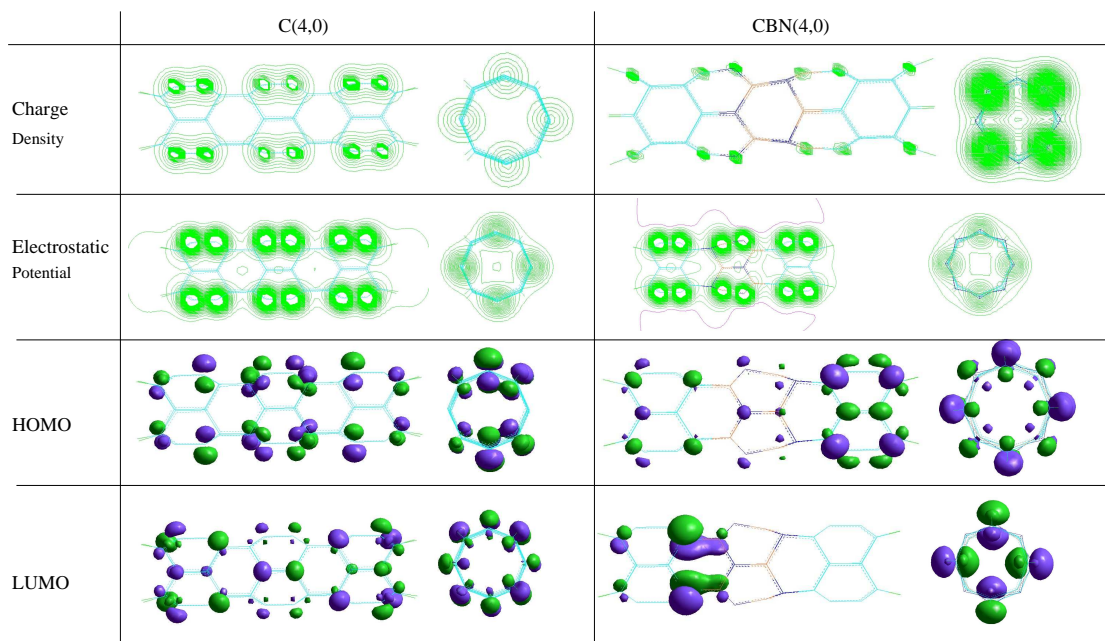
Figure 5.3: Various 3D molecular plots of C(4,0) and CBN(4,0) nanotubes from DFT calculations. Color coding: Green: Negative, other colors: Positive

The initial geometries of Carbon nanotubes are obtained using corresponding definitions from Saito et al's book [66]. Due to nature of the dopant and size limitations, the system needs to be studied as a macromolecular entity in this calculation. Thus, the ends are hydrogenated, so that the coordination number of all the carbons is three.

As mentioned earlier, carbon nanotubes assume an electronic behaviour in terms of the structural geometry. In general, all C(n,n) are metallic. In addition to this, when n+m is a multiple of three, the tube also assumes metallic properties. All the remaining nanotubes are semi conductors, with varying band gaps [66].

First, all eight models were geometry optimized using molecular mechanics method [29] considering MM+ force field. Then, geometry optimization using Austin Model 1 (AM1) [10] in restricted Hartree-Fock formalism [107] was performed. Polak-Ribiere optimizer [37] was used in geometry optimizations. The convergence criteria considered

is gradient reaching less than 0.001 kcal/(A mol). Finally, single point electronic calculations were performed using Density Functional Theory (DFT) considering B3-LYP exchange-correlation functional [21, 25] in STO-3G basis set [108]. Although this basis set is relatively small, it is sufficient for qualitative analysis.

All the calculations were performed in ground state of the system in its singlet state configuration. HyperChem 7.51 Professional [109] package was used in the calculations.

5.3 Results and Discussion

Numerical results of AM1 calculation, presented in Tables 5.1 and 5.2, show that addition of a BNNT ring reduces the binding energy in all the models considered. On the other hand, although all the models are structurally stable, heat of formation of all the models are endothermic, except the CBN(5,5), which is exothermic. Furthermore, comparision of the heat of formation energies suggests that the doped structures are obtainable from nanotubes by chemical exothermic reactions. Numerical results from DFT calculation at least confirm that electrons reside in energetically lower orbitals after doping. (Tables 5.3-5.4).

Table 5.1: Calculated energies (in kcal/mol) from AM1, for C(n,m) and CBN(n,m) nanotubes. E_{tot}: Total Energy; E_{bind}: Binding energy; E_{atom}:Isolated atomic energy; E_{elec}: Electronic energy; $E_{\text{c-c}}$: Core-core Interaction energy; ΔH_f^O: Heat of formation

Quantity	C(4,0)	CBN(4,0)	C(4,4)	CBN(4,4)
E_{tot}	-143202.179	-147500.156	-287926.581	-296398.517
E_{bind}	-7365.140	-7144.453	-16252.504	-15687.111
E_{atom}	-135837.038	-140355.703	-271674.077	-280711.406
E_{elec}	-1657998.349	-1646005.185	-5024230.043	-4997026.045
$E_{\text{c-c}}$	1514796.170	1498505.029	4736303.462	4700627.528
ΔH_f^O	1254.396	730.443	986.568	62.681

A further look in these tables (Tables 5.3-5.4), indicate that in general interfrontier molecular orbital eigenvalues (LUMO-HOMO gap) become lower, meaning a more readily excitable system. The largest doped model CBN(5,5) is an exception, having a

|	C(4,4)	CBN(4,4)
Charge Density		
Electrostatic Potential		
HOMO		
LUMO		

Figure 5.4: Various 3D molecular plots of C(4,4) and CBN(4,4) nanotubes from DFT calculations. Color coding: Green: Negative, other colors: Positive

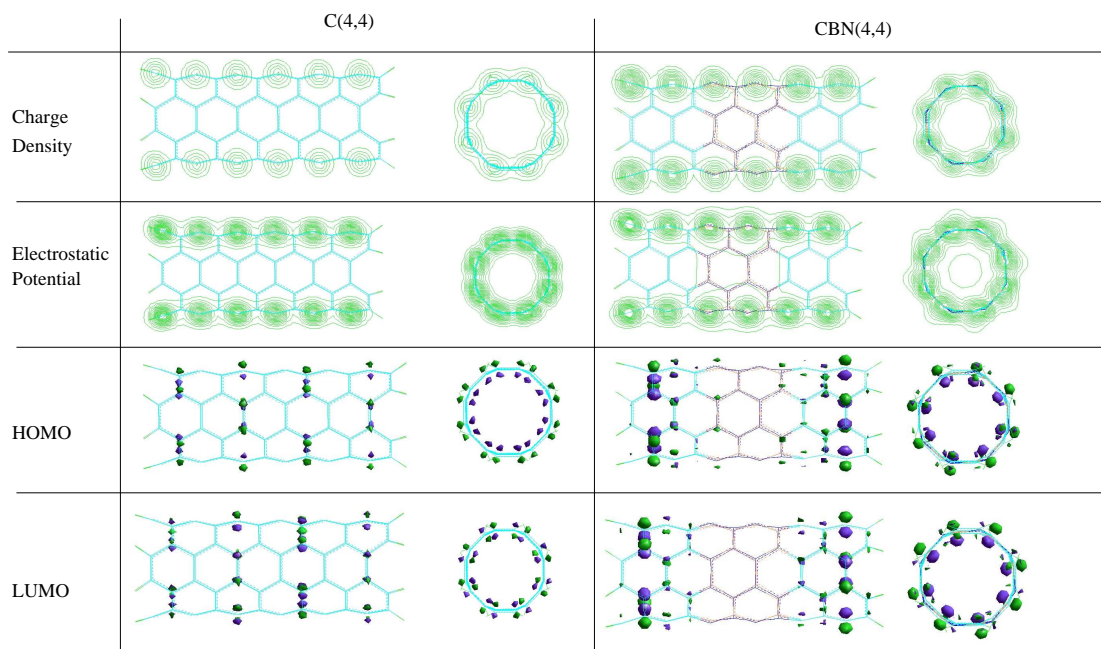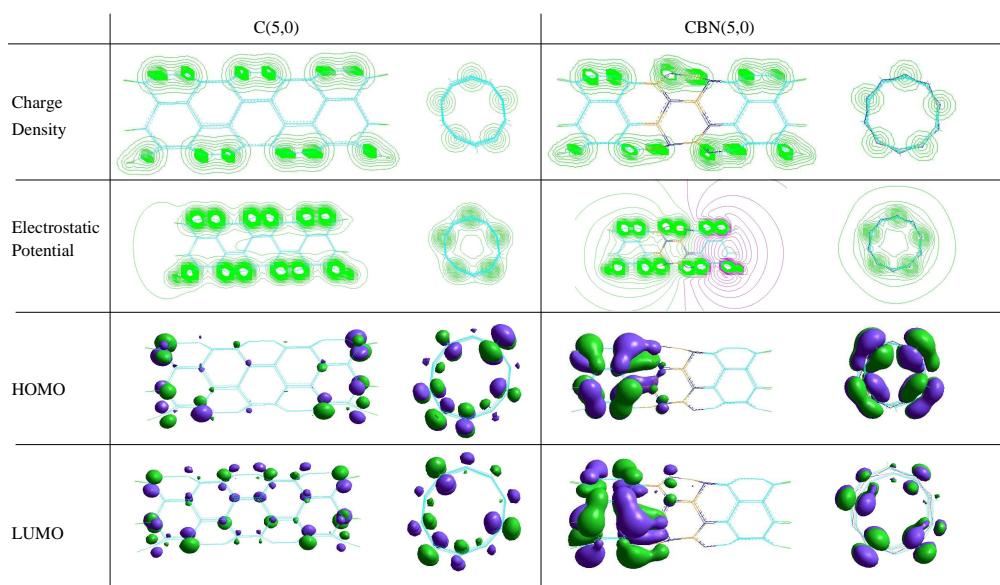|	C(5,0)	CBN(5,0)
Charge Density		
Electrostatic Potential		
HOMO		
LUMO		

Figure 5.5: Various 3D molecular plots of C(5,0) and CBN(5,0) nanotubes from DFT calculations. Color coding: Green: Negative, other colors: Positive

Table 5.2: Calculated energies (in kcal/mol) from AM1, for C(n,m) and CBN(n,m) nanotubes. E_{tot}: Total Energy; E_{bind}: Binding energy; E_{atom}:Isolated atomic energy; E_{elec}: Electronic energy; $E_{\mathrm{C\text{-}C}}$: Core-core Interaction energy; ΔH_f^O: Heat of formation

Quantity	C(5,0)	CBN(5,0)	C(5,5)	CBN(5,5)
E_{tot}	-179433.373	-184787.219	-360176.622	-370723.002
E_{bind}	-9637.074	-9342.590	-20584.026	-19833.744
E_{atom}	-169796.298	-175444.629	-339592.596	-350889.258
E_{elec}	-2398240.785	-2382366.812	-7112912.784	-7073242.899
$E_{\mathrm{C\text{-}C}}$	2218807.413	2197579.593	6752736.162	6702519.897
ΔH_f^O	1137.346	501.030	964.814	-146.504

Table 5.3: Calculated energies (in kcal/mol, unless otherwise stated) and dipole moment from DFT, for C(n,m) and CBN(n,m) nanotubes.

Quantity	C(4,0)	CBN(4,0)	C(4,4)	CBN(4,4)
E_{tot}	-1135270.831	-1152474.083	-2271964.046	-2306266.543
$E_{\mathrm{e,k}}$	1118465.605	1135691.198	2234909.956	2269772.557
$E_{\mathrm{e,v}}$	-4736229.593	-4717254.046	-13277858.216	-13231173.854
$E_{\mathrm{n\text{-}n}}$	3600958.762	3564779.963	11005894.170	10924907.311
E_{H} (eV)	-3.441	-3.547	-2.590	-2.863
E_{L} (eV)	-3.354	-3.497	-2.365	-2.758
$E_{\mathrm{L}} - E_{\mathrm{H}}$ (eV)	0.087	0.050	0.226	0.105
$\vec{p}$ (Debye)	0.291	2.051	1.448	0.059

E_{tot}: Total energy; $E_{\mathrm{e,k}}$: Electron kinetic energy; $E_{\mathrm{e,v}}$: Electron interaction terms; $E_{\mathrm{n\text{-}n}}$: Nuclear repulsion energy; E_{H}: Eigenvalue of HOMO; E_{L}: Eigenvalue of LUMO; $\vec{p}$: Electric dipole moment

greater gap compared to undoped C(5,5). This may be due to peculiar orientation of nearly free electron band in BNNT [112], which should be more observable when the nanotube grows larger. Some details of the molecular parameters from DFT calculations are presented in Tables 5.5-5.6.

Various molecular electronic plots are shown in Figures 5.3-5.6. Addition of Boron - Nitride ring drastically changes HOMO - LUMO and electrostatic potential configuration of the Carbon nanotube. In general, the probability density of these orbitals tend to be away from BNNT ring dopant.

Investigating the metallic carbon nanotube based models, CBN(4,4) and CBN(5,5), an electrostatic potential barrier in the middle is observed. This barrier is not present in the C(4,4) and C(5,5) counterparts. Although it is uncertain that this barrier would

Table 5.4: Calculated energies (in kcal/mol, unless otherwise stated) and dipole moment from DFT, for C(n,m) and CBN(n,m) nanotubes.

Quantity	C(5,0)	CBN(5,0)	C(5,5)	CBN(5,5)
E_{tot}	-1419459.882	-1440862.226	-2840255.769	-2883099.176
$E_{\text{e,k}}$	1397586.475	1419467.939	2793278.386	2836904.105
$E_{\text{e,v}}$	-6649315.097	-6622694.237	-18429548.608	-18359130.023
$E_{\text{n-n}}$	5229855.215	5181832.011	15589292.839	15476030.847
E_{H} (eV)	-1.535	-1.420	-2.041	-2.850
E_{L} (eV)	-0.993	-1.399	-1.128	0.140
$E_{\text{L}} - E_{\text{H}}$ (eV)	0.542	0.021	0.914	2.991
$\vec{p}$ (Debye)	5.192	100.563	0.025	0.031

E_{tot}: Total energy; $E_{\text{e,k}}$: Electron kinetic energy; $E_{\text{e,v}}$: Electron interaction terms; $E_{\text{n-n}}$: Nuclear repulsion energy; E_{H}: Eigenvalue of HOMO; E_{L}: Eigenvalue of LUMO; $\vec{p}$: Electric dipole moment

Table 5.5: Some molecular parameters of C(n,m) and CBN(n,m) nanotubes in DFT calculations.

Quantity	C(4,0)	CBN(4,0)	C(4,4)	CBN(4,4)
Number of Electrons	296	296	592	592
Number of Doubly Occupied Levels	148	148	296	296
Number of Virtual Orbitals	148	148	296	296
Number of Total Orbitals	248	248	496	496
Number of primitive Gaussians	744	744	1488	1488

still be effective in an electronic current condition, theoretical models on graphitic conduction suggest that its presence is promising. Furthermore, this potential barrier is effective inside the nanotube, and there are no evident holes. Thus, for example, a hypothetical memory device application, which relies on physical position of a fullerene inside a nanotube, may benefit from its presence [117]. Electronic charge density distribution plot is not significantly altered (i.e. atoms are still the focus of the density distribution with magnitude changes), but, due to polar nature of the newly added ring, there is some uneven distribution. Figure 5.7 shows that in these nanotubes, there is a charge accumulation to the BNNT ring compared to undoped models.

Consequences of the polar behaviour of the BNNT ring is apparent in CBN(4,0) and CBN(5,0). Especially in CBN(5,0), there is a large electric dipole moment directed along the tube axis (Table 5.4). The dipole moment of CBN(4,0), is also considerably

Table 5.6: Some molecular parameters of C(n,m) and CBN(n,m) nanotubes in DFT calculations.

Quantity	C(5,0)	CBN(5,0)	C(5,5)	CBN(5,5)
Number of Electrons	370	370	740	740
Number of Doubly Occupied Levels	185	185	370	370
Number of Virtual Orbitals	185	185	370	370
Number of Total Orbitals	310	310	620	620
Number of primitive Gaussians	930	930	1860	1860
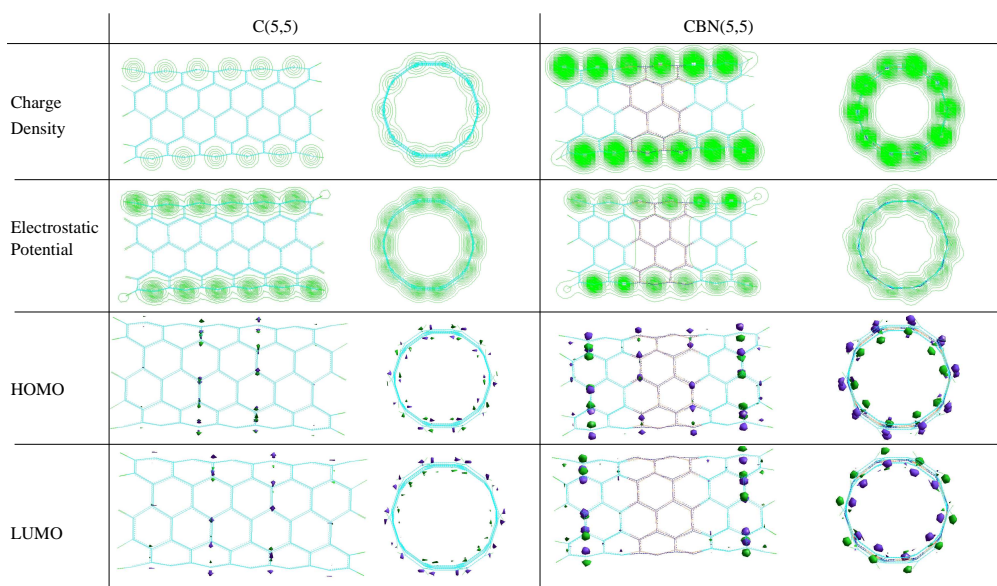
Figure 5.6: Various 3D molecular plots of C(5,5) and CBN(5,5) nanotubes from DFT calculations. Color coding: Green: Negative, other colors: Positive

grater than that of C(4,0). This time dipole moment is not entirely aligned in the tube axis, but has significant transverse components. It seems that there is no direct correlation between the dipole moment values and the HOMO-LUMO gap values of the models considered.

It should be noted that, AM1 predicts nonzero dipole moments only for CBN(4,0) and CBN(5,0) nanotubes. It is most possible that the non-zero dipole moments encountered in the DFT calculation is due to lack of mirror symmetry in the models, and, although small, the nonzero polar vector displaces electrons to the asymmetrical site. This may lead to a slightly different geometrical orientation in a DFT geometry
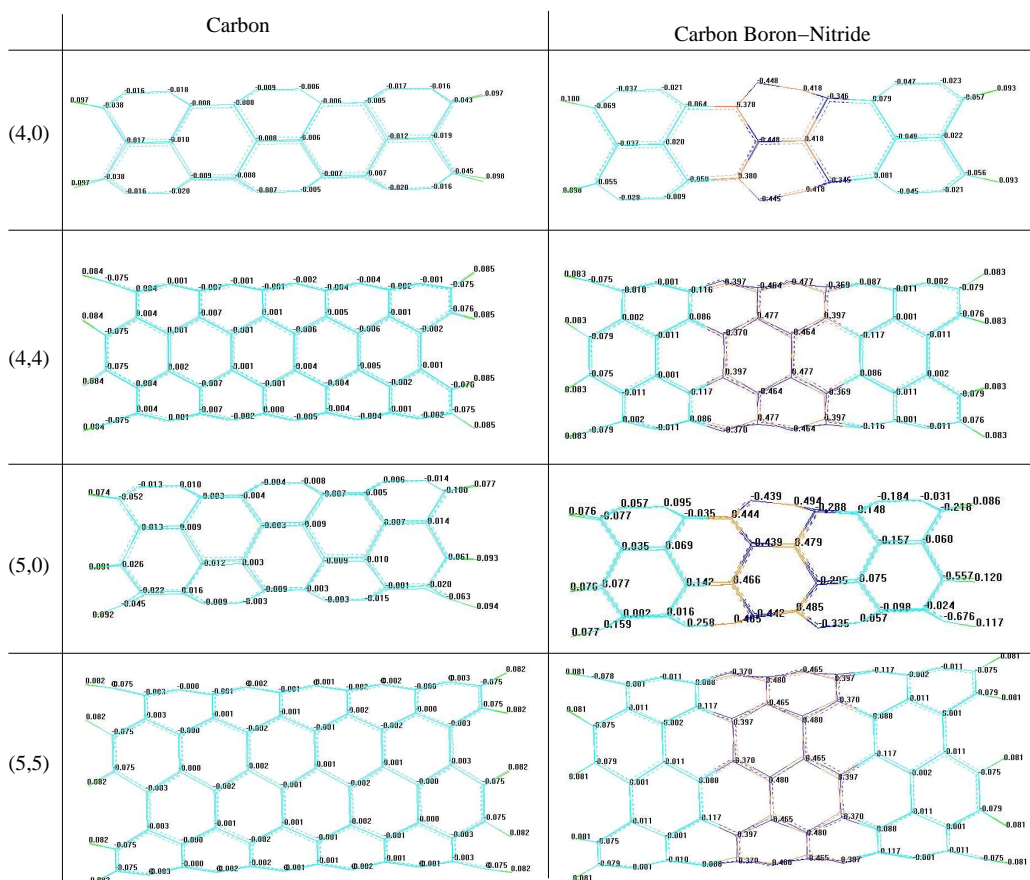
Figure 5.7: Calculated excess charge on atoms in the nanotubes considered. (DFT results).
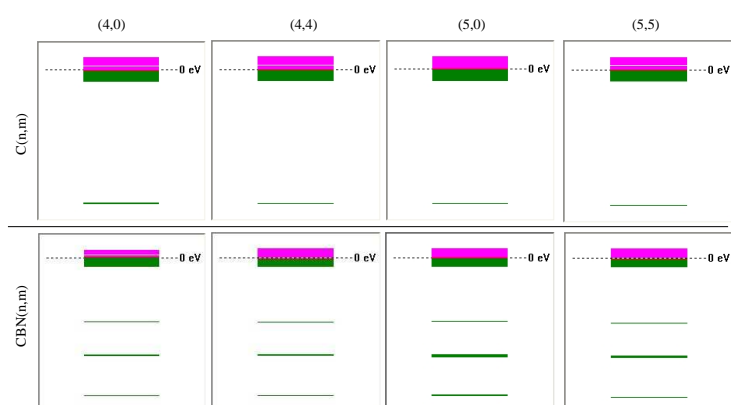
Figure 5.8: Molecular orbital eigenvalue spectra of the nanotubes considered. (DFT results).
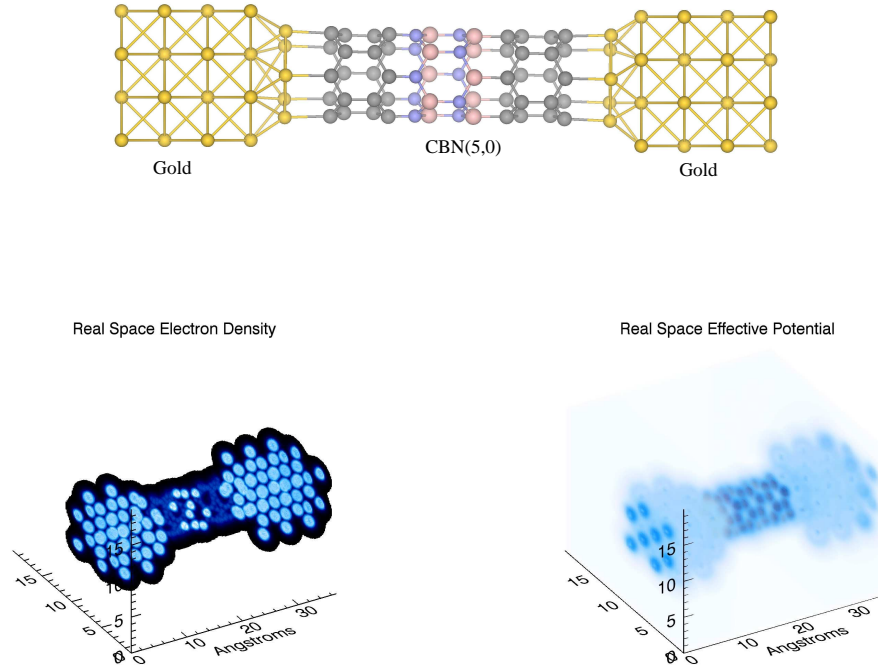
Figure 5.9: The model used in studying the conduction characteristics of CBN(5,0), and ρ and V_{eff} graphs for the model at 0 bias.

optimisation calculation, which is inefficiently costly in computational effort.

Molecular orbital eigenvalue spectrum is shown in Figure 5.8. Among the above mentioned HOMO-LUMO changes, there are some intermediate levels introduced. These levels may have some interesting contribution in a band calculation. Changes in inter-frontier moleculer eigenvalue is often accompanied by changes in optical behaviour.

When the contribution of s and p orbitals of individual atoms to the bonds are investigated, it is seen that the s orbital contribution is dominant. Nitrogen atoms, however, have a larger p orbital contribution, that leads to stronger hybridization characteristics.

These models are very promising candidates for two-terminal devices. The effects
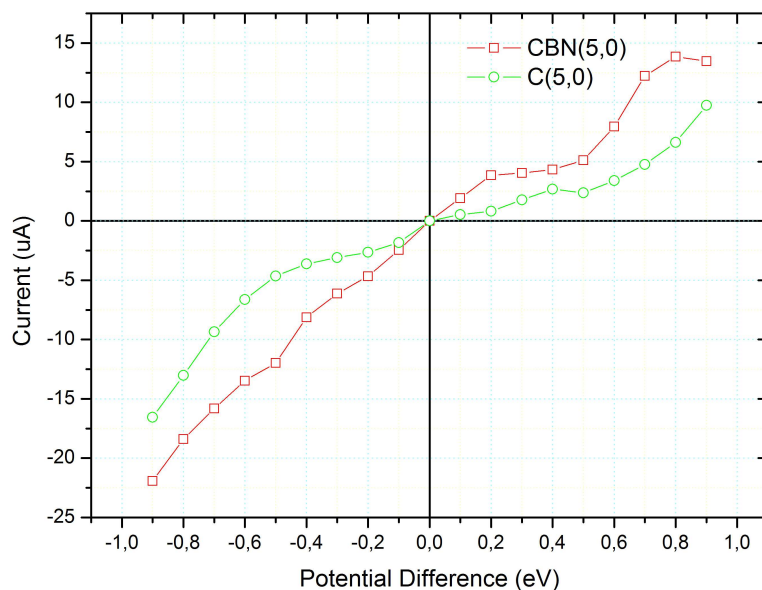
Figure 5.10: I-V trace for the CBN(5,0) and C(5,0) in the model described above.

of addition of BNNT ring is mostly charge oriented. Thus an external field may be used to control this behaviour, possibly leading to Field-Effect devices such as FETs. Furthermore, there is a charge oriented potential barrier, and its presence may be used in a number of applications.

Using a simple model, for example the one shown in Figure 5.9 some of these predicted characteristics can be approximated roughly. In this model, gold contacts at both ends serve as electron reservoirs. The contact region is modelled by relaxing the surface atoms using DFT (B3LYP exchange correlation 6-31g basis set, Hyperchem 7.52) and the same calculation procedure for conductance described in the previous chapter is proceeded. Again for comparison purposes, reference calculations on clean C(5,0) are presented accorodingly.

The current versus applied potential energy difference (bias) is presented in Figure
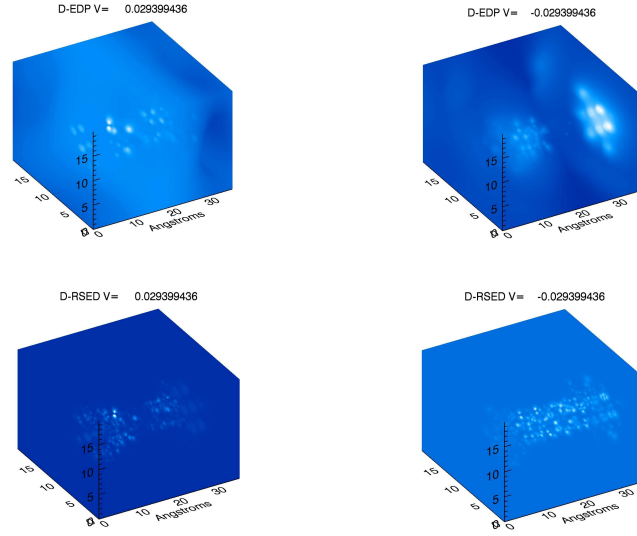
Figure 5.11: Comparison of the changes in electrostatic potential (shown at top row) and the charge density (shown at the bottom row) with respect to 0 bias, at +4 eV and -4 eV respectively.

5.10. C(5,0) is not a nanotube with metallic conduction properties, which results in the non-linear behaviour visible in the graph. In CBN(5,0), however there exists a linear region where the conduction can be modelled ohmically. Furthermore the conductivity increases significantly in the ring doped model. There also exists a non-linear region for the CBN model, which although considerably dominant in positive bias, becomes negligible in negative bias. This asymmetric behaviour can be explained by a formation of a p-n junction like interface region at the dopant region. This assumption is also in correspondance with the previous observations.

The difference in charge density in the BN ring region seen in Figure 5.9 (in correspondance with the previous calculations) has some interesting consequences. In Figure 5.11 the diffrences in electrostatic potential and charge density with respect to zero bias at ±4 eV (the non-linear region) is shown. Under positive bias, a big electrostatic barrier builds up at the center, and it is seen that the charge density remains unchanged.

However, under negative bias, the size of the barrier is significantly low, and there is a charge accumulation at the interface.

In effect, the BN ring acts as a p-n junction interface, with a visible alteration in the real space electrostatic potential, which hints a possible application in field emmission, or tuning via control of these fields just like a FET.

Note: This chapter is based on published work [118]

CHAPTER 6

CLOSING REMARKS

In a material point of view, each of the topics discussed in this work is self contained, and the discussion on the specific material can be found within the corresponding chapter. In this chapter, the underlying methodology in studying the structural and electronic properties of these materials is discussed.

There are various methods available for studying molecular and crystal structures, and in most cases they come packed with easy-to-use graphical interfaces, such as Hyperchem, or Gaussview. No matter how easy the package is to use, the fact that the many-body problem presented by inter-atomic interaction being unsolvable remains. It must be kept in mind that the results presented even by the most sophisticated calculation are still approximations, and it is the users responsibility to interpret the results physically according to the nature of the approximation(s) used.

Almost always, the complexity of the system requires parametrization, in some way or another. The parametrization is often system specific, and there are more than one consideration in their realization. This is the main source of problems in studying novel nanomaterials, by definition, experimental studies on that particular structure does not exist, thus how can we adjust a suitable parameter set? A second problem is the

size limitations. Even a supercomputer can not handle more than a couple of hundred atoms in an highly optimized DFT calculation, which is sadly where the hot topics in nanotechnology reside. Thus, studying such materials require a different approach.

In this work, a ground-up, coarse to fine methodology is employed, trying to circumvent these problems. First of all, it must be emphasized that in carbon based nanotechnology, spatial geometry of a structure is probably the most important consideration. Once the geometry is fixed, most (if not all) of the ground state physical properties are also fixed (through Hohenberg-Kohn theorems)[1]. Thus, the first step is to start with testing the structural stability of the proposed novel nanostructure. For this purpose, the system is modeled in an atomic and molecular physics point of view, using coarse, semi-classical parametric interaction functions between atoms that are modeled for structures resembling the one under study, and with tools of statistical physics the discrepancies with a more complicated equation of motion are averaged out. The procedure is nothing but the pseudo annealing procedure described in the Chapter 2. This exposes the proposed geometry under random fluctuations with a gradually increasing amplitude, and being a macromolecular entity, geometrical re-alignments are possible, like in the benzorod case, which can be studied separately. The pseudo annealing method allows adiabatic introduction of large fluctuations, which are required to compensate the coarse interaction potential, by permitting the structure to realize the most energetically optimized form, thus decreasing the chance of transformations to non-resembling geometrical configurations (see Figure 6.1).

Again, in this step, the structure can be investigated as a 1D periodic entity, if there are any foresight regarding the periodicity resulting in geometrical realignments, like in Bamboo shaped carbon nanotube case.

However, due to semi-classical nature, only structural information (which need to be approached skeptically due to statistical fluctuations) can be obtained in this step.

---

[1]Non-carbon atoms add complications that often need to be handled in a different and more precise manner
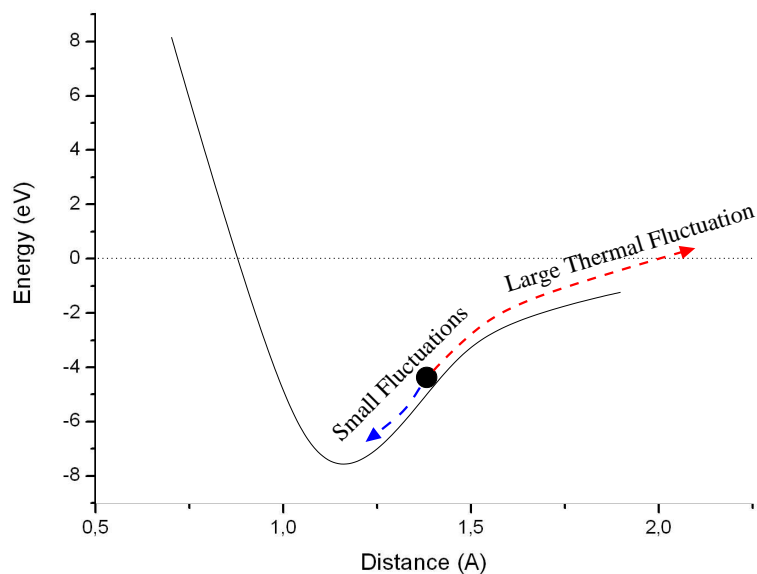
Figure 6.1: Large thermal fluctuations can "free" an atom that is not in its optimal configuration, whereas smaller fluctuations can not overcome the restoring force. Thus adiabatic introduction of thermal fluctuations is mandatory in a model geometry.

Also, being parametric and coarse, one must be familiar with the shortcomings and behavior of the PEF utilized, and act accordingly before proceeding any further. One good example of this kind of intervention is in Chapter 2, where the information on the modeling of Tersoff PEF is used to add hydrogen explicitly in modeling the relaxed benzorod geometry, which otherwise relaxes to a nanotube unit cell.

In "doped" structures, where non-carbon atoms are present, the characteristics of a structure is to a large extent defined by the dopant. The structural stability under fluctuations becomes a secondary concern here, primary concern being a precise definition of dopant interaction, thus the MD step described previously can be replaced by a geometry optimization procedure, that permits more precise interaction schemes due to considerably lesser number of steps involved. Chapter 4 and Chapter 5 are the two

examples of such occurrences. For example in Chapter 5, Boron is a problematic atom in handling using the methods at hand. A MD study is unfeasible (and unnecessary) due to complexities involved. In order to compensate, the complexity of the interaction scheme is increased gradually, starting from MM+ empirical force field then going to semi-empirical methods, performing geometry optimization at each step and using the previous result as an initial configuration for the next, reducing the cost of calculation considerably in each step.

Second step is to model the electronic structure of the system, again in a macro-molecular point of view, using DFT whenever possible. Localized basis sets are utilized which require a lot of chemical intuition in handling. The purpose of this step is mul-tifold: First the chemical stability of the system can be asserted, secondly a geometry optimization results in an increased precision in structural geometry, without the pre-viously mentioned statistical fluctuations. A lot of interesting observables that may be of use for application purposes are within reach at this point, such as molecular density of states, which above all provides information about optical properties, elec-tric dipole field, and the spatial location of HOMO and LUMO which can be used to determine active regions where the structure is most susceptible to corrosion. Due to large number of atoms involved, some structures can not be studied further, for example the Bamboo shaped nanotube of Chapter 3, and one has to be satisfied with structural properties. Keeping in mind the primary application, this does not pose a problem for this particular structure.

The last step is to model system in a solid-state point of view, as a periodic entity. Due to previous steps, the system can be described more precisely now, and most of the discrepancies due to constraining boundary conditions imposed by the periodicity is bypassed due to previous macromolecular treatment. There are new complications, however, since the set of approximations are somewhat different in a solid-state ap-proach. For example, when studying a structure using DFT in a macromolecular point

of view, localized basis sets are used, which are intrinsically different in handling compared to the plane wave basis sets often employed in solid-state physics. For example, in solid state physics, the contribution of the delocalized orbitals is the focal point, and localized segments are modeled only coarsely, if not omitted completely using valance orbital theory via an extension to interaction potential. Whereas in a macromolecular point of view, the core orbitals still can be handled somewhat coarsely, but due to localized nature of whole the inter-atomic orbitals, their definition is definitely more precise, and their contribution need to be almost always handled. In the end, a re-parametrization is required to employ tools of solid state physics. The biggest problem arises from approximate handling of core orbitals, one needs to find a suitable pseudo potential describing the system adequately. For this purpose, "resembling" structures are used, and a pseudo potential is tested to see whether it can describe those systems adequately. For example in Chapter 2, poly-ethylene and 3x3x3 slab of graphite was used in choosing the pseudo potential, it was seen that although the pseudo potential tends to slightly underestimate the hybridized bonds (with temperature scaling in mind) and overestimate the p-p coordination in graphite, the differences are within tolerance limits, and it is the most widely applicable among the tested. Luckily, there exists a systematic way of increasing level of detail for the rest in plane wave basis sets, unlike localized basis sets where intuition on the bonding scheme of the structure is required. Then by comparison with the results from the previous macromolecular step, a parametrization can be obtained rather effortlessly. An optimization procedure based on golden search and energy fitting is used to deduce the parameter set. In order not to increase complexity of calculation needlessly, only convergence of physicals observables such as the lattice parameter is sought.

Some systems can not be handled in a periodic manner. For example in order to observe the change in band structure due to attachment of a corrosive as in Chapter 4, a periodic model may have been devised where corrosive-corrosive interaction is

negligible. However, this would involve more than 300 atoms, which is well above the limits of DFT for the frameworks available. Instead, using NEGF formalism, the system is modeled as a standalone perturbation to an ideal nanotube connected to ideal contacts at infinity, and changes in conductance are observed. Although this simplifies modeling considerably, the model structure is still sizable, and only relatively coarse parametrization is possible. Again, due to precise modeling in macromolecular step, the impact of using a coarse parameter set is lowered. In Chapter 5, a similar procedure is present, but this time due to possible application as a FET or FED, the contacts are metallic, in order to see if the presence of a p-n junction like interface region is adequate to form a p-n device from a semiconductor.

Nanoscale resides at the borderline between the realms of solid state physics and atomic and molecular physics, which have intrinsically different approaches to the design of new materials. Top-down or bottom-up approaches are possible for known materials at nanoscale, however, in order to model novel materials at this scale, concepts of both approaches need to be used together, until a better formalism connecting both worlds can be found. This methodology is gaining importance in literature in the recent years, as the motivation for studying novel materials and effects increase (see for example, [119])

APPENDIX A

LIST OF ABBREVIATIONS

μVT Grand Canonical statistical ensemble

AM1 Austin Model 1, a semi emprical quantum chemistry method [10]

AMBER An empirical force field [30, 31, 32]

B3LYP A Hybrid Exchange correlation functional which uses Becke - 3 parameter approximation in combination with GGA of Lee Yang and Parr

BIO+ An empirical force field [33, 34]

BNNT Boron-Nitrade nanotube

CNT Carbon Nanotube

DFT Density Functional Theory

DOS Density of states

GGA Genaralized Gradients Approximation

LDA Local Density Approximation

LSDA Local Spin Density Approximation

LU Decomposition A diagonalization method which decomposes a matrix into Lower
    and Upper parts

MC Monte Carlo

MD Molecular Dynamics

MM+ An empirical force field [28, 29]

MPI Message passing interface

MPSH Molecular projected self consistent eigenvalues

NEGF Non-equilibrium Green's function

NPT Isothermal–isobaric statistical ensemble

NVE Microcanonical Statistical Ensemble

NVT Canonical Statistical Ensemble

OPLS An empirical force field [35, 36]

PBC Periodic Boundary Condition

PDOS Partial or Projected density of states

PDOS Partial or Projected density of states

PEF Potential Energy Function

PM3 Parametrized Model number 3, a semi emprical quantum chemistry method [11,
    12, 13]

SCF Self Consistent Field

STM Scanning Tunnelling Microscope

STO Slater type orbital

SWCNT Single Wall Carbon Nanotube

REFERENCES

[1] Ş. Erkoc, T. Uzer, *Atomic and Molecular Physics*, (World Scientific, Singapore, 1996).

[2] M. Springborg, *Methods of Electronic Structure Calculations*, (John Wiley&Sons, New York, 2000).

[3] A.R. Leach, *Molecular Modelling: Principles and Applications*, Second Ed. (Pearson Prentice Hall, Harlow, 2001).

[4] Ş. Erkoc, Physics Reports **278**, 79(1997).

[5] Ş. Erkoc, in *Annual Review of Computational Physics IX*, Ed. D. Stauffer, (World Scientific, Singapore, 2001), pp.1-103.

[6] *Hyperchem 7: Tools for Molecular Modelling*, Hypercube. Inc, 2002.

[7] J.H. Knox, *Molecular Thermodynamics*, (Wiley-interscience, New York, 1971).

[8] F. Mandl, *Statistical Physics*, (Wiley, New York, 1988).

[9] D.W. Heerman, *Computer Simulation Methods*, (Springer-Verlag, Berlin, 1990).

[10] M. J. S. Dewar, , Zoebisch, E. G., Healy, E. F. and Stewart, J. J. P., Journal of the American Chemical Society, 107, 3902, (1985).

[11] J. J. P. Stewart, J. Comput. Chem. **10**, 209 (1989).

[12] J. J. P. Stewart, J. Comput. Chem. **12**, 320-341 (1991).

[13] J. J. P. Stewart, J. of Mol. Mod. **10**, 155-164 (2004).

[14] P. Hohenberg and W. Kohn, Phys. Rev. B **864** 136 (1964).

[15] W. Kohn and L. J. Sham, Phys. Rev. A **1133** 140 (1965).

[16] G. D. Mahan, *Many–Particle Physics*, (Kluwer Academic/Plenum publishers, 2000).

[17] J. P. Perdew, A. Zunger, Phys. Rev. B **23,** 5048 (1981).

[18] A.D. Becke . Phys. Rev. a **38,** 3098 (1988).

[19] J. Perdew, *Electronic Structure of Solids,* (ed. P. Ziesche and H. Eschrig) (Akademie Verlag, Berlin 1991)

[20] J. P. Perdew, Y. Wang, Phys. Rev. B **33**, 8800 (1986).

[21] A.D. Becke . J. Chem. Phys. **98**, 1372-1377 (1993).

[22] J. Harris. Phys. Rev A **29**, 1648-1659 (1984).

[23] H. Hellmann, *Einfuhrung in die Quantenchemie* 1936.

[24] R. P. Feynman, Phys. Rev. **56**, 340 (1939).

[25] C. Lee, W. Yang, and R. G. Parr, Phys. Rev. **B 37** 785 (1988)

[26] J. C. Phillips, L. Kleinman Phys. Rev **116**, 287 (1959).

[27] D. Vanderbilt. Phys. Rev. B, **41** 7892, (1990).

[28] U. Burkert and N.L. Allinger, *Molecular Mechanics*, (ACS Monograph 177, 1982).

[29] N.L. Allinger, J. Am. Chem. Soc. **99**, 8127(1977).

[30] S.J. Weiner, P.A. Kollman, D.A. Case, U.C. Singh, C. Ghio, G. Alagona, S. Jr. Profeta , P. Weiner, J. Am. Chem. Soc. **106**, 765(1984).

[31] S.J. Weiner, P.A. Kollman, D.T. Nguyen, D.A. Case, J. Comput. Chem. **7**, 230(1986).

[32] W.D. Cornell, P. Cieplak, C.I. Bayly, I.R. Gould, K.M. Jr. Merz, D.M. Ferguson, D.C. Spellmeyer, T. Fox, J.W. Caldwell, P.A. Kollman, Journal of the American Chemical Society **117**, 5179(1995).

[33] B.R. Brooks, R.E. Bruccoleri, B.D. Olafson, D.J. States, S. Swaminathan, M. Karplus, J. Comput. Chem. **4**, 187(1983).

[34] A.D. Jr. MacKerell, D. Bashford, M. Bellott, R.L. Jr. Dunbrack, J. Evanseck, M.J. Field, S. Fischer, J. Gao, H. Guo, S. Ha, D. Joseph, L. Kuchnir, K. Kuczera, F.T.K. Lau, C. Mattos, S. Michnick, T. Ngo, D.T. Nguyen, B. Prodhom, W.E. III Reiher, B. Roux, M. Schlenkrich, J. Smith, R. AStote, J. Straub, M. Watanabe, J. Wiorkiewicz-Kuczera, D. Yin, M. Karplus, J. Phys. Chem B, **102**, 3586(1998).

[35] W.L. Jorgensen, J. Tirado-Rives, J. Am. Chem. Soc. **110**, 1657(1988).

[36] J. Pranate, S. Wierschke, W.L. Jorgensen, J. Am. Chem. Soc. **113**, 2810(1991).

[37] P. Fletcher, *Practical Methods of Optimization*, (Wiley, Chichester, 1990).

[38] J. Tersoff, Phys. Rev. B **37**, 6991(1988).

[39] J. Tersoff, Phys. Rev. Lett. **61**, 2879(1988).

[40] D.W. Brenner, Mater. Res. Soc. Symp. Proc. **141**, 59(1989).

[41] Y. Omata, Y. Yamagami, K. Tadano, T. Miyake, S. Saito, Physica E, **29**, 454 (2005).

[42] W.H. Press, S.A. Teukolsky, W.T. Vetterling, B.P. Flannery, *Numerical recipes in C : the art of scientific computing* (Cambridge University Press, New York, 1992.)

[43] P. S. Pacheco, *Parallel programming with MPI*, (Morgan Kaufmann Publishers, San Francisco, 1997).

[44] P. Vashista, R.K. Kalia, A. Nakano, J. Nanoparticle Res. **5**, 119(2003).

[45] D.C. Rapaport, *The Art of Molecular Dynamics Simulation*, (Cambridge Univ. Press, Cambridge, 1995).

[46] M. Knalpia, Self organized supramolecules of π-conjugated rodlike polymers, Thesis, Helsinki University of Technology, ISBN 951-22-7147-8, 2004.

[47] Erkoç Ş 2003 Structural and electronic properties of "benzorods" *J. Mol. Struc. (Theochem)* **639** 157–66 .

[48] H.W. Kroto, J.R. Heath, S.C. O'Brien, R.F. Curl, R.E. Smalley, Nature **318**, 162(1985).

[49] Man Z., Pan Z., Xie J. and Ho Y. Nuc. Inst. Meth. Phys. Res. B. 135 (1998), 342

[50] S. Baroni, A. Dal Corso, S. de Gironcoli, P. Giannozzi, 7 C. Cavazzoni, G. Ballabio, S. Scandolo, G. Chiarotti, P. Focher, A. Pasquarello, K. Laasonen, A. Trave, R. Car, N. Marzari, A. Kokalj, http://www.pwscf.org/; Last visited, 19/03/2008.

[51] DEMOCRITOS Center, http://www.quantum-espresso.org/; Last visited 19/03/2008

[52] Axel Kohnmayer, http://www.pwscf.org/pseudo/upfdetails.php?upf=C.blyp-van_ak.UPF; Last visited 19/03/2008

[53] H. J. Monkhorst and J. D. Pack, Phys. Rev. B 13, 5188 (1976).

[54] L. Wirtz et al. Solid State comm. 131 141-152.

[55] The Engineering ToolBox, http://www.engineeringtoolbox.com/young-modulus-d_417.html; Last visited 19/03/2008

[56] C. A. Klein, G. F. Cardinale Proceedings of SPIE – Volume **1759** Editors, 178-193 (1992).

[57] H.J. McSkimin, P. Andreatch, J. Appl. Phys. **43** 2944-2948 (1972).

[58] C.-L. Fu , K.-M. Ho, PRB **28**, 6687 (1983).

[59] M. Methfessel, A. T. Paxton, PRB **40**, 3616 (1989).

[60] N. Marzari, D. Vanderbilt, PRL **82**, 3296 (1999).

[61] S. Iijama, Nature 354, 56–58 (1991)

[62] The periodic table, http://periodictable.com/Elements/082/data.html; Last visited 19/03/2008

[63] O.B. Malcioglu and S. Erkoc, "Stability of C_{60} chains: Molecular Dynamics Simulations", J. Molecular Graphics and Modelling 23, 367(2004).

[64] O.B. Malcioglu and S. Erkoc, "Thermal Stability of Benzorod Arrays: Molecular-Dynamics Simulations", Int. J. Mod. Phys. C 16, 827(2005).

[65] O.B. Malcioglu and S. Erkoc, "Thermal Stability of Benzorods: Molecular-Dynamics Simulations", J. Molec. Graph. Modeling 24, 213(2005).

[66] R.Saito, G.Dresselhaus, and M.S.Dresselhaus, *Physical Properties of Carbon Nanotubes*, (Imperial College Press, London, 1998).

[67] Eds. M.S. Dresselhaus, G. Dresselhaus, and Ph. Avouris, *Carbon Nanotubes Synthesis, Structure, Properties, and Applications* (Springer–Verlag, Berlin, 2001), Vol. 80 of Topics in Applied Physics.

[68] G. Shaun, S. Bao, Physica E **35**, 161(2006).

[69] S. Suen, W. Whang, B. Wu, Y. Lai, Appl. Phys. Lett. **84**, 3157(2004).

[70] S. Ahmad, Nanotechnology **16**, 1739(2005).

[71] G.G. Tibbetts, J. Cryst. Growth **66**, 632(1984).

[72] C.J. Lee, J.H. Park, J. Park, Chem. Phys. Lett. **323**, 560(2000).

[73] W.Z. Li, S.S. Xie, W. Liu, R.A. Zhao, Y. Zhang, W.Y. Zhou, G. Wang, J. Mater. Sci. **34**, 2745(1999).

[74] C.J. Lee, J. Park, Appl. Phys. Lett. **77**, 3397(2000).

[75] J.W. Jang, C.E. Lee, T.J. Lee, C.J. Lee, S.J. Noh, Solid State Commun. **127**, 29(2003).

[76] R. Hoffmann, J. Chem. Phys **39**, 1397-1412 (1963).

[77] O.B. Malcioglu, E. Tasci, and S. Erkoc, "Single wall bamboo shaped carbon nanotube: A molecular dynamics and electronic study", Int. J. Mod. Phys. C 17, 187(2006).

[78] J.P. Novak, E.S. Snow, E.J. Houser, D. Park, J.L. Stepnowski, R.A. McGill, Appl. Phys. Lett. **83** (2003) 4026.

[79] C. Staii, A.T. Johnson Jr., M. Chen, A. Gelperin, Nano Lett. **5** (2005) 1774.

[80] S. Chen, W. Shen, G. Wu, D. Chen, M. Jiang, Chem. Phys. Lett. **402** (2005) 312.

[81] Y. Wang, Z. Iqbal, S.V. Malhotra, Chem. Phys. Lett. **402** (2005) 96.

[82] S. Niyogi, M.A. Hamon, H. Hu, B. Zhao, P. Bhowmik, R. Sen, M.E. Itkis, R.C. Haddon, Acc. Chem. Res. **35** (2002) 1105.

[83] A. Hirsch, Angew. Chem. Int. Ed. **41** (2002) 1853.

[84] D.K. Ferry, S.M. Goodnick, *Transport in Nanostructures*, (Cambridge University Press 1997).

[85] S. Datta, *Quantum Transport Atom to Transistor*, (Cambridge University Press 2005).

[86] Gaussian 03, M.J. Frisch, et al., Gaussian, Inc., Wallingford CT, 2004.

[87] J.J.P. Stewart, J. Compt. Chem. **10** (1989) 209 .

[88] Transiesta-C 1.3.4, www.atomistix.com

[89] S. Datta, *Electronic Transport in Mesoscopic Systems*, (Cambridge University Press 1995).

[90] J. Taylor, H. Guo, J. Wang, Phys. Rev. B **63** (2001) 245407.

[91] M. Brandbyge, J.-L. Mozos, P. Ordejon, J. Taylor, K. Stokbro, Phys. Rev. B **65** (2002) 165401 .

[92] J.M. Soler, E. Artacho, J.D. Gale, A. Garcia, J. Junquera, P. Ordejon, D. Sanchez-Portal, J. Phys.: Cond. Mat. **14** (2002) 2745 .

[93] J. Taylor, M. Brandbyge, K. Stokbro, Phys. Rev. Lett. **89** (2002) 138301 .

[94] O.B. Malcioglu and S. Erkoc, "Functionality of C(4,4) carbon nanotube as molecular detector", J. Nanosci. Nanotech. (in press).

[95] E. Borowiak-Palen, T. Pichler, G. G. Fuentes, A. Graff, R.J. Kalenczuk, M. Knupfer, J. Fink, AIP Conference Proceedings **685**, 374 (2003).

[96] W.-Q. Han, W. Mickelson, J. Cumings, A. Zettl, Appl. Phys. Lett. **81**, 1110 (2002).

[97] R. Ma, Y. Bando, Sci. Tech. Adv. Mat. **4**, 403 (2003).

[98] L. Hultman, S. Stafstrom, Z. Czigany, J. Neidhart, N. Hellgren, I.F. Brunell, K. Suenaga, C. Colliex, Phys. Rev. Lett. **87**, 225503 (2001).

[99] B. Wei, R. Spolenak, P. Kohler-Redlich, M. RÃŒhle, E. Arzt, Appl. Phys. Lett. **74**, 3149 (1999).

[100] M. Terrones, P. M. Ajayan, X. Blase, W. Blau, W. Blau, D. L. Carroll, J. C. Charlier, R. Czerw, B. Foley, N. Grobert, R. Kamalakaran, Ph. Kohler-Redlich, M. RÃŒhle, T. Seeger, H. Terrones, Electronic Properties of Molecular Nanostructures, American Instute of Physics, (2001) p212.

[101] J. Yu, J. Ahn, S. F. Yoon, Q. Zhang, Rusli, B. Gan, K. Chew, M. B. Yu, X. D. Bai, E. G. Wang, Appl. Phys. Lett. **77**, 1949 (2000).

[102] J.-X. Zhao, B.-Q. Dai, Mater. Chem. Phys., In press, doi:10.1016/j.matchemphys.2003.10.018

[103] E. J. Mele, P. Kral, D. Tomanek, Phys. Rev. Lett. **88**, 056803 (2002).

[104] E. J. Mele, P. Kral, Phys. Rev. Lett. **88**, 056803 (2002).

[105] J. Cumings, A. Zettl, Solid State Com. **129**, 661 (2004).

[106] V. Meunier, C. Roland, J. Bernholc, M. B. Nardelli, Applied Physics Letters **81**, 46 (2002).

[107] C. C. J. Roothan, Rev. Mod. Phys. **23**, 69 (1951).

[108] W. J. Hehre, R. F. Stewart, J. A. Pople, J. Chem. Phys. **51**, 2657 (1969).

[109] HyperChem(TM), Hypercube, Inc., 1115 NW 4th Street, Gainesville, Florida 32601, USA.

[110] M. Menon, D. Srivastava, Phys. Rev. Lett. **79**, 4453 (1997).

[111] X. Blase, J.-C. Charlier, A. De Vita, R. Car, Appl. Phys. Lett. **70**, 197 (1997).

[112] M. Ishigami, S. Aloni, A. Zettl, Scanning Tunneling Microscopy/Spectroscopy and Related Techniques: 12th Int. Conf., 94 (2003).

[113] S. Erkoc, J. Mol. Str. (THEOCHEM) **542**, 89 (2001).

[114] Y. Chen, J. Zou, S. J. Campbell, G. Le Caer, Appl. Phys. Lett. **84**, 2430 (2004).

[115] S. Erkoc, J. Mol. Str. (THEOCHEM) **684**, 117 (2001).

[116] R. S. Lee, H. J. Kim, J. E. Fischer, A. Thess, R. E. Smalley, Nature (lett.) **388**, 255 (1997).

[117] J. W. Kang, H. J. Hwang, Carbon **42**, 3018 (2004).

143

[118] O.B. Malcioglu, E. Tasci, and S. Erkoc, "Structural and molecular electronic properties of BN ring doped single-wall carbon nanotubes", Physica E 28, 296(2005).

[119] J.-L. Li, K. N. Kudin, M. J. McAllister, R. K. Prud'homme, I. A. Aksay, and R. Car, PRL **96**, 176101 (2006).

Curriculum Vitae

Osman Barış Malcıoğlu

   Office : (+90 312) 210 4336 / Fax : (+90 312) 210 5099

   e-mail : mbaris@metu.edu.tr

Department of Physics, Middle East Technical University 06531, Ankara TURKEY

PERSONAL INFORMATION

Date of Birth: May, 1979

   Maritial status: Single

   Nationality: Turkish

FIELDS OF INTEREST

- Investigation of various properties of Carbon nanomaterials with an emphasis on nanocage structures.

- Finite-size all-quantum description of nanomaterials.

- Perturbative approaches to DFT.

EDUCATIONAL INFORMATION

- B.S. : Department of Physics, Middle East Technical University.
  "Effect of Chirality on the Stability of Carbon Nanotubes: Molecular-Dynamics Simulations",
  Supervisor: Prof. Ş. Erkoç (2001).

- M.S. : Department of Physics, Middle East Technical University.
  "Stability of Carbon Nanotubes and Nanorods Under Heat Treatment: Molecular-Dynamics Simulations",
  Supervisor: Prof. Ş. Erkoç (2003)

- Ph.D. : Department of Physics, Middle East Technical University.
  " Tailoring one dimensional novel nano structures for specific applications using tools of molecular modelling ",
  Supervisor: Prof. Ş. Erkoç (ongoing).

SCIENTIFIC HIGHLIGHTS

Publications in international refereed journals

1. S. Erkoc and O.B. Malcioglu, "Effect of Chirality on the Stability of Carbon Nanotubes: Molecular-Dynamics Simulations" Int. J. Mod. Phys. C 12, 865(2001). (Based in part to M.S. thesis of Osman Barış Malcıoğlu)

2. S. Erkoc and O.B. Malcioglu, "Structural properties of carbon nanorods: Molecular-dynamics simulations", Int. J. Mod. Phys. C 13, 367(2002). (Based in part to M.S. thesis of Osman Barış Malcıoğlu)

3. O.B. Malcioglu and S. Erkoc, "Structural properties of diamond nanorods: Molecular-Dynamics Simulations", Int. J. Mod. Phys. C 14, 441(2003). (Based in part to M.S. thesis of Osman Barış Malcıoğlu)

4. S. Erkoc and O.B. Malcioglu, "Structural and electronic properties of AlP doped Huckel type cyclacene with 4 benzonoid rings", Int. J. Mod. Phys. C 14, 1183(2003).

5. S. Erkoc, O.B. Malcioglu, and E. Tasci, "Structural and electronic properties of single-wall GaN nanotubes: Semi-empirical SCF-MO calculations", J. Mol. Struc. (Theochem) 674, 1(2004).

6. E. Yazgan, E. Tasci, O.B. Malcioglu, and S. Erkoc, "Electronic Properties of Carbon Nanotoroidal Structures", J. Mol. Struc. (Theochem) 681, 231(2004).

7. O.B. Malcioglu and S. Erkoc, "Stability of C_{60} chains: Molecular Dynamics Simulations", J. Molecular Graphics and Modelling 23, 367(2004).

8. E. Tasci, E. Yazgan, O.B. Malcioglu, and S. Erkoc, "Stability of Carbon Nanotori Under Heat Treatment: Molecular-Dynamics Simulations", Fullerenes, Nanotubes, and Carbon Nanostructures 13, 147(2005).

9. O.B. Malcioglu, E. Tasci, and S. Erkoc, "Structural and molecular electronic properties of BN ring doped single-wall carbon nanotubes", Physica E 28, 296(2005).

10. O.B. Malcioglu and S. Erkoc, "Thermal Stability of Benzorod Arrays: Molecular-Dynamics Simulations", Int. J. Mod. Phys. C 16, 827(2005).

11. E. Tasci, O.B. Malcioglu, and S. Erkoc, "Junction Formation in Crossed Nanotubes Under Pressure: Molecular-Dynamics Simulations", Int. J. Mod. Phys. C 16, 1371(2005).

12. O.B. Malcioglu and S. Erkoc, "Thermal Stability of Benzorods: Molecular-Dynamics Simulations", J. Molec. Graph. Moddeling 24, 213(2005).

13. O.B. Malcioglu and S. Erkoc, "Structural stability of CmTin microclusters and nanoparticles: Molecular-dynamics simulations", Computing Letters 1, 204(2005) (e-journal). [This issue, issue 4, of the Computing Letters 1(4) has been also

published as a book Lecture Series on Computer and Computational Sciences, Vol. 5, "Structures and Properties of Clusters: From a few Atoms to Nanoparticles", Ed. G. Maroulis, Brill Academic Publishers, Leiden, 2006, pp: 61-66.]

14. O.B. Malcioglu, E. Tasci, and S. Erkoc, "Single wall bamboo shaped carbon nanotube: A molecular dynamics and electronic study", Int. J. Mod. Phys. C 17, 187(2006).

15. E.D. Calisir, O.B. Malcioglu, S. Erkoc, "Density functional theory investigation of 1-chloroborepin and propargyl benzene planar molecules", Int. J. Pure Appl. Chem. 1, 509(2006).

16. O.B. Malcioglu and S. Erkoc, "Impact of geometry on the hydrogen storage properties of titanium carbide: A DFT study on the model TiC4H4", Int. J. Mod. Phys. C 18, 1951(2007)..

17. E. Tasci, O.B. Malcioglu, S. Erkoc, "Structural properties of carbon nanogears", Fullerenes, Nanotubes and Carbon Nanostructures 16, 30(2008).

18. O.B. Malcioglu and S. Erkoc, "Functionality of C(4,4) carbon nanotube as molecular detector", J. Nanosci. Nanotech. (in press).

Proceedings published in national and international meetings

1. O.B. Malcioglu, V. Tanriverdi, A. Yildiz, and S. Erkoc, "Structural stability of carbon nanocapsules: Molecular-dynamics simulations", NATO-ASI, Nanoengineered Nanofibrous Materials, Antalya, 1-12 September 2003. (Poster). Proceeding: NATO Science Series II/169, Eds. S. Guceri, Y.G. Gogotsi, and V. Kuznetsov, 2004 Kluwer, p. 219.

2. E. Tasci, O.B. Malcioglu, and S. Erkoc, "Simulation of carbon nanotube junction formation", NATO-ASI, Nanoengineered Nanofibrous Materials, Antalya, 1-12 September 2003. (Poster). Proceeding: NATO Science Series II/169, Eds. S.

Guceri, Y.G. Gogotsi, and V. Kuznetsov, 2004 Kluwer, p. 237.

3. E. yazgan, E. Tasci, O.B. Malcioglu, and S. Erkoc, "Stability of carbon nan-otori", NATO-ASI, Nanoengineered Nanofibrous Materials, Antalya, 1-12 September 2003. (Poster). Proceeding: NATO Science Series II/169, Eds. S. Guceri, Y.G. Gogotsi, and V. Kuznetsov, 2004 Kluwer, p. 241.

4. O.B. Malcioglu and S. Erkoc, "Structural properties of carbon nanorods: Molecular dynamics simulations", Avrupa Birligi 6. Cerceve Programi: Nanoteknoloji, Akilli Malzemeler ve Yeni Uretim Surecleri Calistayi, Bilkent Universitesi, Ankara, 12 Temmuz 2002. (Poster).

5. O.B. Malcioglu and S. Erkoc, "Effect of chirality on the stability of carbon nanotubes: Molecular dynamics simulations", Avrupa Birligi 6. Cerceve Programi: Nanoteknoloji, Akilli Malzemeler ve Yeni Uretim Surecleri Calistayi, Bilkent Universitesi, Ankara, 12 Temmuz 2002. (Poster).

6. O.B. Malcioglu ve S. Erkoc, "Karbon nanotup ve nanocubuklarin yapisal ozellikleri", Turk Fizik Dernegi 22. Fizik Kongresi (TFD22), Bodrum, 14-17 Eylul 2004. (Poster).

7. E. Yazgan, E. Tasci, O.B. Malcioglu ve S. Erkoc, "Karbon nanotoroid yapilarin kuramsal incelenmesi", Turk Fizik Dernegi 22. Fizik Kongresi (TFD22), Bodrum, 14-17 Eylul 2004. (Poster).

8. O.B. Malcioglu, E. Tasci, S. Erkoc, "Structural and molecular electronic properties of BN ring doped single–wall carbon nanotubes", Nano-TR-I, Nanoscience and Nanotechnology 2005, Bilkent University, Ankara, 25–27 May 2005. (Poster).

9. E. Tasci, O.B. Malcioglu, S. Erkoc, "Modelling and Simulation of Carbon Nano Gears", Nano-TR-I, Nanoscience and Nanotechnology 2005, Bilkent University, Ankara, 25–27 May 2005. (Poster).

Chapters in Books

1. S. Erkoc, O.B. Malcioglu, E. Tasci, "Thermal Stability of Carbon Nanosystems: Molecular-Dynamics Simulations", in "Nanomaterials: Design and Simulation", Eds. P.B. Balbuena, J.M. Seminario, Elsevier, 2007, pp: 201–226. (Invited chapter).

2. O.B. Malcioglu and S. Erkoc, "Thermal stability of carbon nanostructures", in Encyclopedia of Nanoscience and Nanotechnology, Ed. H.S. Nalwa, American Scientific Publishers, 2007 (in press). (Invited chapter).

Conferences and Workshops attended

1. The science and technology of spin transport in nanostructures, ICTP 2002

2. NATO-ASI, Nanoengineered Nanofibrous Materials, Antalya, 2003

3. NANOTR I, Ankara 2005

4. NANOMAT, Antalya 2006

5. 13th International Workshop on Computational Physics and Materials Science: Total Energy and Force Methods, ICTP 2007

6. Advanced Workshop on Nanomaterials: A Partnership between ICTP and ICMR, ICTP 2007

Other:

- Participated as a research assistant in a collaboration between Stefano Fabris and Hande Üstünel at Elettra (Trieste/Italy) between 29 July - 15 September 2007.

COMPUTATIONAL SKILLS

- Coordinator for the computational framework of the Atomic & Molecular Physics Laboratory, and administrator of the Linux cluster therein.

- Extensively used Hyperchem and Gaussian03, adept in PWSCF, VMD and have some limited experience in NWChem, ABINIT,Atomistix toolkit, IDL.

- Adept in C++ and various scripting languages including tcl/tk.

- Teaching Assistant to computational physics courses 443 and 444 in METU since 2001.